

DESIGN, CONSTRUCTION AND PERFORMANCE EVALUATION OF A
CENTRIFUGAL PUMP FOR AN ENERGY EFFICIENT DISHWASHER

A THESIS SUBMITTED TO
THE GRADUATE SCHOOL OF NATURAL AND APPLIED SCIENCES
OF
MIDDLE EAST TECHNICAL UNIVERSITY

BY

DORUK TURGUL

IN PARTIAL FULFILLMENT OF THE REQUIREMENTS
FOR
THE DEGREE OF MASTER OF SCIENCE
IN
MECHANICAL ENGINEERING

DECEMBER 2015

Approval of the thesis:

**DESIGN, CONSTRUCTION AND PERFORMANCE EVALUATION OF A
CENTRIFUGAL PUMP FOR AN ENERGY EFFICIENT DISHWASHER**

submitted by **DORUK TURGUL** in partial fulfillment of the requirements for the degree of **Master of Science in Mechanical Engineering Department, Middle East Technical University** by,

Prof. Dr. Gülbin Dural Ünver
Dean, Graduate School of **Natural and Applied Sciences**

Prof. Dr. R. Tuna Balkan
Head of Department, **Mechanical Engineering**

Prof. Dr. Kahraman Albayrak
Supervisor, **Mechanical Engineering Dept., METU**

Examining Committee Members:

Prof. Dr. Haluk Aksel
Mechanical Engineering Dept., METU

Prof. Dr. Kahraman Albayrak
Mechanical Engineering Dept., METU

Assoc. Prof. Dr. Mehmet Metin Yavuz
Mechanical Engineering Dept., METU

Assist. Prof. Dr. Cüneyt Sert
Mechanical Engineering Dept., METU

Prof. Dr. Nuri Yücel
Mechanical Engineering Dept., Gazi University

Date: 18.12.2015

I hereby declare that all information in this document has been obtained and presented in accordance with academic rules and ethical conduct. I also declare that, as required by these rules and conduct, I have fully cited and referenced all material and results that are not original to this work.

Name, Last name: Doruk Turgul

Signature:

ABSTRACT

DESIGN, CONSTRUCTION AND PERFORMANCE EVALUATION OF A CENTRIFUGAL PUMP FOR AN ENERGY EFFICIENT DISHWASHER

Turgul, Doruk
M. S., Department of Mechanical Engineering
Supervisor : Prof. Dr. Kahraman Albayrak

December 2015, 121 pages

Energy efficiency has become one of the most important concerns of the world recently. Rate of decrease of energy resources have been accelerated due to increased population and unconscious consumption. As a result, energy efficient new generation products are on the agenda for environmental issues. Furthermore, the more efficient the product, the less costly it consumes energy. Hence, people are encouraged to use energy efficient products which enables them to save more money. In addition, it has become obligatory to manufacture energy efficient products rather than being an option. This is regulated by certain rules determined by relevant commissions around the world. White goods, so dishwashers, have to obey certain consumption levels according to these regulations as well.

In this thesis, a centrifugal pump for circulating the washing liquid in an energy efficient dishwasher, especially Arçelik dishwasher, is designed and constructed. The pump is required to deliver 60 l/min at 3020 rpm against a 300 mbar system. After the construction, its performance is evaluated by means of both Computational Fluid Dynamics (CFD) and laboratory experiments. CFD helps the designer save time and money. Several geometries and conditions can be analyzed in certain time without requiring any real product but eligible hardware and software. After deciding the final design, prototypes are produced and tested under actual conditions. At the end of this study, performance target is reached with acceptable energy efficiency.

Keywords: Centrifugal pump, Energy efficiency, Dishwasher, CFD analysis, CFD validation

ÖZ

ENERJİ VERİMLİ BİR BULAŞIK MAKİNESİ İÇİN SANTRİFÜJ BİR SİRKÜLASYON POMPASI TASARIM, KONSTRÜKSİYON VE PERFORMANS DEĞERLENDİRMESİ

Turgul, Doruk

Yüksek Lisans, Makine Mühendisliği Bölümü

Tez Yöneticisi : Prof. Dr. Kahraman Albayrak

Aralık 2015, 121 sayfa

Enerji verimliliği son dönemlerde dünyanın en önemli konularından biri haline geldi. Artan nüfus ve bilinçsiz tüketim, enerji kaynaklarının tükenme hızını artırdı. Bu nedenle çevresel meseleler için enerji verimli yeni nesil ürünler gündeme geliyor. Ayrıca, ürünün enerji verimliliği arttıkça, daha ucuz enerji tüketimi gerçekleşir. Daha fazla tasarruf edebilmek için insanlar enerji verimli ürünleri tüketmeye teşvik ediliyor. Ayrıca enerji verimli ürünler üretmek bir seçenekten ziyade zorunluluk haline geldi. Bu kurallar dünyanın çeşitli bölgelerinde ilgili birimler tarafından belirleniyor. Beyaz eşyalar da, dolayısıyla bulaşık makineleri de, bu kurallar çerçevesinde belli başlı tüketim değerlerine uymak zorundadır.

Bu tezde, enerji verimli bir bulaşık makinesinin, özellikle Arçelik bulaşık makinesi, yıkama suyu sirkülasyon pompası tasarlanıp inşa edilecektir. Pompa, 3020 rpm devirde, 300 mbar basınç karşısında dakikada 60 litre su basacaktır. İnşa işleminden sonra Hesaplamalı Akışkanlar Dinamiği (HAD) ve laboratuvar deneyleri ile pompa performansı ölçülecektir.

HAD, tasarımcıya zaman ve maliyet kazancı sağlamaktadır. Pek çok geometri ve koşul, belirli bir zamanda ve gerçek ürünün varlığına gerek olmaksızın analiz edilebilmektedir. Bunun için sadece uygun donanım ve yazılıma ihtiyaç vardır. Son

tasarıma karar verildikten sonra, pompanın prototipi yapılarak farklı çalışma koşullarında performans testi yapılacaktır. Çalışma sonunda performans hedefine kabul edilir enerji verimliliği sınırlarında ulaşılmıştır.

Anahtar kelimeler: Santrifüj pompa, Enerji verimliliği, bulaşık makinesi, HAD analizi, HAD doğrulaması

To My Parents

ACKNOWLEDGEMENTS

The author would like to thank his thesis supervisor, Prof. Dr. Kahraman Albayrak, for his great helps, guidance, encourage, support, positive altitude and patience throughout the study. He always made constructive criticism to move the author to improved levels. By organizing regular meetings, he never let the author deviate from the route.

The author wishes to express his sincere gratitude to his team leader, Dr. Songül Bayraktar, who never hesitated to help the author complete his study with her great knowledge and experience. She provided the author with all the required materials and opportunities. Moreover, she appreciated every steps of the study which in turn increased the courage of the author.

The author can never forget the love, encourage, belief and support of his family. Without the feeling of making them happy, this study may not be completed.

The author expresses his special thanks to his guide in Arçelik Dishwasher Plant, Gökhan Ak. He has been teaching every details of a dishwasher from the beginning of the author's work life.

The author wants to thank Dr. Ertuğrul Başıme, who taught the specifics of CFD, especially by providing technical support for Autodesk Simulation CFD. The author was able to complete CFD analyses by applying all the steps that Mr. Başıme taught.

The laboratory experiments could have been conducted by great effort of Mr. Orhan Atabey, who converted raw prototypes into testable pump parts. With his help, proper alignment of the pump parts and prevention of leakage problem may have been achieved.

The author also feels debted to his best schoolmate Onur Öztürkmen for his everlasting supports throughout his academic life.

The author would like to express his best wishes to his dear colleagues Mr. Uğur Kan, Ms. Ayla Kuran, Nasır Efe Aras, Didem Polat, Hasret Gürsoy Külahcı, Mahmut Murat Göçmen and Erkan Kütük for their great support.

Finally, the author would like to thank whole Arçelik Inc. family for unlimited support and peaceful ambience throughout the study.

TABLE OF CONTENTS

ABSTRACT.....	v
ÖZ.....	vii
ACKNOWLEDGEMENTS.....	x
TABLE OF CONTENTS	xii
LIST OF TABLES.....	xv
LIST OF FIGURES.....	xvi
LIST OF SYMBOLS.....	xxii

CHAPTERS

1. INTRODUCTION.....	1
1.1. General.....	1
1.2. Literature Survey.....	1
1.2.1. General Information on Dishwashers.....	1
1.2.2. General Information on Centrifugal Pumps.....	3
1.2.2.1. Classification of Pumps.....	3
1.2.2.2. Construction and Operation of Centrifugal Pumps.....	7
1.2.3. General Information on CFD.....	12
1.2.4. General Information on Energy Efficiency of Pumps and Dishwashers.....	14
2. DESIGN OF THE CENTRIFUGAL PUMP.....	19
2.1. Design Parameters.....	19
2.2. Design of Hydraulic Parts.....	20
2.2.1. Design of Impeller.....	21
2.2.2. Design of Volute.....	38

2.3. Design of the Dishwasher Circulation Pump.....	49
2.3.1. Design of the Impeller.....	50
2.3.2. Design of the Volute.....	56
2.3.3. Mechanical Parts and Electric Motor of the Pump.....	61
3. CFD ANALYSES OF THE DISHWASHER CIRCULATION PUMP...63	
3.1. General Information on CFD Analyses and Software.....	63
3.2. Pre-processing Steps for CFD Analyses.....	65
3.2.1. Solid Modeling.....	65
3.2.2. Material Assignment.....	67
3.2.3. Boundary Conditions.....	68
3.2.4. Meshing.....	68
3.3. Analyses and Results.....	70
3.3.1. Analysis and Results for Case 1.....	70
3.3.2. Analysis and Results for Case 2.....	80
4. EXPERIMENTAL SETUP AND PROCEDURE.....	91
4.1. General about the Tests.....	91
4.2. Test Setup.....	92
4.3. Experimental Procedure and Calculations.....	93
4.3.1. Experimental Procedure.....	93
4.3.2. Data Processing and Calculations.....	94
4.4. Experimental Results.....	95
4.5. Validation of CFD Analysis Results.....	96
4.6. Improvement in Energy Efficiency Compared to Current Pump.....	98
5. SUMMARY AND CONCLUSION.....	99
5.1. Summary.....	99

5.2. Conclusion.....	100
5.3. Additional Contributions and Future Work.....	101
REFERENCES.....	103
APENDICES.....	109
A. PICTURES OF PROTOTYPES AND EXPERIMENTAL SETUP.....	109
B. SAMPLE VISUALS OF MS EXCEL [®] PUMP DESIGN SHEET.....	115
C. CODES OF MACROS FOR ITERATIONAL CALCULATIONS.....	119

LIST OF TABLES

TABLES

Table 1.1- Change of ideal pump efficiency with respect to outlet blade angle.....	7
Table 1.2- Hydraulic pump components and arrangements.....	10
Table 1.3- Losses in pumps and their influence on the pump curves.....	18
Table 2.1- Results of the study on the effects of blade number on pump performance.....	26
Table 2.2- Design point parameters of the pump.....	49
Table 2.3- Impeller dimensions.....	51
Table 2.4- Blade surface area per unit blade parameters.....	54
Table 2.5- Partial volute section heights.....	58
Table 3.1- Number of elements with respect to different mesh size combinations...	70
Table 3.2- Comparison of hydraulic performance parameters between theory and analysis (case 1)	76
Table 3.3- Comparison of hydraulic performance parameters between theory and analysis (case 2)	85

LIST OF FIGURES

FIGURES

Figure 1.1- Basic components of a dishwasher.....	3
Figure 1.2- Comparison of pump profiles according to specific speed variation.....	5
Figure 1.3- Blade shapes depending on outlet angle (a) forward-swept, (b) radial exit, (c) backward-swept	5
Figure 1.4- Theoretical pump curves calculated based on formula (1.2)	6
Figure 1.5- Theoretical power vs. flow rate curves.....	6
Figure 1.6- Main components of a closed-impeller centrifugal pump.....	8
Figure 1.7- Schematics of (a) volute pump and (b) diffuser pump.....	9
Figure 1.8- Diffusion of the fluid across a pipe.....	9
Figure 1.9- Meridional section and plan view of a radial impeller.....	11
Figure 1.10- CFD analysis process.....	13
Figure 1.11- (a) Energy Guide for US, (b) Energy Label for EU, (c) Energy Rating for AU.....	14
Figure 1.12- Priorities when purchasing a new pump.....	15
Figure 1.13- LCC of centrifugal pump.....	16
Figure 1.14- Reduction of theoretical Euler head due to losses.....	17
Figure 1.15- Increase in power consumption due to losses.....	17
Figure 2.1- Geometric profile and dimensions of the radial impeller (a) plan view, (b) meridional view.....	22
Figure 2.2- Hydraulic efficiency vs. specific speed.....	23
Figure 2.3- Pressure coefficients.....	24
Figure 2.4- Non-dimensional blade outlet width vs. specific speed.....	28
Figure 2.5- Inlet velocity triangle and geometric parameters.....	30

Figure 2.6- Outlet velocity triangle and geometric parameters.....	30
Figure 2.7- Impeller blade leading edge profiles.....	31
Figure 2.8- Drawing of a single blade by Single-arc method.....	32
Figure 2.9- Drawing of a single blade by Double-arc method.....	33
Figure 2.10- Drawing of a single blade by Point-by-point method.....	35
Figure 2.11- Drawing of the radial view of the impeller.....	36
Figure 2.12- Channel cross-section between successive blades.....	37
Figure 2.13- Weinig diagram for moving circular cascade.....	38
Figure 2.14- Volute casing types.....	39
Figure 2.15- Flow rate components through the impeller.....	40
Figure 2.16- Cross-section shapes of volute casings.....	40
Figure 2.17- Rectangular, circular, and trapezoidal volutes of the same cross-sectional area.....	41
Figure 2.18- CFD analysis results for different cross-section volutes of the same cross-sectional area, (a) Head coefficient, (b) Hydraulic efficiency, (c) Radial force with respect to flow coefficient ratio	41
Figure 2.19- Volute casing.....	43
Figure 2.20- Meridional section of volute.....	44
Figure 2.21- Cutwater and throat.....	45
Figure 2.22- Diffuser shapes, (a) tangential, (b) radial.....	46
Figure 2.23- Performance characteristics of tangential and radial diffusers, (a) head coefficient, (b) efficiency, (c) radial force with respect to flow coefficient ratio.....	46
Figure 2.24- Diffuser efficiency in straight and curved diffusers.....	47
Figure 2.25- Flow regimes inside a diffuser.....	48
Figure 2.26- Blade profile by Single-arc method.....	52
Figure 2.27- Blade profile by Double-arc method.....	52
Figure 2.28- Blade profile Point-by-point method with: (a) 5 equal elements, (b) 3 equal elements, (c) 2 equal elements	52

Figure 2.29- Comparison of Single-arc and Double-arc methods on the same plane.....	53
Figure 2.30- Channel cross-section control circles: (a) Single-arc (b) Double-arc.....	54
Figure 2.31- Channel breadth x blade width for the mid-stream line sections.....	54
Figure 2.32- Meridional view of the impeller.....	55
Figure 2.33- Final blade profile (plan view)	56
Figure 2.34- Final impeller model.....	56
Figure 2.35- Volute outer limits.....	57
Figure 2.36- Design limits for partial volutes.....	58
Figure 2.37- Volute bottom profile obtained by connecting 8 partial volute sections.....	59
Figure 2.38- Completed volute design (without heater plate): (a) top view, (b): side view	60
Figure 2.39- Pump hydraulic parts.....	61
Figure 2.40- Full pump assembly.....	62
Figure 3.1- Fluid domain CAD model with inlet-outlet extensions.....	66
Figure 3.2- Impeller inside the fluid domain.....	66
Figure 3.3- Rotating region between volute wall and impeller.....	67
Figure 3.4- Rotating region speed-time table.....	68
Figure 3.5- Analysis results for different mesh sizes at Q=60 l/min for case 1.....	70
Figure 3.6- Exploded view of pump assembly for case 1.....	71
Figure 3.7- Pump assembly model for case 1.....	71
Figure 3.8- Generated mesh-general view (case 1)	72
Figure 3.9- Generated mesh-sectional view (case 1)	72
Figure 3.10- Generated mesh at impeller.....	73
Figure 3.11- Mesh refinement at blade leading edge.....	73
Figure 3.12- Mesh refinement at cutwater region (case 1)	74

Figure 3.13- Convergence plot for design point analysis (case 1) (a) Inlet pressure and inlet velocity, (b) residual values for pressure.....	75
Figure 3.14- Hydraulic torque values for design point analysis (case 1).....	76
Figure 3.15- Absolute velocity vectors inside the pump on a vertical cut plane (case 1)	76
Figure 3.16- Static pressure distribution inside the pump on a vertical cut plane (case 1).....	77
Figure 3.17- Absolute velocity vectors inside the pump on a horizontal cut plane (case 1)	77
Figure 3.18- Relative velocity vectors inside the pump on a horizontal cut plane (case 1)	78
Figure 3.19- Relative velocity vectors through the blades (case 1)	78
Figure 3.20- Flow development in extension pipe (case 1)	79
Figure 3.21- Static pressure distribution inside the pump on a horizontal cut plane (case 1)	79
Figure 3.22- Pressure rise versus flow rate and efficiency versus flow rate curves obtained by CFD analysis (case 1)	80
Figure 3.23- Exploded view of pump assembly for case 2.....	80
Figure 3.24- Pump assembly model for case 2.....	81
Figure 3.25- Generated mesh-general view (case 2)	82
Figure 3.26- Mesh refinement at cutwater region (case 2)	83
Figure 3.27- Convergence plot for design point analysis (case 2) (a) Inlet pressure and inlet velocity, (b) residual values for pressure.....	84
Figure 3.28- Hydraulic torque values for design point analysis (case 2).....	84
Figure 3.29- Absolute velocity vectors inside the pump on a vertical cut plane (case 2).....	85
Figure 3.30- Static pressure distribution inside the pump on a vertical cut plane (case 2).....	85
Figure 3.31- Absolute velocity vectors inside the pump on a horizontal cut plane (case 2).....	86

Figure 3.32- Relative velocity vectors inside the pump on a horizontal cut plane (case 2).....	86
Figure 3.33- Relative velocity vectors through the blades (case 2)	87
Figure 3.34- Flow development in extension pipe (case 2)	87
Figure 3.35- Static pressure distribution inside the pump on a horizontal cut plane (case 2).....	88
Figure 3.36- Pressure rise versus flow rate and efficiency versus flow rate curves obtained by CFD analysis (case 2)	88
Figure 3.37- Hydraulic performance comparison of case 1 and case 2 by CFD analyses –(a) pressure rise versus flow rate, (b) efficiency versus flow rate.....	89
Figure 4.1- SLS process-I.....	91
Figure 4.2- SLS process-II.....	92
Figure 4.3- Test setup schematic.....	93
Figure 4.4- Test results for case 1.....	95
Figure 4.5- Test results for case 2.....	95
Figure 4.6- Comparison of CFD and test results for case 1.....	97
Figure 4.7- Comparison of CFD and test results for case 2.....	97
Figure 4.8- Efficiency comparison of current and new pump designs.....	98
Figure A.1- Prototype of designed impeller (top view)	109
Figure A.2- Prototype of designed impeller (side view)	109
Figure A.3- Prototype of designed impeller (isometric view)	110
Figure A.4- Prototype of designed impeller assembled to shaft and wet rotor	110
Figure A.5- Prototype of designed volute (top view)	111
Figure A.6- Prototype of designed volute (side view)	111
Figure A.7- Prototype of designed volute (front view)	112
Figure A.8- Prototype of designed volute (bottom view)	112
Figure A.9- Prototype of designed volute assembled to electric motor and inlet hose (with water-resistant glue on it)	113

Figure A.10- Silicon reinforcement at the top of the volute prototype.....	113
Figure A.11-Experimental setup in Prof. Dr. Cahit Eralp Laboratory in Arçelik Dishwasher Plant.....	114

LIST OF SYMBOLS

SYMBOLS

a	diameter at throat
b	impeller width
c	velocity
d	diameter
e	thickness
f_q	number of stages (see Eq. 2.1)
f_{d1}	coefficient (see Eq. 2.5)
f_l	constant (see Eq. 2.16)
g	gravitational acceleration
i	incidence
k_z	coefficient (see Eq. 2.4)
k_w	coefficient (see Eq. 2.15)
l	impeller length
n	rotational speed (in revolutions per minute)
n_q	specific speed (metric)
p	pressure
r, R	radius
t	pitch
u	circumferential velocity
w	relative velocity
z	elevation
z_{la}	number of blades
z_{le}	number of cutwater
A	area
H	head
L	diffuser length

N_s	specific speed (non-dimensional)
P	power
T	torque
Q	volumetric flow rate
X_{sp}	factor (see Eq. 2.38)
α	absolute fluid angle, camber angle
β	relative fluid angle
δ	deviation angle, displacement thickness (see Fig. 2.24)
δ_r	factor (see Eq. 2.5)
ε	wrap angle (for volute)
ε_{lim}	factor (see Eq. 2.14)
ϕ	central angle (for blade)
γ	slip factor
Γ	circulation
η	efficiency
λ_{Le}	angle between blade and impeller disk
π	pi number
ρ	density
τ	blockage
ϑ	diffuser opening angle
ξ_p	lift coefficient
ψ	head coefficient
ω	angular speed

INDICES

1	inlet of the blade
2	outlet of the blade
3	inlet of the volute
b	arithmetic average
B	blade
h	hydraulic

L_a	related to blade
L_e	related to volute
m	mean, meridional, mechanical
n	hub
w	shaft
u	tangential direction
v	volumetric
∞	infinite
opt	operating
min	minimum
max	maximum
$NPSH_R$	Net Positive Suction Head-required
$NPSH_i$	Net Positive Suction Head-required for cavitation inception

CHAPTER 1

INTRODUCTION

1.1 General

The subject of this thesis is design, construction and performance evaluation of a centrifugal pump to be used in a dishwasher, especially for Arçelik Inc. Dishwasher Plant. Not only laboratory experiments but also numerical experiments by means of Computational Fluid Dynamics (CFD) are to be conducted in order to approach the problem from two sides. Using CFD will provide the agent with save of time, money, and effort since the parameters which are included in hydraulic design can easily be manipulated and their effects can easily be investigated by this method.

This thesis covers the issue within three main parts: theoretical design, numerical experimentation (CFD), and laboratory experimentation. In theoretical part, the desired pump is to be designed by using the basic empirical methods commonly used in literature. In CFD part, theoretically obtained parameters are to be used to generate Computer-Aided Design (CAD) models. Then these models are to be tested under several conditions by using commercial CFD software. In the final part –laboratory experimentation part-, previously analyzed models (by CFD method) are to be prototyped and tested at the same conditions to validate the accuracy between numerical and actual tests.

1.2 Literature Survey

1.2.1 General Information on Dishwashers

“A dishwasher is a mechanical device for cleaning dishes and eating-utensils.”, [1]. A domestic dishwasher operates according to the following principle: Dishes are loaded into the device manually. Upon starting any desired program, residual water from the previous operation is drained first by means of a drain pump. Then the

dishwasher takes certain amount of water from the mains and fills a sump located at the bottom to collect washing water. Then a circulation pump takes water from the sump and delivers to spray arms, which are the main actuators of the cleaning action. The spray arms rotate with momentum supplied by the circulating water, and spray water towards the dishes. The water then passes through the filtration system located at the bottom center by means of gravitational force and reaches to the sump again. Circulation of washing water continues in this manner up to a certain time. When a washing step ends, soiled water is drained, [2].

There are mainly four steps in standard programs in which water circulation mentioned above takes place: pre-wash, main wash, cold rinse, and hot rinse. The last step of a dishwasher operation is the drying step, but water is not circulated here. In main wash step, detergent is added to solve the soil and to provide hygiene; whereas in rinsing steps, rinsing agent is added for superior drying performance. In main wash and rinsing steps, the water is heated for optimum detergent/rinsing agent activation, [2]. It is seen that, the circulation pump of a dishwasher is operated with water which is first clean, then soiled, then mixed with detergent and rinsing agent. This requires a suitable design which is flexible enough to withstand these condition changes.

To summarize, a dishwasher takes water, circulates it to clean the dishes (according to the step, water is heated, mixed with detergent, and mixed with rinsing agent), drains the soiled water, and dries the dishes, [2].

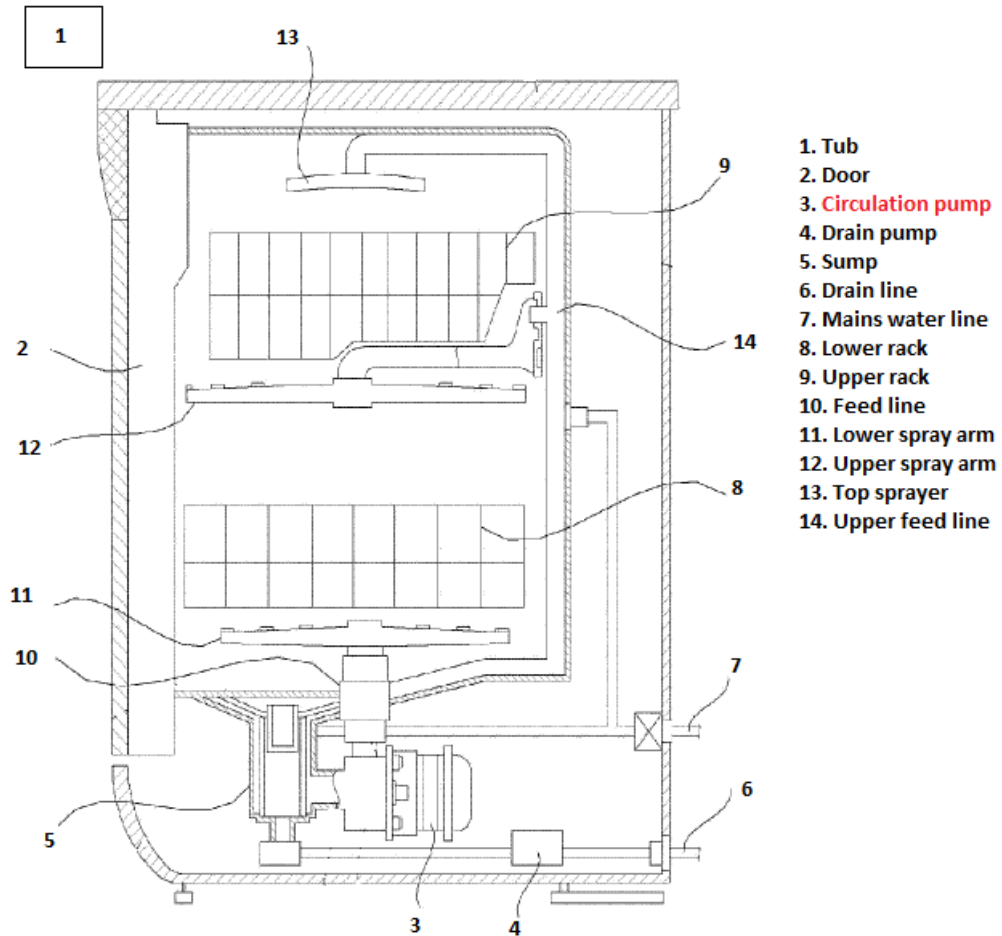


Figure 1.1- Basic components of a dishwasher [3]

Although there are a lot of detailed systems which play crucial roles, such as safety systems, water softening system, electronic control system and so on, only the circulation system is mentioned up to here since this thesis covers only the design of its circulation pump.

1.2.2 General Information on Centrifugal Pumps

1.2.2.1 Classification of Pumps

It is better to start with the concept of “turbomachine” since a pump is a kind of this device. “Turbomachine is a device that exchanges energy with a fluid using continuously flowing fluid and rotating blades”. A pump is a type of turbomachines which extracts energy from a liquid, [4]. Pumps are also classified into several types, but mainly into two: rotodynamic (or simply dynamic) pumps, where the fluid velocities within the pump are increased by continuous energy adding such that they exceed the values of discharge velocities resulting in pressure rise towards the outlet;

and positive displacement pumps, where a fixed amount of fluid is forced by adding energy periodically resulting in pressure rise up to desired values to move the fluid within the system, [5]. Yet another classification is made under the rotodynamic pumps according to the geometry of the flow pattern: centrifugal (radial) pumps, mixed-flow (semi-axial) pumps, and axial pumps, [6]. In centrifugal pumps, velocity is increased by the centrifugal forces created during the operation of rotating impeller, [5].

According to Reti (1963, p. 290), the history of centrifugal pumps dates a treatise about a mud lifting machine by Francesco di Giorgio Martini, who is an Italian Renaissance engineer, in 1475. On the other hand, the real centrifugal pumps as understood today were developed in late 17th century by Denis Papin with straight vanes, and by John Appold with curved vane, [7].

As stated above, according to the direction of the flow paths, dynamic pumps are divided basically into three: centrifugal, mixed flow, and axial. It is the specific speed, a special parameter for pumps, which decides the flow path geometry of dynamic pumps. There are numerous definitions for specific speed in the literature. However, to be consistent throughout this study, the expression (non-dimensional specific speed) in Eq. (1.1) is used, [8]:

$$N_s = \frac{\omega\sqrt{Q}}{(gH)^{0.75}} \quad (1.1)$$

where ω is in rad/s, Q is in m³/s, H is in m, and g is the gravity [m/s²]. According to Gülich (2008), if the application is “universal” or standard, a single-stage radial pump should be used due to low investment costs, [6]. A dishwasher application can be counted under this type of application since the only duty of the circulation pump is to circulate certain amount of water with relatively low flow rate and low head. Moreover, construction of dishwashers requires use of this type of pumps. Figure 1.2 illustrates how the profile and efficiency of the pump is varying according to specific speed (note that, dimensional specific speed is used in most of the sources in literature for this type of charts).

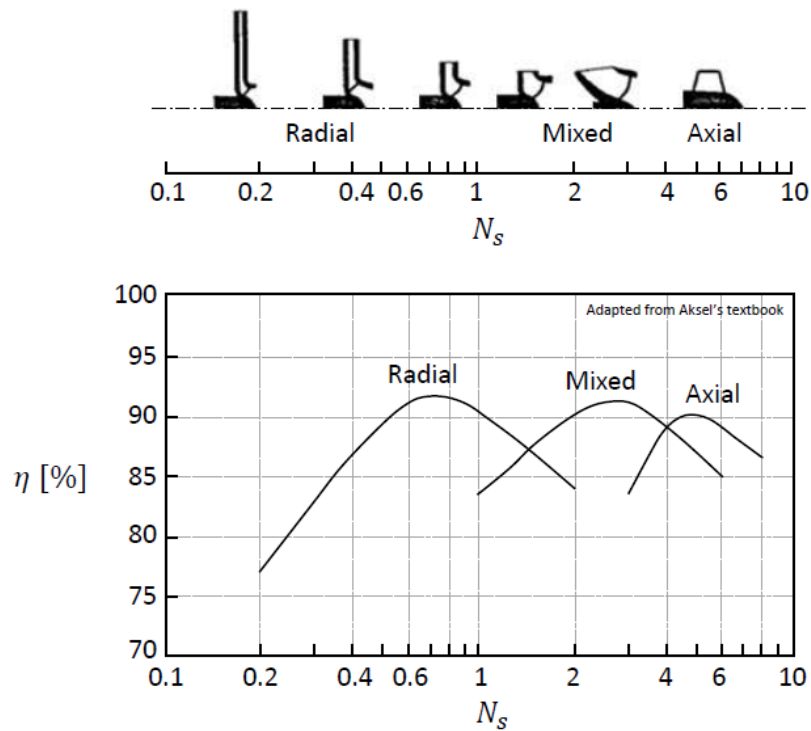
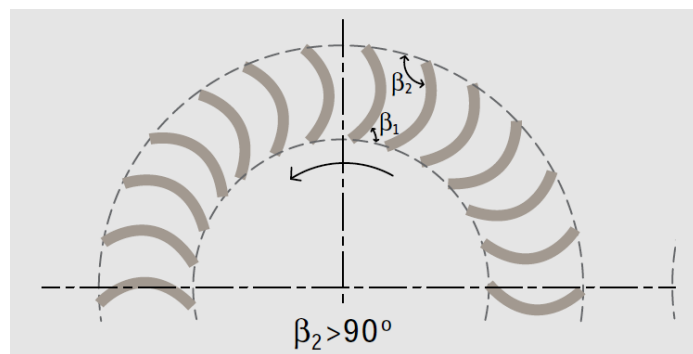


Figure 1.2- Comparison of pump profiles according to specific speed variation [9]

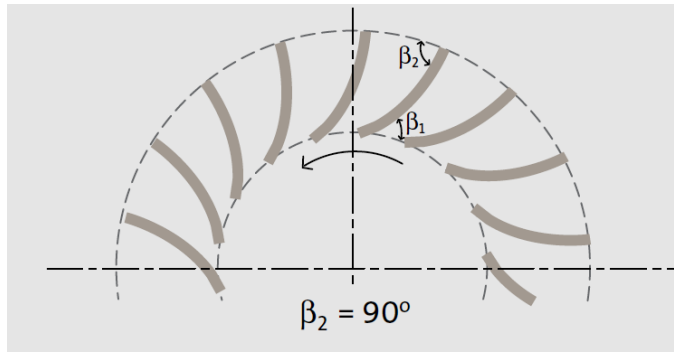
Other than the vane area profile, the blade shape of the impeller depending on outlet angle is also important for the performance of the pump. There are three types of blade shapes: forward-swept/curved/leaning, backward-swept/curved/leaning, and radial exit. Characteristics trends of these three different blade types can be calculated theoretically by using Eq. (1.2), [10]:

$$H = \frac{c_2^2}{g} - \frac{c_2}{\pi \cdot d_2 \cdot b_2 \cdot g \cdot \tan(\beta_2)} Q \quad (1.2)$$

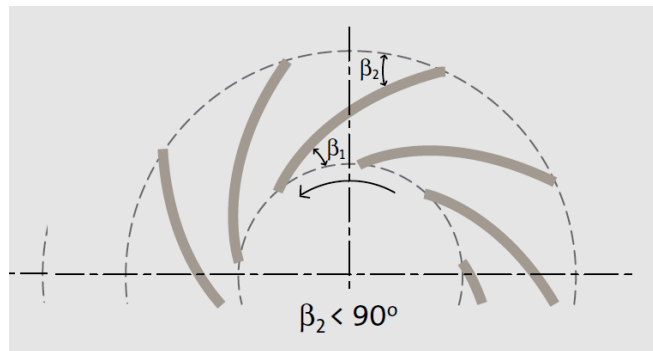
Figures 1.3 to 1.5 illustrate the appearances and the characteristics of these three types:



(a)



(b)



(c)

Figure 1.3- Blade shapes depending on outlet angle (a) forward-swept, (b) radial exit, (c) backward-swept [10]

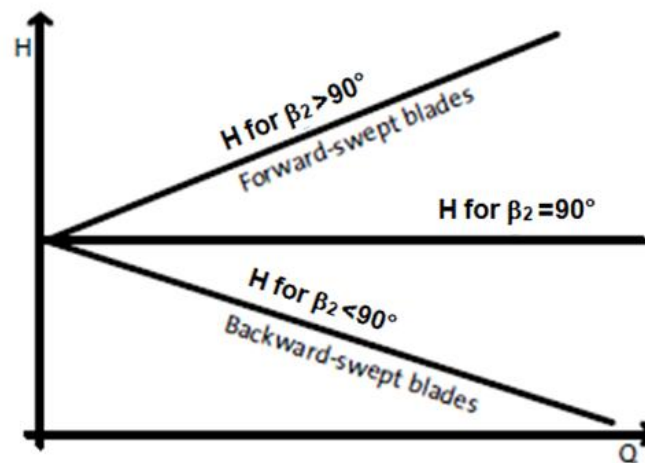


Figure 1.4- Theoretical pump curves calculated based on formula (1.2) [10]

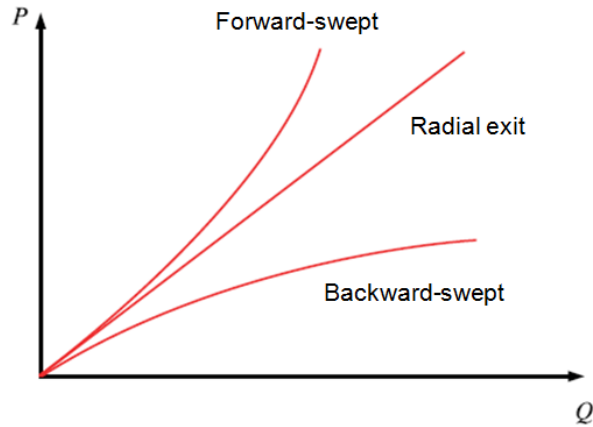


Figure 1.5- Theoretical power vs. flow rate curves [4]

As seen from Figure 1.5, backward leaning blades exhibit a decreasing gradient of power as the flow rate is increased. Moreover, they have higher efficiencies since they have lower exit swirl and forward leaning blades have increasingly steep power curve. These are the basic reasons which favor backward leaning blades over the others, although the head is decreasing as the flow rate is increasing, [4]. In dishwashers, circulation pumps have backward leaning blades for the aforementioned reasons.

In backward-curved blades, as the exit blade angle increases, tangent value increases resulting in a decrease in the second term in Eq. (1.6). Due to the minus sign of that term, overall value of the equation increases. Thus, the larger the blade angle, the higher the head. On the other hand, the ideal efficiency decreases with increased energy. A comparative example in which all the parameters are kept constant while the blade angle is changed illustrates some numerical results:

Table 1.1-Change of ideal pump efficiency with respect to outlet blade angle, [11]

β_2 (degrees)	20	45	90
η_{ideal} (%)	73	58	47

1.2.2.2 Construction and Operation of Centrifugal Pumps

According to Karrassik (2011, p. 2.97), [5], a centrifugal pump is composed of mainly two parts: the first being a rotating element consisting of an impeller and a shaft, and the second being a stationary element consisting of a casing, casing cover, and bearings. However, there are other components which complete a centrifugal pump assembly as shown in Figure 1.6:

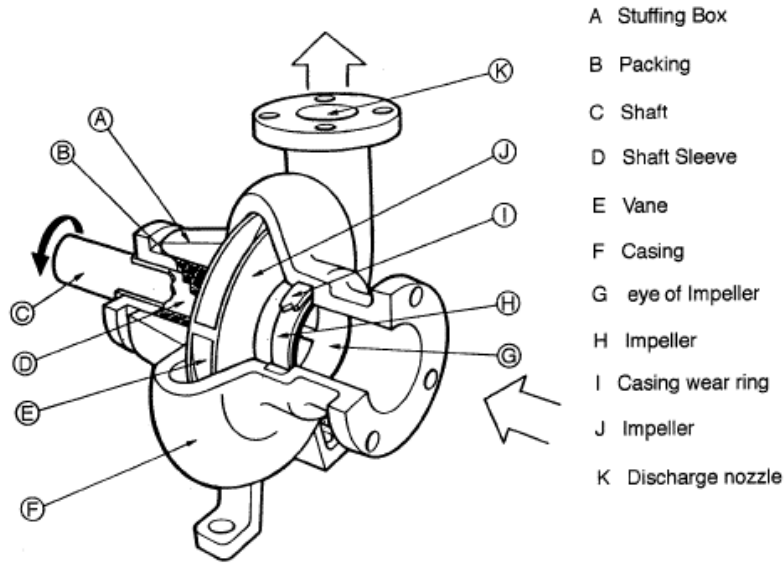


Figure 1.6- Main components of a closed-impeller centrifugal pump [12]

The working principle of centrifugal pumps is as follows: a pressure means forces the fluid into the impeller, which is composed of a set of vanes. As the impeller rotates, the fluid is discharged by centrifugal force towards the periphery gaining a higher velocity. There is a volute (in volute pumps) or stationary diffusers (in diffuser pumps), as shown in Figure 1.6, surrounding the impeller designed such that the previously increased velocity is converted into pressure energy, [5]. The physics behind this phenomenon may be described as follows: The fluid leaving the impeller is collected in the volute. The volute has an increasing cross-sectional area so that as the fluid travels across there, its velocity decreases resulting in a pressure rise according to Bernoulli's equation (Eq. (1.3)), [10]. The illustrative figure of diffusion process in the volute/diffuser is shown in Figure 1.8:

$$\frac{p}{\rho} + \frac{c^2}{2} + gz = Constant \quad (1.3)$$

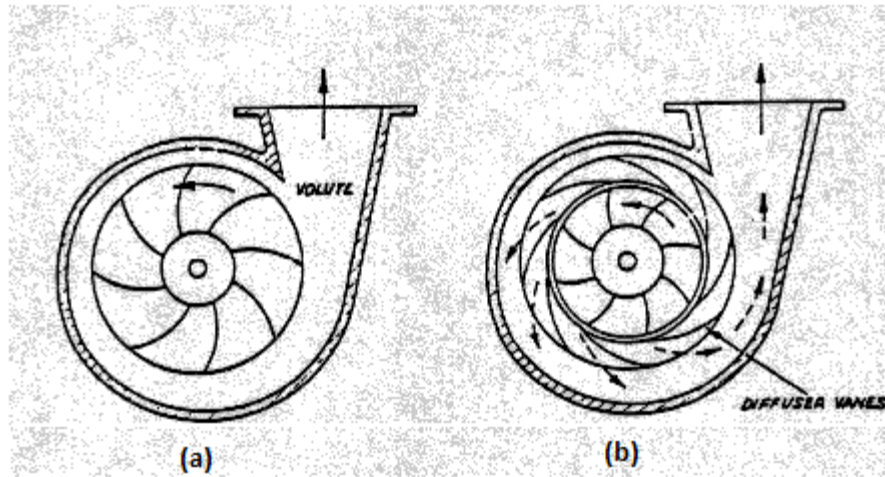


Figure 1.7- Schematics of (a) volute pump and (b) diffuser pump [13]

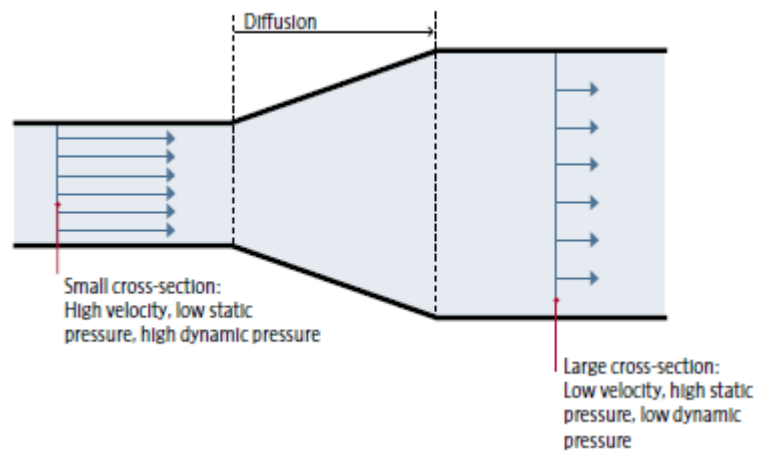

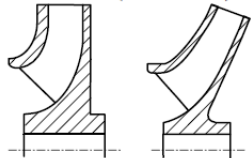
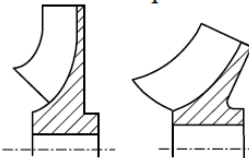
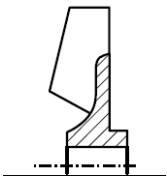

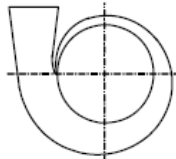
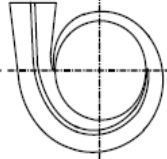
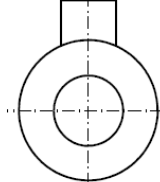
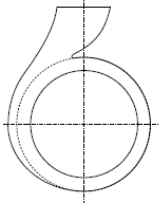
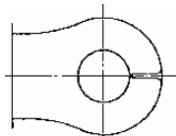
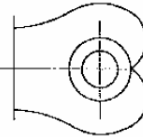
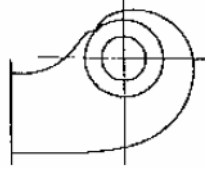
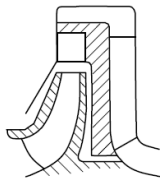
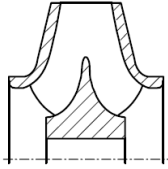


Figure 1.8- Diffusion of the fluid across a pipe [10]

There are several other classifications which describe the type of a centrifugal pump, including impeller, volute, diffuser, and casing characteristics. The most common classifications are summarized as shown in Table 1.2:

Table 1.2- Hydraulic pump components and arrangements of a centrifugal pump [6]

Impeller form: Characteristic: flow direction at impeller exit	Radial 			
Impeller type	Closed (shrouded) 	Semi-open 	Open 	
Diffuser Characteristic: flow direction at diffuser	Radial 			
Outlet casing	Single-volute 	Double-volute 	Concentric annulus 	Concentric annulus plus volute 
Inlet casing	Annular inlet chamber 	Symmetric inlet 	Asymmetric inlet 	
Impellers in series: multi-stage pumps				
Impellers in parallel: double-entry impellers	Single stage 			

In a standard dishwasher, the circulation pump has a closed impeller, a single volute outlet casing, and an annular inlet chamber. In Figure 1.9, a typical radial impeller is shown:

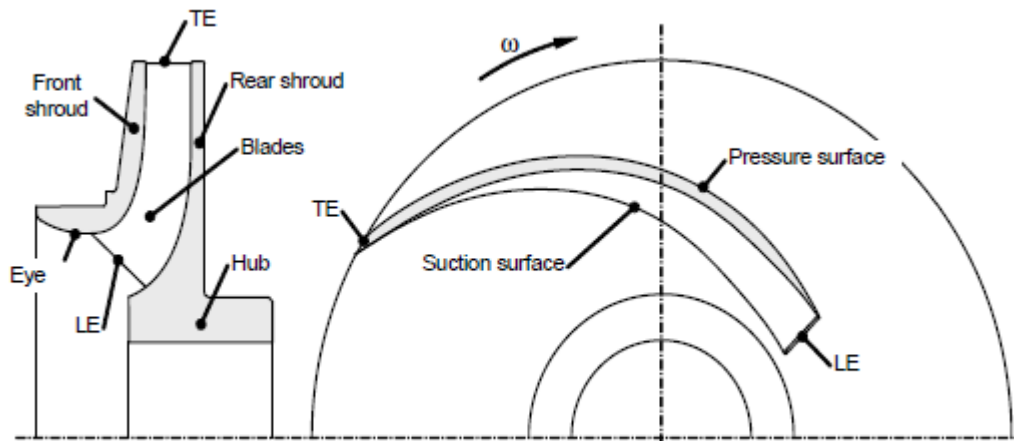


Figure 1.9- Meridional section and plan view of a radial impeller (LE: Leading edge, TE: Trailing edge) [6]

Having explained the types, the parts, and the working principle of centrifugal pumps, the prime movers can now briefly be mentioned to complete this section. According to Karrassik (2011), pumps can be driven by electric motors, by steam turbines, by internal combustion engines, by hydraulic turbines, and by gas turbines depending on the application, [5]. Since electric motors are used as the prime mover in dishwashers, the details are presented only for this driver only in this study.

Electric motors can most basically be classified into two: alternating current (AC), and direct current (DC) motors. The mechanism of these electric motors is that, mechanical energy is obtained from electrical energy by means of the magnetic flux linkage of the two magnetic circuits, one of which is in the stator and the other is in the rotor. Due to magnetic flux created between the circuits, a torque is produced resulting in the relative rotation of the motor shaft. The value of the torque is so important such that it determines the output power of the motor when multiplied by the rotational speed, [5]

AC motors operate with 50-60 Hz alternating voltages from public mains. The number of magnetic poles and the sinusoidal frequency of the voltage determine the speed of the motor. DC motors, on the other hand, requires additional storage batteries or a DC generator. AC motors are much more preferred over DC motors

due to their ease of availability, excellent reliability, excellent performance characteristics, and ease of replacement. On the contrary, DC motors are also preferred in some cases. The reason is its variable speed capability by simply changing the voltage. Despite DC motors' not having a long useful life without maintenance, the brushless DC (BLDC) motors began to eliminate this problem with higher reliability, superior performance, and longer life. Yet, AC motors seem to be the dominant one since they may also have variable speed by using AC converters and vector drivers, [14].

1.2.3 General Information on CFD

Although the experimental fluid dynamics have prospered for years, it is sometimes not possible to construct a test setup for every design study. This may be due to time considerations, economical reasons, space availability, and so on. Thus, an alternative branch of fluid dynamics to solve this problem is developed called computational fluid dynamics (CFD). It is a cost-effective way to simulate real flows numerically by solving related governing equations by means of advanced computers, [15]. Today, there are several commercial or open source CFD software, some of which are Fluent, CFX, SimulationCFD (CFdesign), OpenFOAM, Star-CD, Cradle, and so on.

As cited in Fletcher (2006, p. 2), Chapman et al., Green, Rubbert, and Jameson point to the following major advantages of CFD compared to experimental approach in fluid dynamics, [15]:

- Reduction in lead time in design and development.
- Simulation opportunity of non-reproducible flow conditions in experimental method.
- Availability of more detailed and comprehensive information.
- Developing cost efficiency compared to wind-tunnel testing.
- Reduction in energy consumption.

Although there are a number of arguments about the first appearance of CFD, the history dates to mid-1900's. According to Wendt (2008, p. 6), the study of Kopal in 1947 can be counted as the first remarkable CFD example, [16]. In the mentioned study, Kopal gathered massive tables of the supersonic flow over sharp cones together by applying numerical solution to the governing differential equations by

means of a primitive digital computer. Nevertheless, it was not until the 1950's, during which superior computers with higher efficiency and speed emerged, that actual CFD solutions of more complicated problems first appeared, [16]. 50 years of CFD can be summarized as follows: between 1960 and 1970, early developments were made; between 1970 and 1980, potential flow equations were solved; between 1980 and 1990, Euler and Navier-Stokes equations are solved; between 1990 and 2000, aerodynamic shape optimization is achieved; and finally, after 2000, discontinuous finite element methods are implemented, [17].

In CFD, the basic governing equations are continuity, momentum and energy equations, but there are more according to the application. These are solved numerically in CFD since analytical solutions cannot be obtained for such complex problems, [16].

CFD is used in heat transfer, mass transfer, and fluid flow problems, which are three of the basic engineering disciplines. Moreover, several application areas may be counted, some of which are the following: aircraft industry, turbomachinery industry, automotive industry, naval industries, as well as meteorology, oceanography, astrophysics, oil recovery, architecture, and so on, [18].

A typical CFD analysis process can be summarized as follows in Figure 1.10, [19]:

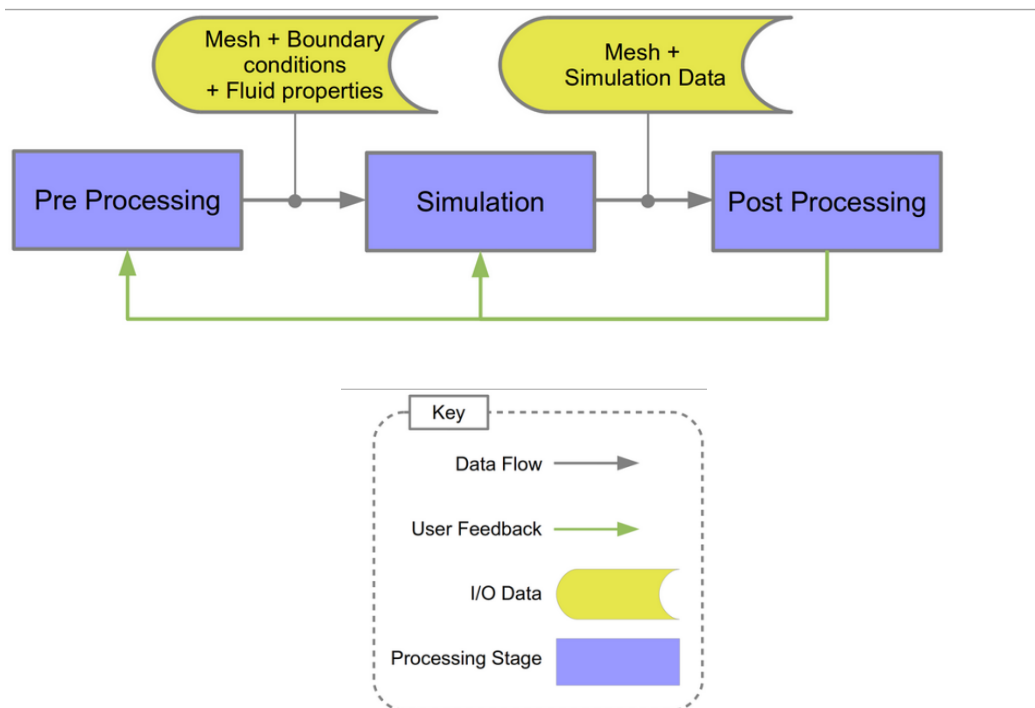


Figure 1.10- CFD analysis process

If one of the convergence criteria of an analysis is fulfilled, then the analysis stops manually or automatically depending on the software. If the analysis diverges, then appropriate modifications should be made at the necessary steps, such as at mesh generation step, until the analysis converges. In the verification part, the results of the analysis are compared with the experimental results. If the results are accurate, then the process can be terminated. If, on the other hand, the results are not accurate enough, then some further modifications should be made.

In this study, CFD analyses for the designed pump under different conditions are made. Detailed information is presented in Chapter 3.

1.2.4 General Information on Energy Efficiency of Pumps and Dishwashers

When buying an appliance, people are concerned not only by the purchase price, but also their energy levels since energy save is a very important issue today. There are different energy standards in different countries. For example, USA uses “Energy Guide”, [20], EU uses “Energy Label”, [21], and Australia uses “Energy Rating” [22] as their indication of how an appliance is efficient. Figure 1.12 shows sample tags for each of them. These guides/labels/ratings provide the user with information about how much energy and water is consumed by the product annually, how noisy is it, how beneficial is it for the globe and so on, [21]. With the increasing consciousness, consumers seek to buy the appliances with better energy guides/labels/ratings to save more money and protect the globe.

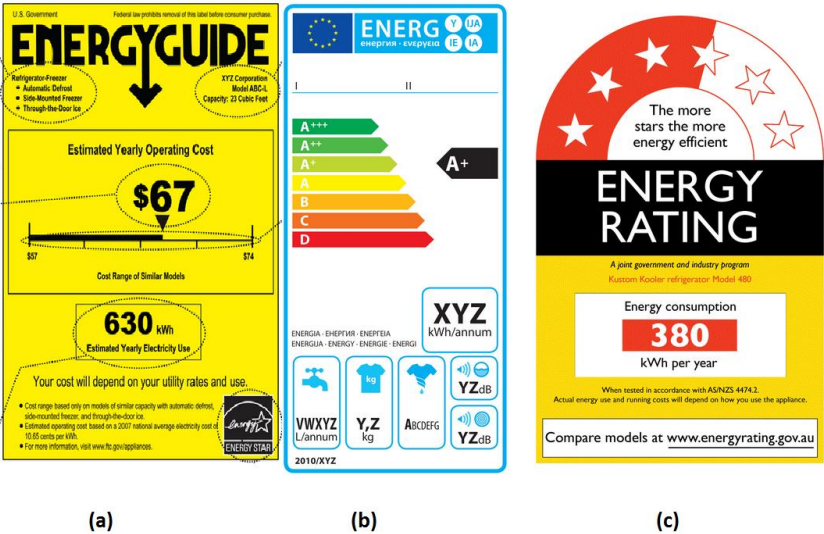


Figure 1.11- (a) Energy Guide for US, [20], (b) Energy Label for EU, [23], (c) Energy Rating for AU, [22]

Although other parameters such as the insulation have effects on determining the energy guide/label/rating of a dishwasher, the biggest role belongs to the electrical heater and then to the circulation pump since it is involved in energy and water consumption, noise level, CO₂ emission and so on. Thus, it is an important task to give higher emphasis on the hydraulic performance. Efficiency of a pump and efficiency of an entire dishwasher system are different issues, but they are strictly interconnected. A highly efficient pump under certain conditions may exhibit inferior efficiency when operated in an inappropriate system. Therefore, both the pump and the system should be considered together in order to decide whether they meet the needs efficiently or not. According to a study by Dries (n. d.), most manufacturers expect to increase the efficiency of a dishwasher by changing the electric motor of the pump although this would only be effective on electrical efficiency, but not on the hydraulic efficiency. He adds that, improving the hydraulic efficiency of a dishwasher by some manipulations on the hydraulic system can be both more economic and more beneficial. In order to achieve this, washing systems and operating conditions should be well analyzed, [24]. On the other hand, the scope of this thesis includes only the pump side of an energy efficient dishwasher, that is, the hydraulic system of the dishwasher is assumed to be fixed, and the modifications are made on the circulation pump.

It is mentioned above that, people try to buy more energy efficient dishwashers. Nonetheless, when it comes to the purchase of a new pump, energy cost is at the least consideration according to a survey of Users, [25]. However, dishwasher manufacturers are firstly concerned about the efficiency. Figure 1.12 illustrates the priorities in other industries when purchasing a new pump according to the survey:

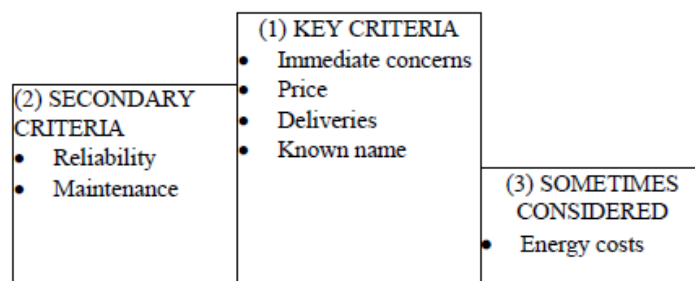


Figure 1.12- Priorities when purchasing a new pump [25]

However, the Figure 1.13 indicates the contradiction between the buyer priorities and the actual life cycle cost (LCC) trend:

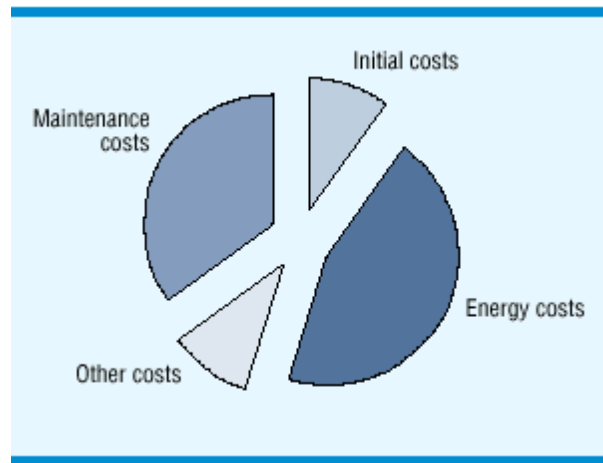


Figure 1.13- LCC of centrifugal pump [26]

According to a study in European Commission (Study on Improving the Energy Efficiency of Pump, 2001), there are mainly three barriers to improving the efficiency of pumps. The first is the organizational behavior: Usually intermediaries such as Distributors and OEM suppliers are responsible for buying pumps in the cheapest manner; hence, energy saving is not concerned at this stage. Moreover, fast revision of pumps results in inadequate repair by non-specialists. The second barrier is the technical and educational factors: Efficiency contradicts with maintenance effort and safety requirements. In addition, system efficiency should be considered together with the pump efficiency. Furthermore, pumps are not correctly selected, and/or they are replaced with the identical ones rather than re-assessing the needs. The last obstacle in front of the efficiency improvement is the economic reasons: As seen in Figure 1.13, energy saving is insignificant compared to other factors according to most users, excluding dishwasher manufacturers. Moreover, amortization of energy saving is not appreciated in short term or in case of low cost installments. Acceptance tests, in addition, are not economic for smaller pumps. To sum up, there are many biases and reasons that overshadow the importance of energy efficiency of pumps. However, on site advice, encouraging third party involvement, and research and development (R&D) may help getting rid of these problems, [25].

In order to improve/maintain the efficiency of a pump, all the losses affecting the pump performance should be well analyzed. There are mainly two types of losses in a pump: mechanical losses and hydraulic losses. Since they result in lower head than theoretical and higher power consumption, efficiency of the pump decreases, [10].

Figures 1.14, 1.15 and Table 1.3 show how losses are effective on the performance, so the efficiency, of the pumps:

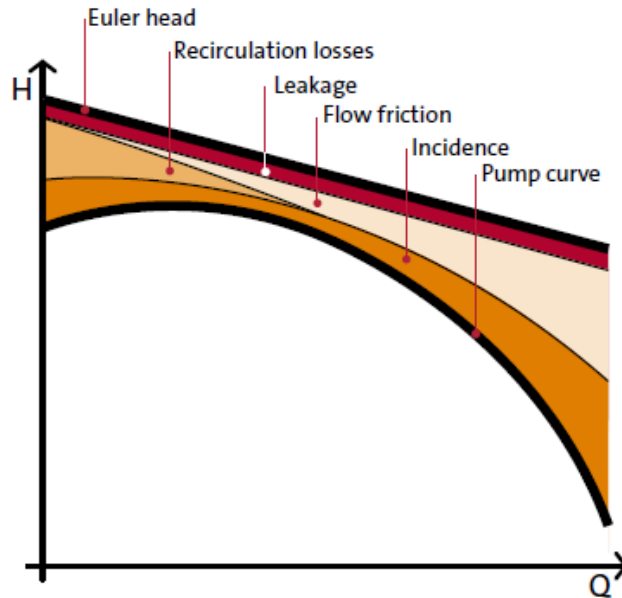


Figure 1.14- Reduction of theoretical Euler head due to losses [10]

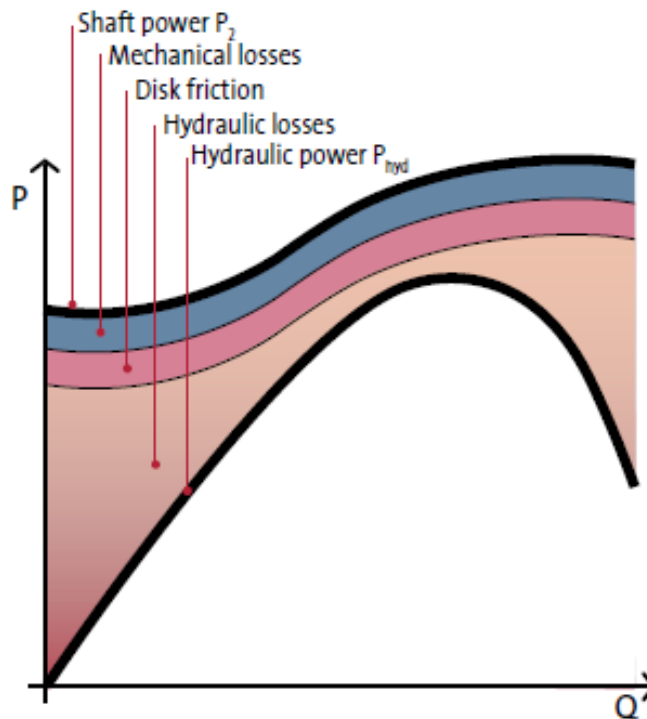










Figure 1.15- Increase in power consumption due to losses [10]

Table 1.3- Losses in pumps and their influence on the pump curves [10]

	Loss		Smaller flow (Q)	Lower head (H)	Higher power consumption (P ₂)
Mechanical losses	Bearing				X
	Shaft seal				X
Hydraulic losses	Flow friction			X	
	Mixing			X	
	Recirculation			X	
	Incidence			X	
	Disk friction				X
	Leakage		X		

Losses are not the only factors affecting the efficiency of pumps. Specific speed, pump type, design, absolute size, operating range, and so on are also very important for determination of the efficiency, [6].

To summarize, in order to produce energy efficient dishwashers, the hydraulic system and the circulation pump are the upmost important elements to be considered. In the scope of this thesis, design of an efficient pump is covered only while the system characteristics for the dishwasher is assumed to be fixed.

CHAPTER 2

DESIGN OF THE CENTRIFUGAL PUMP

2.1 Design Parameters

The pump to be designed should deliver approximately 3.1 m of head, 60 l/min of volumetric flow rate, and should operate at 3020 rpm at its design point. According to Eq. (1.1), the pump has a specific speed of 0.78 with these design values. Although the blades with $N_s < 0.57$ and $Q < 140$ l/s are better to be designed with double curvature according to Lazarkiewicz [27], it is difficult to manufacture this type of blades for dishwasher pumps having much smaller dimensions compared to other industrial applications. Moreover, flow rates are much less than 140 l/s (around 1 l/s). As a result, a single curvature blade is sufficient for this application.

The pump operates between 15°C and 70°C. Thus, the structure should bear this temperature difference. Moreover, the water contains food soils, detergent, rinsing aid and such chemicals. So, the pump should maintain its performance stability under these conditions.

Due to increasing environmental consciousness and high level of competition between brands, one of the most important targets is to decrease water consumption as much as possible. Hence, it is important for the pump to be designed to overcome the risk of air entrainment. If the pump sucks air bubbles, outlet pressure starts to pulsate resulting in severe loss of flow supply to the spray arms of the dishwasher. Furthermore, the pump will mechanically be damaged after some time just like in cavitation case.

There are geometric restrictions due to dense structural design of dishwasher. This affects not only the dimensions of the pump, but also the flow conditions. For example, there are sudden elbows which should actually be avoided for smooth

guidance. Thus, geometrical restrictions of the other parts affecting inlet and outlet of the pump should be considered during the design approach.

For the aforementioned conditions, theoretical methods are to be supported with experimental background of the factory. By doing so, real operating conditions are better simulated.

2.2 Design of Hydraulic Parts

There are two main hydraulic parts of centrifugal pumps: impeller and volute (or diffuser) as stated in Chapter 1. In this study, a volute type pump is to be designed. There are several methods for designing this type of pumps in literature. Although they constitute a base for the design, they should be manipulated so as to fulfill the exact demands since the theoretical methods are somehow generalized. There are mainly three types of methods: semi-empirical, direct, and inverse, [6]. In the case of semi-empirical methods, geometry and performance of the pump is predicted by means of basic flow equations supported with experimental correlations. At the beginning of the design, a specific speed value is chosen, which fixes the pump type and efficiency. In this method, 1-D mean line method, which is based on streamline theory and ideal fluid theory, is used. In this case, secondary motions are neglected, and the method gives an insight about the performance up to a few percent accuracy. In "Direct method", on the other hand, the geometry of the pump is prescribed first. Then the flow field is predicted. The third method, "Inverse method", is based on numerical iterations. Pressure distribution is the input of this method. At the end, the geometry which provides the prescribed pressure distribution is obtained. This method is mostly used in special cases, such as where cavitation is of high-importance.

In this study, semi-empirical methods, which is the most suitable one for dishwasher application, is to be used. There are several methods introduced in the literature. Some of them are the methods of Pfleiderer, Gülich, Stepanoff, Lazarkiewicz, and so on. A good design may synthesize all of those methods, and may be optimized by self-experimental background of the application area. Throughout the design stage, Gülich's design methodology and nomenclature is taken as base; on the other hand, some modifications and additions are made using other sources where it is needed.

2.2.1 Design of Impeller

Impeller is the most critical part in a pump since it is the dynamic part and the major energy gain is obtained here. Therefore, it is the first component to be designed. Then the volute design starts using the outputs of the impeller design.

Impeller design starts with selection of the specific speed. Gülich uses a different specific speed than the non-dimensional one. It is stated to be common in Europe and is indicated as follows, [6]:

$$n_q = n \frac{\sqrt{Q_{opt}/f_q}}{H_{opt}^{0.75}} = N_s * 52.9 \quad (2.1)$$

where n is in rpm, Q_{opt} is the operating flow rate in m^3/s , f_q is the number of impeller entries (number of stage), and H_{opt} is the operating head in m. This expression may also be obtained by multiplying the non-dimensional specific speed, N_s , by the constant shown in Eq. (2.1). In this study, a single-stage pump is designed which makes $f_q=1$.

There are some points to be obeyed in order to have an efficient design. Among them, the suitable ones for this study can be listed as follows, [6]:

- Considering that the design is made according to the best efficiency point (BEP), the pump should operate within $0.8 < Q_R/Q_{opt} < 1.1$, Q_R being the actual (or rated) operating point.
- Cavitation characteristics should be considered while defining the maximum flow rate, Q_{max}
- Again considering the cavitation, the suction conditions may be of high importance in many designs
- Stability of Q-H curves is demanded in many cases, which is "the higher the head, the lower the flow rate" condition is obtained continuously.
- The operation of the pump must be in the planned range, noise and vibrations must be limited, and damage must be avoided considering cavitation characteristics.
- The head coefficient is generally chosen near the upper limit when pump size and cost is critical.
- To have a higher and healthier operation life, excitation forces and pressure pulsations must be kept in allowable range.

There are basically three calculation models for impeller design: Cascade model, channel model, and airfoil model. As the name implies, impeller and diffuser are considered as cascades. In this model, velocity vectors, incidences and the slip conditions are the main parameters. In the channel model, on the other hand, impeller and diffuser are sliced into cross-sections along the stream. Instead of vectorial velocity concept, velocity magnitudes according to continuity equation are of interest. Different from the former two, airfoil model is applied when widely-spaced blades are to be designed, [6]. In this study, cascade and channel models are combined in order to obtain the desired flow path to the best extend.

Having mentioned some key points, the design procedure may be covered starting from here. The radial impeller to be designed has the form shown in Figure 2.1:

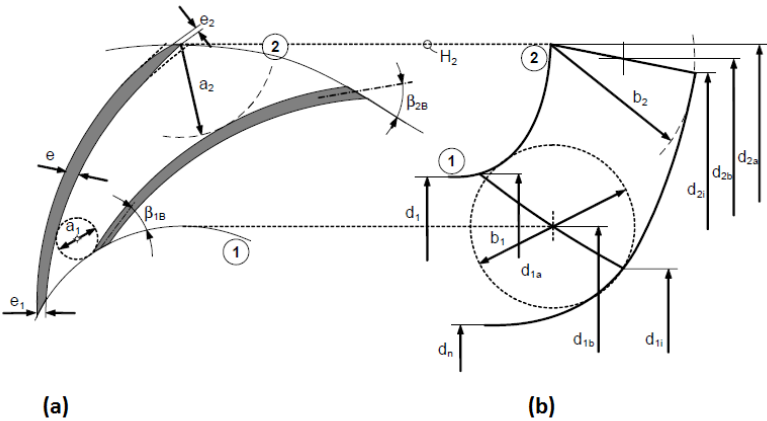


Figure 2.1- Geometric profile and dimensions of the radial impeller (a) plan view, (b) meridional view, [6]

The design starts with determining the boundary conditions of the operation (n , H_{opt} , and Q_{opt}). This will give the specific speed, n_q , of the pump according to Eq. (2.1). It should be noticed that the operation point should be chosen as the *BEP* bewareing that the actual pump may operate at some distance from this point.

Upon getting the specific speed, hydraulic and volumetric efficiencies are assumed. The hydraulic efficiency directly affects the head of the pump; thus, considering the reduction in head, a conservative efficiency should be selected. Since there is leakage in the impeller through the gap between impeller and volute, the volumetric efficiency of the pump should be considered. There are several experimental charts for those efficiencies. Other than empirical values, there are also some rules of thumb used in literature for an initial value of the efficiency. The minimum flow rate is

limited to 0.005 m³/s in Centrifugal Pumps of Gülich, [6]. Since this is larger than that of the design of this study, different sources are used for determining the efficiencies. It is proper to choose volumetric efficiency between 0.90-0.95 for an initial approach [28]. Baysal (1975, p.22) tabulates hydraulic efficiency with respect to specific speed regardless of flow rate, [29]. The plotted version of the data (with the proper conversion of specific speed to n_q as used in this study) is presented in Figure 2.2:

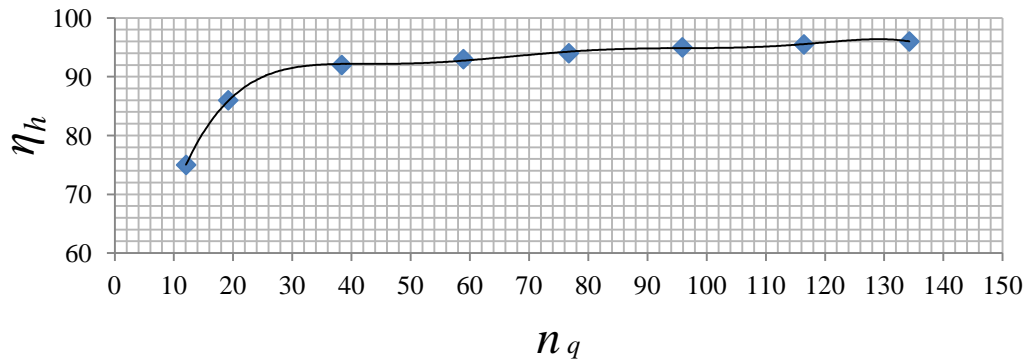


Figure 2.2- Hydraulic efficiency vs. specific speed, [29]

After assuming the efficiency values, shaft diameter which endures the torque safely is calculated. In order to do this calculation, the material and the allowable stress should be decided. The remaining parameters are obtained from already decided boundary conditions. Eq. (2.2) is used for the shaft diameter, [6]:

$$d_w = 3.65 \left(\frac{P_{max}}{n \tau_{al}} \right)^{\frac{1}{3}} \quad (2.2)$$

where d_w is in m, P_{max} is in W, n is in rpm, and τ_{al} in N/m². It is wise to choose a larger value of shaft diameter than the calculated one to handle other factors than the transmitted torque. Hub diameter of the impeller can be chosen as (1.3-1.4)x d_w considering the manufacturing, [8].

In order to get the outer diameter, d_2 , the pressure coefficient is calculated. Figure 2.3 may be used to find the pressure coefficient as a function of specific speed:

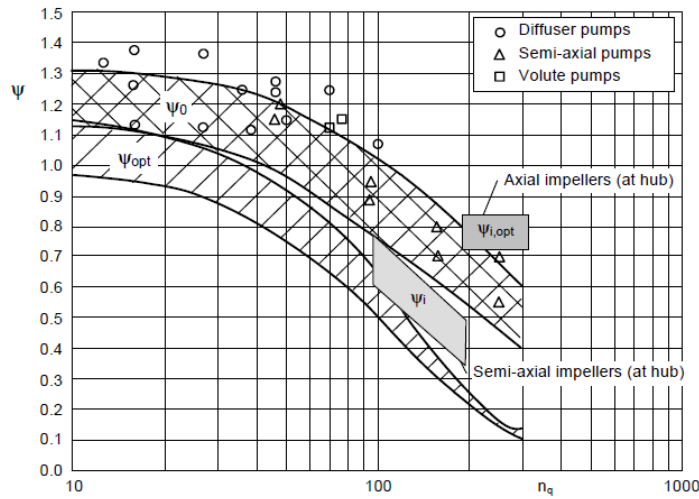


Figure 2.3- Pressure coefficients, [6]

Despite it is stated above that the pressure coefficient is selected near the upper limit for the cost and size considerations, it increases instability of the $Q-H$ curve due to flat characteristics. It means that, the lower limits of the pressure coefficients are better for steeper $Q-H$ curves. Thus, it is an optimization problem depending on the application and restrictions. After a suitable pressure coefficient is obtained, it is possible to calculate the outer diameter as:

$$d_2 = \frac{84.6}{n} \sqrt{\frac{H_{opt}}{\psi_{opt}}} \quad (2.3)$$

where n is in rpm, and H_{opt} is in m, resulting d_2 in m. It is the outer diameter which plays an important and pioneer role on the head of the pump. It should be taken 10% greater than the calculated value according to Eq. (2.3) in case of that the required head may not be achieved due to losses. If the manufactured impeller can supply higher head values than the design value, trimming can be applied, [29].

Number of blades is another parameter which is highly important. There are several ways to choose or calculate the number of blades in literature. There is a general consideration which brings a need for optimization: If the number of blades is low, there is less frictional loss and less blockage; nonetheless, the flow is more prone to separation. In the case of higher number of blades, there is more frictional loss and blockage; however, the flow is better guided.

Some methods for the selection of blade number consider vibration and noise characteristics, some others consider blade loading and its effects. When the stability is considered, eight or more blades should be avoided. If the head per stage is higher

than 100 m, less than five blades should be avoided since it would result in highly non-uniform flow and pressure pulsations. Combining all these criteria, a narrower range of choice (5 to 7 blades) emerges for $10 < n_q < 120$, [6].

A study conducted by Liu et al (2010), [30], provides one with an insight for preliminary design. The study covers the effect of number of blades on head capacity, efficiency, and $NPSH_R$ versus flow-rate. Moreover, the participants interpret phenomena occurring within the blade passages and within the diffuser. There are both numerical experimentation (CFD) and laboratory experimentation results which strengthen the argument.

In the study, only the blade number of the impeller is changed while all other parameters are kept constant. As a result, the effects only caused by the number of blades may be seen.

The tests are made for number of blades 4, 5, 6, and 7, where the model pump has an impeller of 5-blade. At the end of the study, it is seen that CFD results and experimental results are in good agreement. For different parameters of concern, different blade numbers show better performance; meaning there is not a unique number making all the outputs superior. As a result, an optimum number of blades is chosen.

As the number of blades increase, static pressure generated within the pump also increases without any exception. On the other hand, the pressure at the suction side of the inlet decreases with increasing number of blades resulting in an increase in the risk of cavitation.

Uniformity of pressure distribution is also affected by blade number. Increasing the number worsens the pressure uniformity at screw section, but betters that at diffuser section.

An important phenomenon occurring through the blades is the “jet-wake” interaction. This may be explained as mixing of “jet” stream at pressure side and “wake” stream at suction side. The study shows that, the increase in the blade number enhances jet-wake characteristics, in other words, jet-wake mixture loss reduces.

Efficiency of the pump does not exhibit an ordered change with respect to blade number. Odd number of blades gives higher efficiencies than those of even-numbered ones.

When all categories are investigated, the results shown in Table 2.1 are reached under design conditions:

Table 2.1- Results of the study on the effects of blade number on pump performance, [30]

Blade number <i>Z</i>	Head <i>H</i> /m	Efficiency η /%	NPSHR H_{RNPS} /m
4	27.51	74.07	4.04
5	30.38	75.63	3.68
6	30.54	74.20	4.66
7	32.91	77.45	4.95

Considering all the results, the following deductions may be made: Best efficient blade numbers: 7, 5; best cavitation characteristics: 5, 4

Although 7-blade impeller gives the highest head and best jet-wake distribution, cavitation limits the preferences. Thus, having relatively higher efficiency and the best cavitation characteristics. 5-blade impeller is the most optimum one for the application, [30].

It should be noted that, the above study just bears a torch to the issue. Thus, the number of blades should be selected depending on the operation conditions; that is, whether performance or cavitation is more critical should be considered.

Eq. (2.4) may also be used to calculate the blade number, but it is an iterative approach due to including yet unknowns, [28]:

$$z_{La} = k_z \frac{d_2 + d_1}{d_2 - d_1} \sin\left(\frac{\beta_{1B} + \beta_{2B}}{2}\right) \quad (2.4)$$

where k is a coefficient depending on the material, d 's are in m, and β 's are in radians.

When inlet diameter is considered, there are more than one way to calculate it. The selection again depends on the application and operational conditions. For example, if a suction impeller is to be designed, a selected suction specific speed is the design

initiator. If cavitation is critical, design methods with $NPSH_R$ or $NPSH_i$. In this study, inlet diameter calculation for minimum inlet relative velocity is made which is appropriate for minimum leakage, friction and shock losses. Eq. (2.5) is used in this case, [6]:

$$d_1^* = f_{d1} \sqrt{d_n^{*2} + 1.48 \times 10^{-3} \psi_{opt} \frac{n_q^{1.33}}{(\eta_V \delta_r)^{0.67}}} \quad (2.5)$$

where $\delta_r = 1 - \frac{c_{1m}}{u_{1m} \tan \alpha_1}$ and f_{d1} is a coefficient between 1.15 and 1.05 for n_q between 15 and 40 for normal impellers. Since "no inlet-whirl" assumption is made throughout the design, the most-right term drops, leaving δ_r as 1.

At the inner streamline, the blade inlet diameter may be different than the nominal inlet diameter. This is limited by the mounting of the blade and the stability of Q-H curve. Thus, the optimum value should be kept. For the case covered in this study, the impeller is relatively small resulting in closer values of inlet diameters from inner to outer streamlines.

The inlet velocity triangle can be established upon determining the diameter of the impeller inlet. There are some parameters to be calculated in order to achieve this. Once the velocity triangle is set, the blade angle at the inlet can be calculated by adding an incidence value of 0° to 4° to the flow angle. The less the incidence, the lower the risk of cavitation. While calculating the flow angle, it is important to consider the effect of blockage due to blade thickness. It plays an important role since reduction in the flow passage area due to finite number of blades causes an accelerated flow through the blades. As seen from Eq's (2.8) and (2.9), the blockage term includes blade angle, and flow angle includes blockage; thus, an iterative process is applied to calculate both, [6]. The steps for the calculation of inlet blade angle are as follows:

$$u_1 = \pi d_1 n / 60 \quad \text{circumferential speed} \quad (2.6)$$

$$c_{1m} = \frac{Q_{La}}{A_1} \quad \text{meridional component of the absolute velocity} \quad (2.7)$$

$$\tau_1 = \left(1 - \frac{z_{La} e_1}{\pi d_1 \sin \beta_{1B} \sin \lambda_{La}}\right)^{-1} \quad \text{blade blockage} \quad (2.8)$$

$$\beta'_1 = \arctan \frac{c_{1m} \tau_1}{u_1 - c_{1u}} \quad \text{flow angle} \quad (2.9)$$

In these expressions, Q_{La} is the total flow rate through the impeller, $A_1 = \frac{\pi}{4}(d_1^2 - d_n^2)$, which is the area between the eye and the hub of the impeller. c_{1u} is zero due to no inlet-whirl assumption. λ_{La} is the angle between the blade and the shroud, and taken as 90° for single-curvature blades. e_1 is the inlet blade thickness, and usually chosen to lay in $(0.016 \text{ to } 0.022) \times d_2$. Upon calculating Eq. (2.9), inlet blade angle can be found by adding the incidence.

Together with the blade number and the blade outlet angle, the blade outlet width is an important parameter which determines the required head of the pump. Despite the fact that the larger the width the higher and the more stable the head, flow separation should be avoided. This means that, the outlet blade width should be kept in an optimum range. Maintaining $b_2 < b_1$, empirical data may be used to calculate the blade outlet width. Figure 2.4 illustrates an empirical approach. It is wise to select b_2^* closer to the lower limit in order to be safe in terms of turbulent losses, [6]:

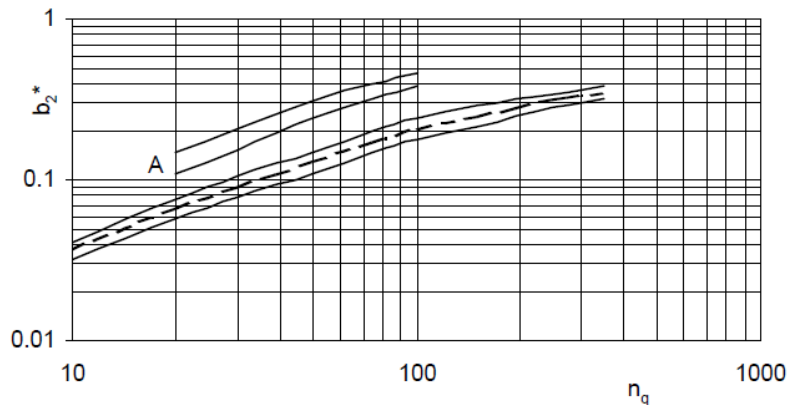


Figure 2.4- Non-dimensional blade outlet width vs. specific speed ("A" for sewage pumps), [6]

The head demanded for the design requires the determination of the blade outlet angle as well. In this case there is one more factor than the blockage which affects the outlet angle: the slip factor. It is the finite number of blades that causes friction losses in a real impeller. As a result of this phenomenon, slip losses merge resulting in reduced outlet flow angle. Then, circumferential component of the absolute

velocity, thus the rated head decreases, [5]. As a result, designers should consider this effect and choose a larger blade angle than that of ideal case. Including both slip and blockage effects, typical centrifugal pumps have outlet blade angles between 15° to 90°. However, it is hardly encountered to use outlet blade angle larger than 40° if the working fluid is water, [28]. In many cases, 20° to 27° are used. If the specific speed is above 60, the outlet blade angle should vary from the inner streamline to the outer, [6]. The governing equations for the outlet blade angle are as follows:

$$u_2 = \pi d_2 n / 60 \quad \text{circumferential speed} \quad (2.10)$$

$$c_{2m} = Q_{La} / A_2 \quad \text{meridional component of the absolute velocity} \quad (2.11)$$

$$A_2 = \pi d_2 b_2 \quad \text{outlet passage area (without blockage)} \quad (2.12)$$

$$\tau_2 = \left(1 - \frac{z_{La} e_2}{\pi d_2 \sin \beta_{2B} \sin \lambda_{La}} \right)^{-1} \quad \text{blade blockage} \quad (2.13)$$

influence factors of inlet diameter on slip:

$$\epsilon_{Lim} = \exp\left(-\frac{8.16 \sin \beta_{2B}}{z_{La}}\right) \quad (2.14)$$

$$k_w = \begin{cases} 1 - \left(\frac{d_{1m}^* - \epsilon_{Lim}}{1 - \epsilon_{Lim}} \right)^3, & d_{1m}^* \geq \epsilon_{Lim} \\ 1, & \text{otherwise} \end{cases} \quad (2.15)$$

$$\gamma = f_1 \left(1 - \frac{\sqrt{\sin \beta_{2B}}}{z_{La}^{0.7}} \right) k_w \quad \text{slip factor for } z_{La} > 2 \text{ with } f_1 = 0.98 \text{ for radial pumps} \quad (2.16)$$

$$c_{2u} = u_2 \left(\gamma - \frac{c_{2m} \tau_2}{u_2 \tan \beta_{2B}} \right) \quad \text{circumferential component of absolute velocity (prediction)} \quad (2.17)$$

$$c_2 = \sqrt{c_{2m}^2 + c_{2u}^2} \quad \text{absolute velocity} \quad (2.18)$$

relative velocity components:

$$w_{2u} = u_2 - c_{2u} \quad (2.19)$$

$$w_2 = \sqrt{c_{2m}^2 + w_{2u}^2} \quad (2.20)$$

$$\beta_2' = \arctan \frac{c_{2m} \tau_2}{w_{2u}} \quad \text{relative outlet angle with blockage} \quad (2.21)$$

$$\delta' = \beta_{2B} - \beta_2' \quad \text{deviation angle with blockage} \quad (2.22)$$

δ' is selected between 10° and 14°

In Eq.(2.13), the outlet blade thickness may be selected within $(0.016 \text{ to } 0.022) \times d_2$ as in the case of inlet blade thickness; moreover, they can be of the same size.

All the these parameters constitute the inlet and outlet velocity triangles. They can be represented together with other descriptive dimensions as follows:

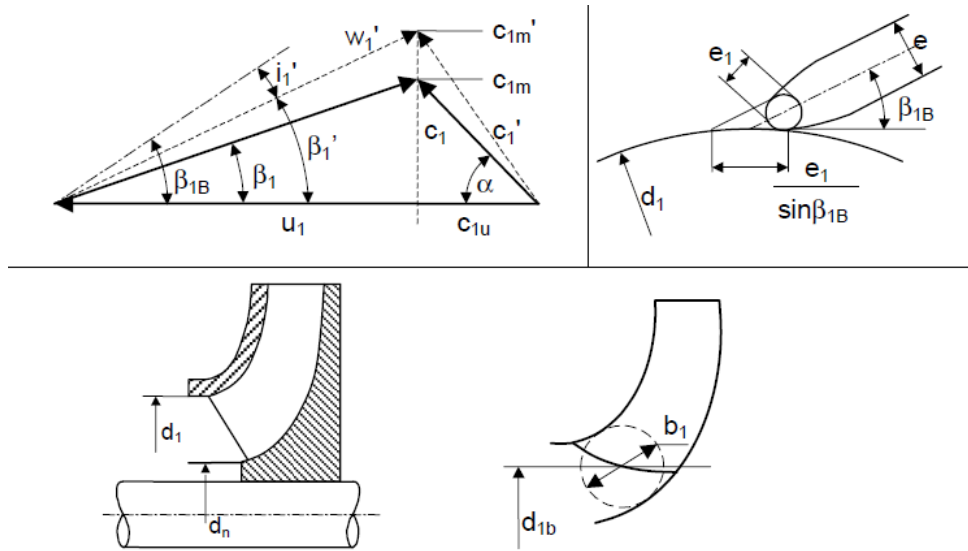


Figure 2.5- Inlet velocity triangle and geometric parameters, [6]

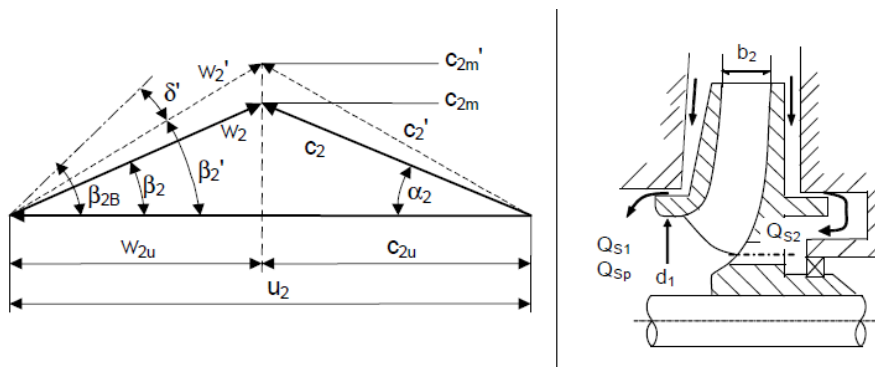


Figure 2.6- Outlet velocity triangle and geometric parameters, [6]

Before proceeding into drawing of the impeller, a last modifying step may be applied to leading and trailing edges of the blade. In order to prevent uneven pressure distributions, strong low pressure peaks, cavitation, and deficiency, an effective leading edge profile should be used. Gülich (2010, p. 347) covers three shapes: semi-circle, elliptic, and wedge-like. Semi-circular leading edges are only suitable for small pumps with low demands. For acceptable pressure distributions, elliptical

profile is preferable, [6]. Only if shock-less entry is needed, wedge-like shaped blade leading edge may be used. The shapes are represented in Figure 2.7:

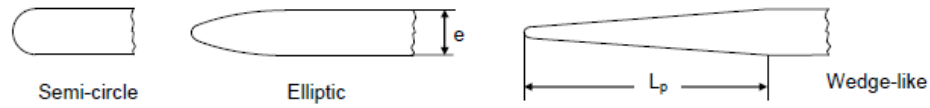


Figure 2.7- Impeller blade leading edge profiles, [6]

There are two options for determining the shape of the trailing edge. The first one as a super group is profiling the edge (symmetrical profiling, under-filing, or over-filing). This is helpful for reducing the wake width, turbulent dissipation losses and pressure pulsations. The other option is not to profile the edge. The idea behind this is that after manufacturing the impeller, there may be head deficit. In order to eliminate this risk, there should be a chance to under-file the trailing edge. Thus, profiling this edge may be postponed to performance test rather than doing it in the design stage, [6].

Having obtained all the necessary geometrical data, drawing of the blades may be conducted. It should be noted that, since a single curvature blade is designed in this study, the drawing methods are covered for this type only. There are basically two methods: circular arc method and point-by-point method. The former one needs only one or two circles to define the blade shape, [27]. The latter one; on the other hand, uses the variation of β_B along the radius of the blade. This method is introduced by Pfleiderer, and is more sensitive since discrete data is used, [28]. If the pump, so the impeller, is small, circular arc is sufficient and less effort-consuming.

Circular arc method, as stated above, is simpler than point-by-point method, and gives acceptable results for smaller impellers. In this method, inlet and outlet diameters of the impeller, inlet and outlet blade angles and number of blades are the main parameters to be used in drawing. The two types of this method are "single-arc method" and "double-arc method". As their names imply, the blade has a single radius of curvature in single-arc method, and double radius of curvature in double-arc method. When size of the impeller is increased, use of "double-arc" method is more appropriate.

In single-arc method, circles with d_1 and d_2 are drawn first. Then, an arbitrary point K is selected on the inner circle and connected to the center point O. A straight line

\overline{FM}_1 , and the length of this line is set to a value $d_2/2$. The point of intersection of the perpendicular bisector of \overline{GO} and \overline{FM}_1 is point M_2 . The second arc of the blade is centered at point M_2 and passes from point F and the circle with diameter d_2 . The shape of blade with 2 radii of curvature is obtained. Again an offset of the blade thickness is given, and the remaining blades are patterned as done in single-arc method, [29]. This procedure may be represented as shown in Figure 2.9:

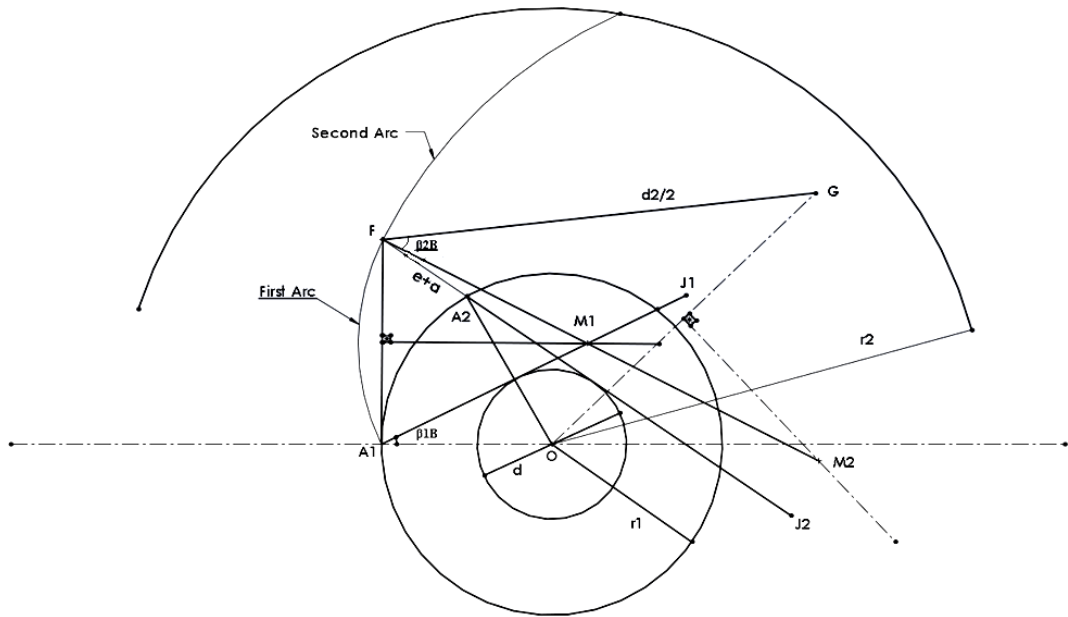


Figure 2.9- Drawing of a single blade by Double-arc method

In point-by-point method, the blade is sliced into small elements. The idea behind the method is to find the variation of β_B as a function of radius. The boundary conditions are the known inlet and outlet blade angles. For each change of Δr , a different β is obtained. At the end, these points are smoothly combined by a spline. Although this is a pure integration method (with dummy variable dr), it can be converted into a summation function in practice. An arbitrary point A is selected on the circle having a diameter d_1 . Another arbitrary point P is set at an arbitrary distance r from the center point O . The angle between \overline{OA} and \overline{OP} is ϕ and called the central angle. The value of this angle is found by the following procedure: The radius r increases by an amount of dr as ϕ increases by $d\phi$, At the same time, a new point P' is set on the blade at $r+dr$. The projection of point P on the new radius line of $r+dr$ is point T and \overline{PT} is perpendicular to dr . From trigonometry:

$$\overline{PT} = r\phi = \frac{\overline{P'T}}{\tan\beta} \quad (2.23)$$

From this equation, defining $\overline{P'T} = dr$:

$$rd\phi = \frac{dr}{\tan \beta} \quad \text{or} \quad d\phi = \frac{dr}{r \tan \beta} \quad (2.24)$$

Integrating Eq. (2.24) between r_1 and r with a multiplier $180/\pi$ gives the local value of ϕ at any r in degrees:

$$\phi^\circ = \frac{180}{\pi} \int_{r_1}^r \frac{dr}{r \tan \beta} \quad (2.25)$$

As stated above, converting Eq. (2.25) into a summation is more common in practice since it enables tabular representation. In this case:

$$\phi^\circ = \frac{180}{\pi} \sum_{r_1}^r \frac{\Delta r}{r \tan \beta} \quad (2.26)$$

In point-by-point method, both ϕ and β seem to be unknown. However, there is an assumption that the variation of β with r is known. Thus, the only unknown is the central angle ϕ . In another case, which is more common especially for water pumps, it is assumed that the variation of relative velocity w with r is known between the boundary conditions w_1 and w_2 . In this case, the variation in β can indirectly be calculated. As a result, there is again only one unknown variable, ϕ , [28]. The construction of the method can be illustrated as shown in Figure 2.10:

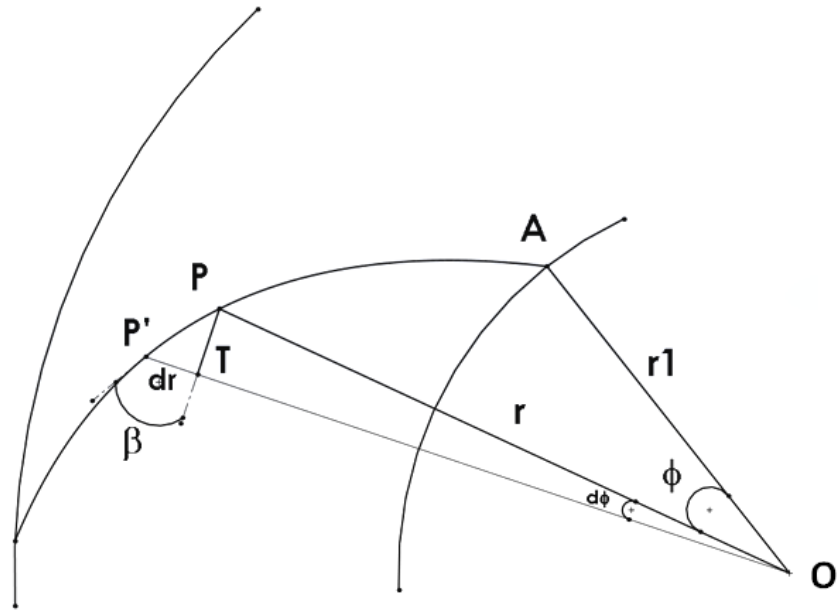


Figure 2.10- Drawing of a single blade by Point-by-point method

Up to here, plan view of the blades is covered. In order to completely define the shape of an impeller, radial view of it should be obtained. There are different methods for this in literature. One of the simplest models is used in this study since a relatively small impeller is designed. Accordingly, the bounding lines which represent the axis of rotation, shaft diameter, hub diameter, average inlet diameter, average outlet diameter parallel to each other. An arbitrary point O on the line representing the inlet diameter is chosen. A circle of diameter b_1 is drawn its center being at point O. A perpendicular line from the point of intersection of this circle to the line at r_2 is drawn which constructs the lower cover of the impeller. The end point is labeled as point B. A distance of b_2 from point B is traveled to point C. An arc passing from point C and tangent to the circle with diameter b_1 is drawn. The lower limit of this arc is the tip diameter. The inner, the mid-section, and the outer streamlines of the blade inlet are connected to each other, constructing the blade inlet edge. As the skeleton of the radial blade section is obtained, proper thicknesses and shapes are given to the drawing depending on the application and volute size, [29]. The radial view can be illustrated as shown in Figure 2.11:

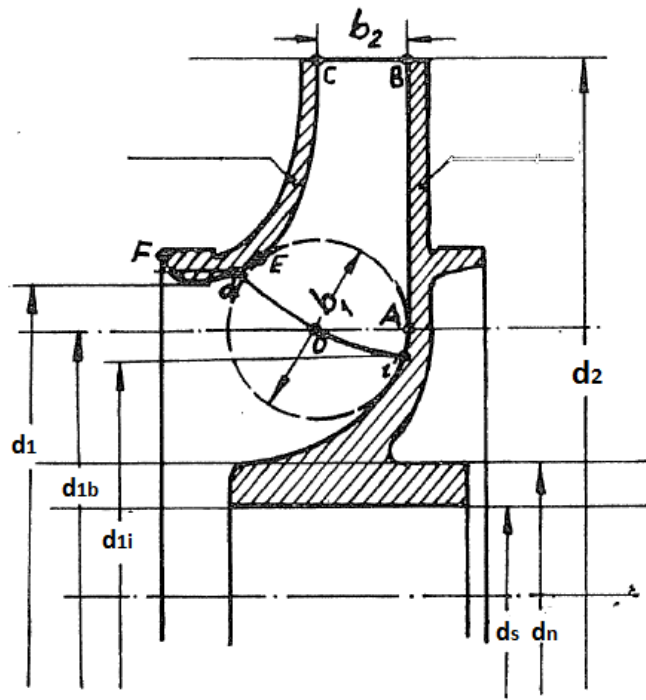


Figure 2.11- Drawing of the radial view of the impeller

At the end of aforementioned procedures, the draft drawing is completed; however, there are some parameters which should be controlled whether they fulfill some necessary specifications or not. The parameters to be controlled may be listed as: channel cross-section between successive blades, cone angle between successive blades, and minimum blade surface, [29].

Channel cross-section should satisfy that the relative velocity throughout the blade is linearly changing. The method for examining this can be explained as follows: The streamline between the centers of the circles of inlet channel breadth (a_1) and outlet channel breadth (a_5) is drawn. Development of that streamline is moved to abscissa, and $(a_x b_x)$ product is moved to ordinate with rectangular cross-section assumption. The connecting curve of the points on the plot should be pure-linear. Otherwise, blade width values should be manipulated to satisfy this rule, not making any change in channel breadth values. Figure 2.12 illustrates the method:

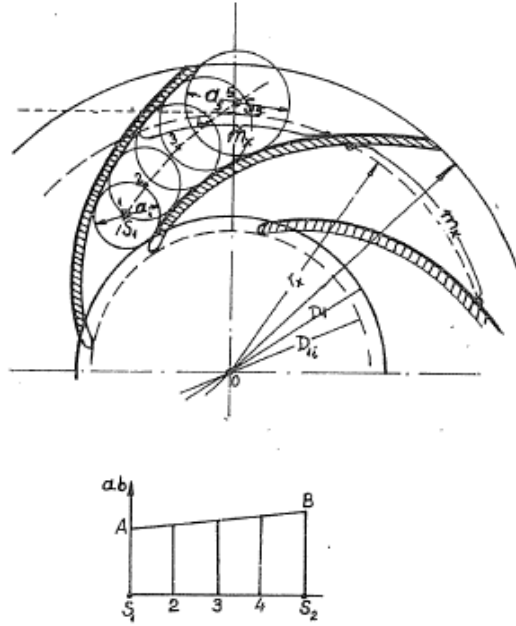


Figure 2.12- Channel cross-section between successive blades, [29]

The last control is made on the blade surface as stated above. In order to get the desired pump head with a sufficient hydraulic efficiency, the blades should possess a minimum surface area per unit blade. This is represented as the product of blade number and blade length. Kovats (1971, pp. 142-146) introduced a method for this issue. According to this method, approximate blade length is calculated first:

$$l = \frac{d_2 - d_1}{2 \sin\left(\frac{\beta_{1B} + \beta_{2B}}{2}\right)} \quad (2.26)$$

Then, mean pitch (t/l), circulation (Γ) at inlet and outlet, and vectorial average of inlet and outlet relative velocities (w_∞) are calculated as:

$$\frac{t}{l} = \frac{\pi(d_1 + d_2)}{2 z_{1a} l} \quad (2.27)$$

$$\tan \beta_\infty = \frac{2 c_{m2}}{u_1 + u_2 - c_{u2}} \quad (2.28)$$

$$w_\infty = \frac{u_1 + u_2 + c_{u2}}{\cos \beta_\infty} \quad (2.29)$$

$$\Gamma_2 = \pi d_2 c_{u2} \text{ and } \Gamma_1 = \pi d_1 c_{u1} \quad (\text{equals to zero for no inlet whirl}) \quad (2.30)$$

Referring to Weinig diagram in Figure 2.13, lift coefficient (ξ_p'/ξ_p) is obtained by using blade mean angle and mean pitch. After getting that parameter, the minimum blade surface area is calculated from Eq. (2.31) for no inlet whirl assumption:

$$(z_{la}l)_{min} = \frac{2\Gamma_2}{1.5 W_\infty \xi_p'/\xi_p} \tag{2.31}$$

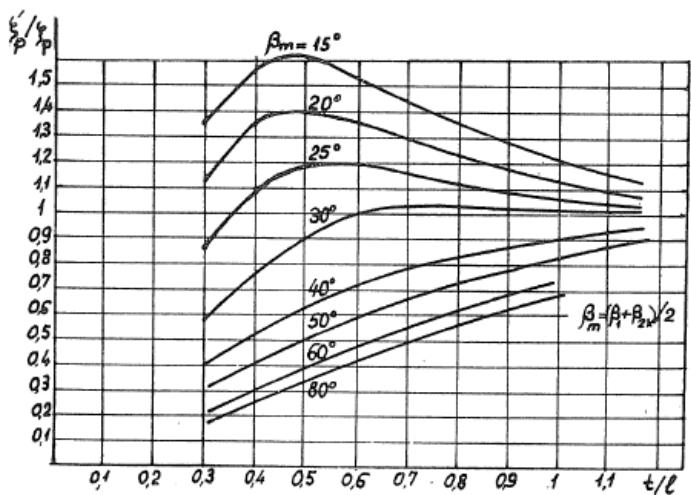


Figure 2.13- Weinig diagram for moving circular cascade, [31]

At the end of this procedure, real ($z_{la} l$) value should be above the calculated minimum value. If this is not satisfied, blade angles at inlet and outlet should be reduced to increase blade length, or number of blade should be increased, [31]. In single curvature blade profiles, blade length can directly measured in drawing. This, moreover, gives better results than approximate calculation, [29]. Having completed the impeller task, the volute design may now be covered in the following section.

2.2.2 Design of Volute

Volute is a part of a “volute-pump” in which kinetic energy created through the impeller is converted into pressure energy. It has a spiral shape enveloping the impeller. From the starting point to the end point which is at 360°, the cross-sectional area of the volute keeps increasing gradually. At the end of the spiral casing, there is a linearly centered section which is the “discharge opening”. This is the final section of a single stage pump where the liquid is pressurized and travels into the system, [5]. There is an extension at the intersection of the initial section and the discharge nozzle named as “cutwater” or “tongue”. This portion, as the name implies, cuts the

water at a specified camber angle with circumferential direction of the volute and deflects it towards the discharge nozzle, [6].

The volute may be classified mainly into two according to the number of sections: single and double, noting that other types may be derived from double volute, such as twin volute. The former one is much simpler than the latter one in terms of design and manufacturing. Radial thrust is the primary parameter in volute type selection. At off-design conditions, radial forces may threaten the mechanical life of single volutes. Thus, double volutes should be used if bearing loads, shaft stresses and shaft deflection is inevitably high despite high design and manufacturing efforts. In single volutes, the head capacity is limited by specific speed. 120 m of head may be reached for $n_q < 40$ if the working fluid is water, [6]. In this study, the design head is approximately 1/40 of this upper limit for the same specific speed; thus, single volute may be safely applied.

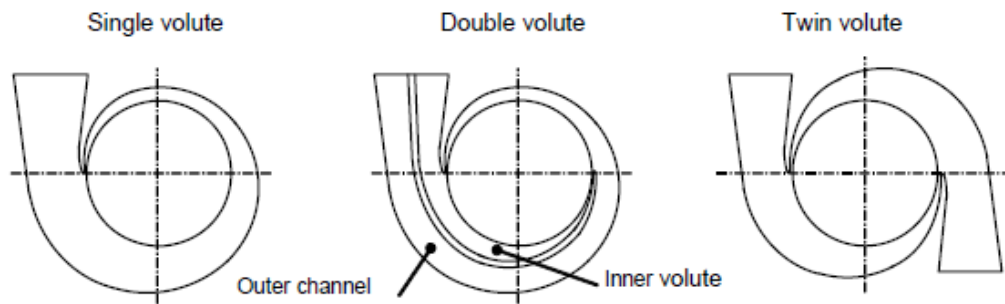


Figure 2.14- Volute casing types

At the beginning of volute design, the first step is to specify the boundary conditions of the flow entering the volute section. Casing design flow rate, Q_{Le} is one of these conditions. This is the total flow rate which includes both discharged flow rate and leakage through the impeller, which depends on the volumetric flow rate of the pump. Considering the leakage, operating flow rate should be used in volute calculations in order to achieve agreement between design and actual best efficiency points, [6].

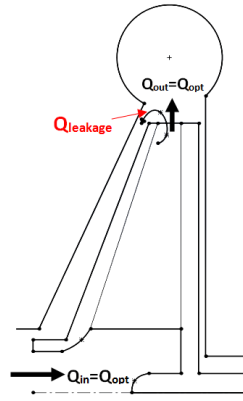


Figure 2.15- Flow rate components through the impeller

In order to keep pressure pulsations and hydraulic excitation forces within allowable limits, there should be a clearance between cutwater and impeller. This distance is represented as the ratio of cutwater diameter to impeller diameter, [6]:

$$d_z^* = \frac{d_z}{d_2} \geq 1.03 + 0.1 \frac{n_q}{n_{q,Ref}} + 0.07 \frac{\rho H_{st}}{\rho_{Ref} H_{ref}} \quad (2.31)$$

where $n_{q,Ref}=40$, $H_{Ref}=1000$ m, $\rho_{Ref}=1000$ kg/m³

Cross-sectional shape of the volute is one of the most important characteristics when mechanical and economic issues are considered. The designer should well analyze stresses to be applied on casing in order to decide the most suitable volute shape. Moreover, the shape should be manufactured as economic as possible considering that the more complex the shape, the more expensive the manufacturing. There are several shapes used in practice depending on the application. Figure 2.16 illustrates some of these shapes:

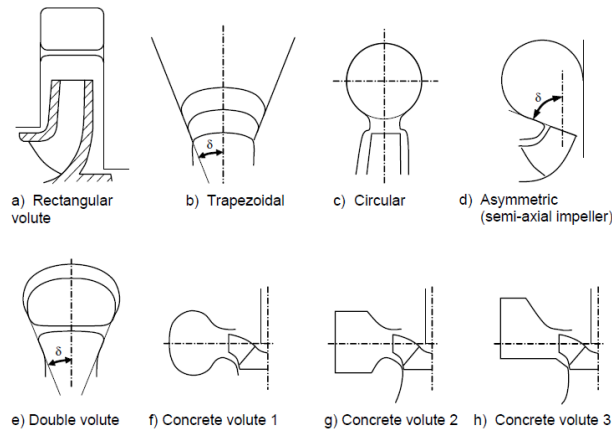


Figure 2.16- Cross-section shapes of volute casings, [6]

Among the shapes shown in Figure 2.16, the most common volute types are rectangular, trapezoidal, circular, and double volute (when needed). In a study conducted by Alemi et al, rectangular, circular and trapezoidal cross-sectioned volutes of the same cross-sectional area are investigated in terms of performance with a common specific speed, [32]:

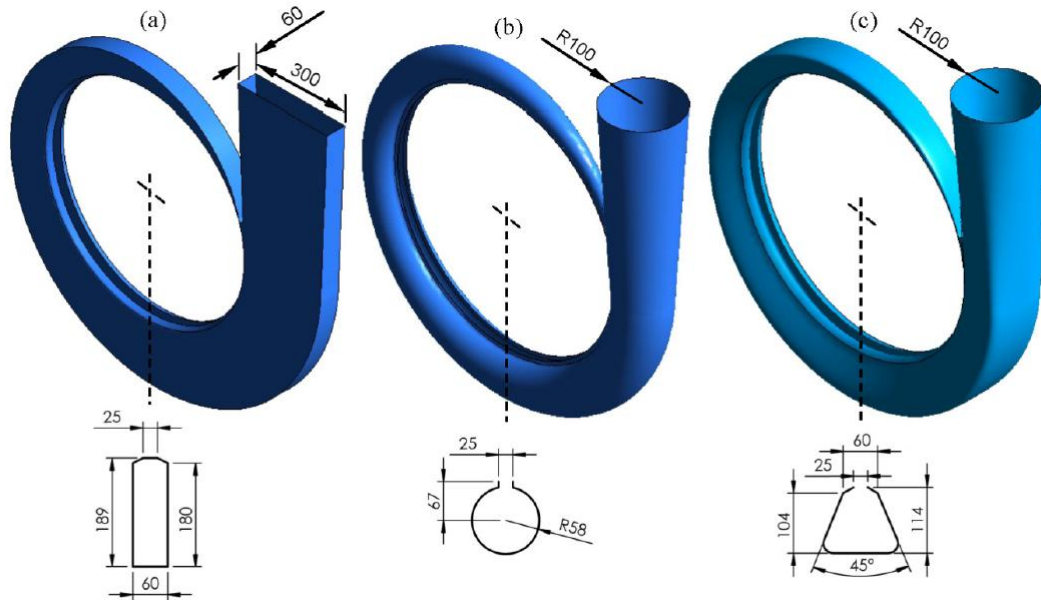


Figure 2.17- Rectangular, circular, and trapezoidal volutes of the same cross-sectional area, [32]

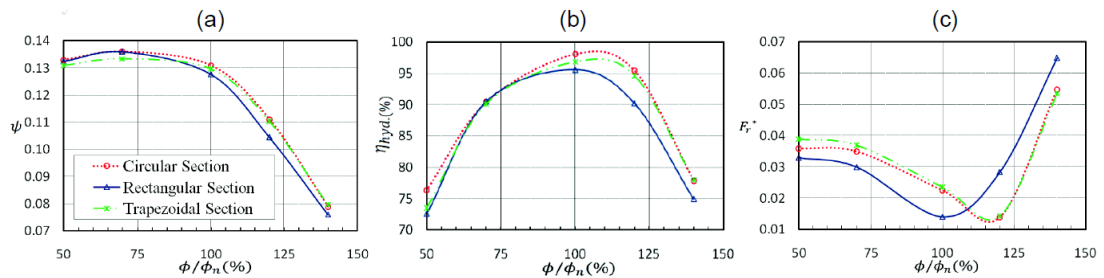


Figure 2.18- CFD analysis results for different cross-section volutes of the same cross-sectional area, (a) Head coefficient, (b) Hydraulic efficiency, (c) Radial force with respect to flow coefficient ratio, [32].

According to the above results, circular cross-section volute has higher head coefficient values at all flow rates; whereas rectangular and trapezoidal cross-section ones change trend at certain flow rates. However, at and above the design flow rate, trapezoidal cross-section volute shows similar performance as the circular one. In terms of hydraulic efficiency, circular cross-section volute is the most efficient among all. The reason that rectangular cross-section volute has worse performance at

and above the design flow rate is that its hydraulic diameter is smaller than the others, so that frictional loss is higher. Below 110% of the design flow rate, rectangular cross-section volute produces lower radial forces. Above that point, circular and trapezoidal cross-section volutes are more preferable. Considering all the cases together, if the pump is to be operated near and below the design flow rate, rectangular cross-section may be used due to lower radial forces. However, if the operation point is above the design flow rate by a certain amount, circular or trapezoidal cross-section volutes are better at head, hydraulic efficiency and radial force characteristics, [32]. In the design of dishwasher circulation pump, the cross-sectional shape is to be trapezoidal. This is due to not only aforementioned performance characteristics, but also the heater unit to be integrated at the top of the volute casing. The integrated heater unit is a flat plate in the majority of its geometry and has only a few sections which are rounded. This shape cannot be changed by the pump designer since its designed by the heater company. As a result, a flatter top plate and a more rounded lower sections restricts the designer to use trapezoidal design, noting that rectangular design is not preferred for the study.

Inlet width, b_3 is chosen such that height to width ratio at the volute inlet is close to 1 in single volutes. Moreover, sufficient side wall gaps between impeller and volute should be kept ensuring that $b_3 > b_2$. Hence, the ratio b_3/b_2 is required to be 2 to 4 for small specific speed pumps. As the specific speed increases, the risk of secondary flow increases as well. For this reason, b_3/b_2 ratio should be chosen smaller, [6].

Cutwater is another highly stressed portion in a volute as it acts like a stationary blade to guide the flow into the discharge nozzle. As a result, the shape of it should be designed so that any damage due to flow is prevented. A rounded leading edge having a diameter, e_3 nearly 1/50 of impeller outlet diameter is suitable for relatively small pumps having single volute. The angle α_{3B} between cutwater and circumferential direction should be selected so that the required guidance is made most effectively. Eq's (2.32) to (2.36) are used to get this camber angle, [6]:

$$c_{3u} = \frac{d_2 c_{2u}}{d_3} \quad \text{circumferential component of absolute velocity at volute inlet} \quad (2.32)$$

where d_3 (volute inner diameter) is obtained by a minimum 2 mm of clearance from the impeller outlet.

$$\tau_3 = \left(1 - \frac{z_{Le} e_3}{\pi d_3 \sin \alpha_{3B} \sin \lambda_{Le}}\right)^{-1} \quad \text{blockage due to cutwater} \quad (2.33)$$

$\lambda_{Le}=90^\circ$ for single curvature blade

$$c'_{3m} = \frac{Q_{Le} \tau_3}{\pi d_3 b_3} \quad \text{meridional component of absolute velocity at volute inlet} \quad (2.34)$$

$$\tan \alpha'_3 = \frac{c'_{3m}}{c_{3u}} \quad \text{flow angle at volute inlet with blockage} \quad (2.35)$$

$$\alpha_{3B} = \alpha'_{3B} + i_3 \quad \text{cutwater camber angle} \quad (2.36)$$

incidence $i_3 = \pm 3^\circ$

Upon shaping the cutwater, the last main parameter of the volute, which is the volute throat area, is to be found. Apart from frictional losses, fluid particles obey the first law of Newton, which is the inertia. As a result, the fluid leaving the impeller tends to keep its angular momentum ($\rho \times Q \times c_{2u} \times r_2$) throughout the volute. Consider Figure 2.19

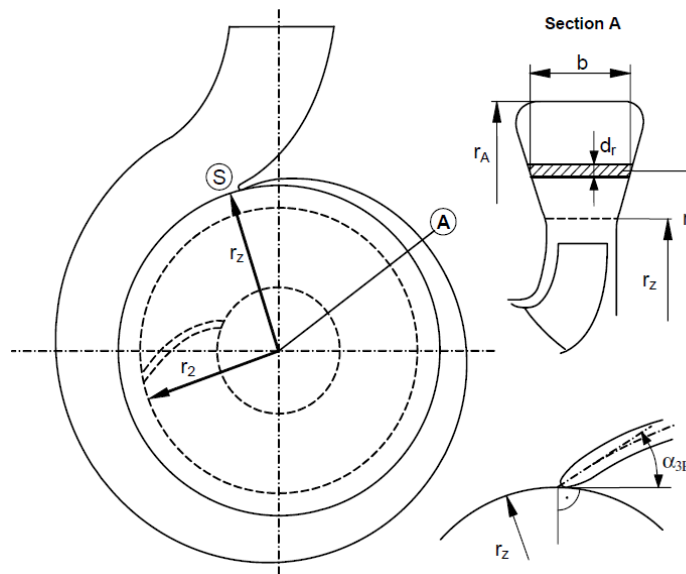


Figure 2.19-Volute casing, [6]

At any section A different from the starting point S, fluid particles flow through the infinitesimal area $dA=b \times dr$ with a circumferential velocity c_u . Due to conservation of angular momentum, $c_{2u} \times r_2 = c_u \times r$ is valid. As a result, the fluid passing through the infinitesimal area element has a differential flow rate $dQ=c_u \times b \times dr=c_{2u} \times r_2/r \times dr$. It is known that Q_{opt} flows within the volute. Hence, the only unknown is the ratio b/r at any section A. In order the flow to obey the conservation of angular momentum, the designer should satisfy Eq. (2.37) equation while evaluating each partial volute throat area, [6]:

$$\int_{r_z}^{r_A} \frac{b}{r} dr = \frac{\epsilon^\circ Q_{opt}}{360^\circ c_{2u} r_2} \quad (2.37)$$

For circular throat area, Eq. (2.37) can be evaluated by Eq's (2.38) and (2.39):

$$X_{sp} = \frac{Q_{Le}}{\pi c_{2u} r_2} \frac{\epsilon_{sp}}{2\pi} \quad \epsilon_{sp} = 2\pi \text{ for single volutes} \quad (2.38)$$

$$d_{3q} = X_{sp} + \sqrt{2d'_z X_{sp}} \quad A_{3q} = \frac{\pi d_{3q}^2}{4} \quad \text{throat area for circular cross-section volute} \quad (2.39)$$

Having obtained all the necessary geometrical parameters, the volute may be designed according to either constant angular momentum method introduced by Pfleiderer, or constant velocity method introduced by Stepanoff. The theory behind the conservation of angular momentum method is introduced above. Since there is not a single analytical expression for the entire volute shape, the cross-sections of it is partially designed in such a way that the circumferential angle of the volute is calculated satisfying the momentum conservation.

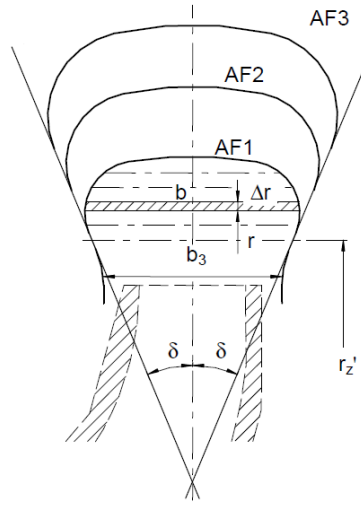


Figure 2.20- Meridional section of volute

$$\epsilon = 360^\circ \frac{c_{2u} r_2}{Q_{Le}} \int_{r'_z}^{r_A} \frac{b}{r} dr = 360^\circ \frac{c_{2u} r_2}{Q_{Le}} \sum_{r'_z}^{r_A} \frac{b}{r} \Delta r \quad (2.40)$$

The right-most hand side of Eq. (2.40) is used when the calculation is done manually. Using δ , r'_z and b_3 , the boundaries of surfaces of revolution are defined first. For a number of cross-sections, AF's, the height is estimated from Eq. (2.39). Then all the cross-sections are sliced into infinitesimal elements of $\Delta r \times b$. For each cross-section,

these parameters are tabulated to evaluate Eq. (2.40). At the end of this procedure, a volute which satisfies the conservation of momentum is obtained, [6].

In the method of constant velocity, throat area is calculated in the same way as in the previous method in order not to deviate from the best efficiency point. Assuming that $c_{3q} = Q_{Le}/A_{3q}$ is constant throughout the volute, area at any wrap angle of the volute may be evaluated as:

$$A(\epsilon) = \frac{Q(\epsilon)}{c_{3q}} = \frac{Q_{Le}}{c_{3q}} \frac{\epsilon}{\epsilon_{sp}} = A_{3q} \frac{\epsilon}{\epsilon_{sp}} \quad (2.41)$$

The efficiencies of both methods are similar to each other. However, for smaller specific speeds, the constant velocity method is more efficient due to lower frictional loss. On the other hand, the other method is better in secondary flow point of view at higher specific speeds. In order to be more certain to decide which method to use, a limiting range is introduced as $n_q \sim 25$ to 35. The constant velocity method for below this range and the constant angular momentum for above this range is highly applicable, [6].

A very important criterion in volute design is to maintain a continuous shape. On the other hand, the blockage effect of the cutwater has to be considered as well. As a result, the designer should use a correction so as to compensate the blockage and maintain the continuity of the shape. Wesche (as cited in Gülich, 2010) introduces an equation for this issue, [6]:

$$\frac{\Delta a_3}{a_3} = 0.2 \left(\frac{e_3}{a_3} \right)^2 \quad (2.42)$$

where a_3 and e_3 are taken from the throat section as shown in Figure 2.21:

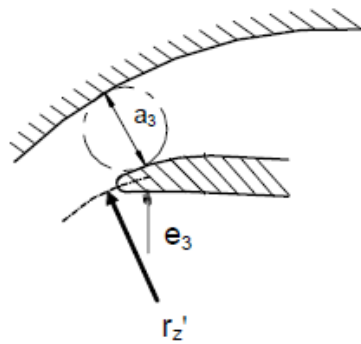


Figure 2.21- Cutwater and throat

The final part of a volute is the discharge nozzle/diffuser. No additional part is applied in single stage pumps since the diffuser part of the volute bears the discharge nozzle itself. This part should be designed aiming a minimum amount of loss due to deceleration, especially for small specific speeds, [6]. The developing trend of the diffuser shows variety. Alemi et al. also attempted to this issue. They analyzed the performances of tangential and radial diffusers shown in Figure 2.22:

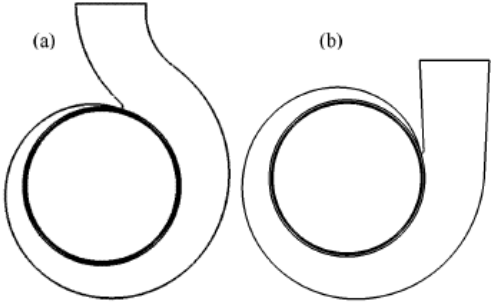


Figure 2.22- Diffuser shapes, (a) tangential, (b) radial, [32]

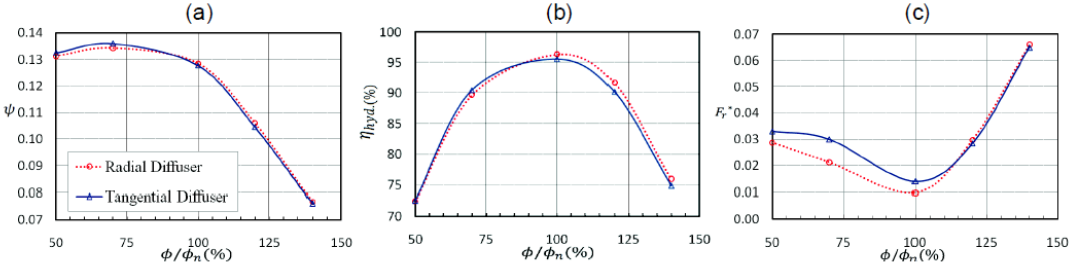


Figure 2.23- Performance characteristics of tangential and radial diffusers, (a) head coefficient, (b) efficiency, (c) radial force with respect to flow coefficient ratio, [32]

As seen in Figure 2.23, both of the shapes exhibit similar characteristics. However, radial diffuser has a bit higher efficiency above the design flow rate and has lower radial force generation below the design flow rate. Therefore, it is design conditions which decides the diffuser shape. In fact, the most important parameters in a diffuser design are length, diffusion angle and inlet flow conditions. These are critical since they play a significant role on boundary layer development, on turbulence characteristics, and solely on discharge flow conditions, which is the output of the diffuser. In a good design, separation should be prevented. The main mechanism behind the separation is the deceleration phenomenon. As the fluid starts to decelerate, pressure increases according to Bernoulli Equation. In a field that deceleration continues, pressure gradient is positive. After a certain point, the kinetic energy inside the boundary layer cannot overcome the pressure at the frontier. As a

result, the flow separates from the walls of the diffuser and causes a significant loss of efficiency. Since this phenomenon occurs inside the boundary layer, keeping the boundary layer thickness as small as possible helps the flow get rid of separation and stall. This necessitates a short diffuser since the longer the pipe the thicker the boundary layer. Level of turbulence has a remarkable effect on separation as well. Due to the fact that increased turbulence increases energy transfer between the main flow and flow inside the boundary layer. This occurs in radial pumps thanks to the centrifugal forces, which in turn increases the level of turbulence, created through the impeller and continuing within the volute, [6].

As cited in Schlichting (1979), Ackeret and Sprenger, following Kline et al. have many studies on the effect of diffuser geometries on diffuser performance. The researches give a light to diffuser efficiency, which is dramatically affected by the boundary layer thickness. The diffuser efficiency is defined as follows, [33]:

$$\eta_D = \frac{p_2 - p_1}{\frac{1}{2}\rho(c_1^2 - c_2^2)} \quad (2.43)$$

where p_1 and p_2 are the static pressure at the inlet and at the outlet of the diffuser, respectively. And c_1 and c_2 are the mean velocities at the inlet and at the outlet of the diffuser, respectively. According to their studies, not only the boundary layer thickness, but also the diffuser included angle and deflection angle (if curved diffuser) are highly effective on the efficiency:

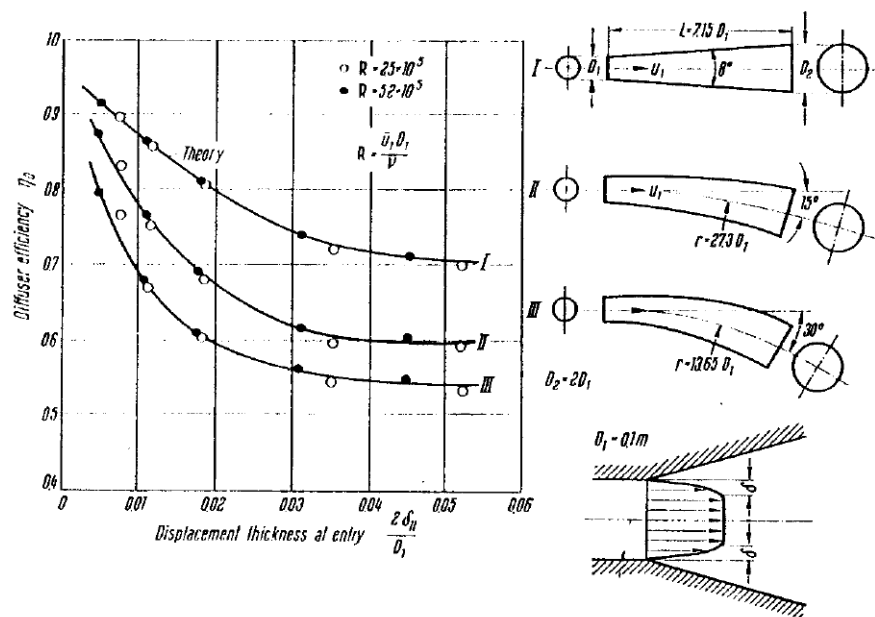


Figure 2.24- Diffuser efficiency in straight and curved diffusers, [33]

As seen in Figure 2.24, increase in both displacement thickness (due to boundary layer) and in deflection angle (represented as I, II and III) causes a deficiency in the diffuser.

The effect of deceleration may be better understood by comparing the flow regimes inside the diffuser. Traupel and Kline (as cited in Gülich, 2010) state that there are four types of regimes seen inside diffusers. According to Figure 2.25, the most desired case is A whereas the case which should strictly be avoided is D. Hence, an optimum length to height (or radius) ratio and an optimum included angle should be chosen. Eq. (2.44) may be used to find a maximum value to included angle provided that the inflow conditions are favorable, [6]:

$$\vartheta_{al} = 16.5^\circ \sqrt{\frac{R_1}{L}} \tag{2.44}$$

Schlichting and Gersten (as cited in Schlichting, 1979), found a range for optimum included angle which maximizes the diffuser efficiency. The range is between $2.9=3^\circ$ and 8° , [33].

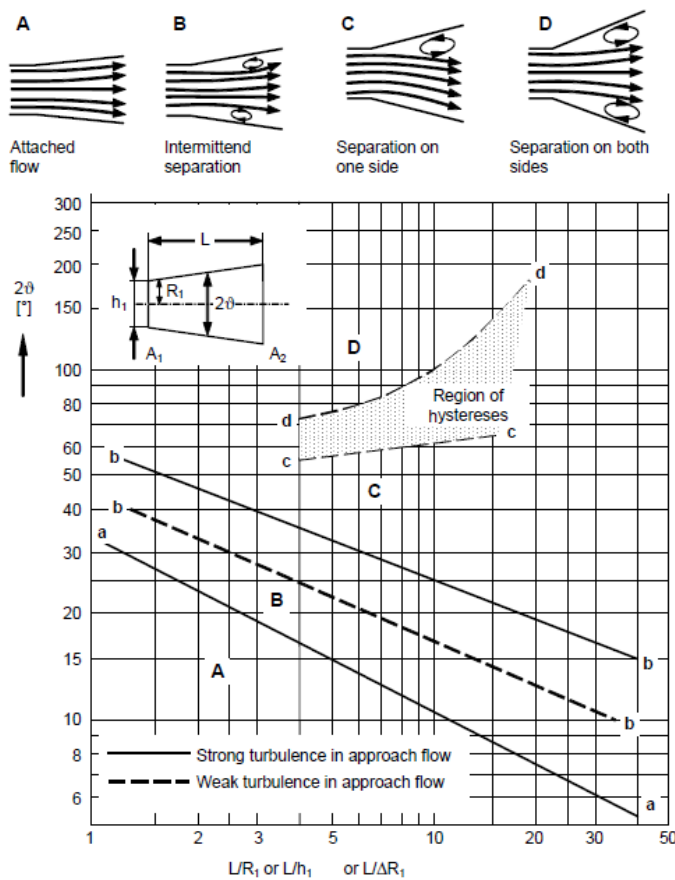


Figure 2.25- Flow regimes inside a diffuser, [6]

In case of non-circular cross-sectioned diffusers, equivalent dimensions are used, [6]:

$$R_{1,eq} = \sqrt{\frac{A_1}{\pi}} \quad \vartheta_{eq} = \text{atan}\left(\frac{R_{1,eq}}{L} \left(\sqrt{\frac{A_2}{A_1}} - 1 \right)\right) \quad (2.45)$$

It should be considered that geometric constraints, manufacturability, adaptation to impeller and so on are also determinant on the design. This means that, above mentioned procedures may be used as guides for a preliminary design. Moreover, a volute does not have to have a certain shape such as circular, rectangular and so on. The installation where the pump is to operate may sometimes forces a genuine design. An example for this case is to be presented in this study since the dishwasher infrastructure requires special pump design.

2.3 Design of the Dishwasher Circulation Pump

In this part, the design procedure for the dishwasher circulation pump specific to this study is to be explained. As stated very early in this chapter, the required operating point of the pump is defined with the parameters listed in Table 2.2:

Table 2.2- Design point parameters of the pump

Parameter	Value
$n (\omega)$	3020 rpm (316 rad/s)
Q	60 l/min=0.001 m ³ /s
$p (H)$	300 mbar (3.07 m)
ρ_{water}	997 kg/m ³

With the above parameters, the pump has a specific speed of $N_s=0.78$ in non-dimensional form. This corresponds to $n_q=41$ in metric form which is used throughout the design in this study (as used in Gülich, [6]).

Majority of the geometric dimensions are determined according to the aforementioned empirical methods in Part 2.2. On the other hand, some parameters are taken from the existing circulation pump designs of Arçelik in order to keep harmony with in-direct parts of the installation such as connection hoses, electrical motor and so on.

In order to make the design in a systematic manner, and to bring a practical and a helpful tool to Arçelik archive, a design sheet is prepared in MS Excel[®] (see Appendix B). The sheet comprises empirical relations, tables, figures and some comments from a variety of sources. The designer inputs the design conditions to the

table, than vast of the parameters are automatically calculated by embedded equations. In some parts, the designer refers to the plots in order to choose a suitable value for his/her application. Moreover, the designer may input his/her desired value(s) for some parameters if the calculated value is not satisfactory or suitable. There are some macros embedded in to evaluate parameters which require iterative calculation. This saves time and effort since otherwise the designer should repeat changing the value of a parameter to get the correct result. At the end, all geometrical dimensions required to model the pump is obtained in a quick way.

2.3.1 Design of the Impeller

Having determined the specific speed of the pump, the design starts with the calculation of shaft diameter according to Eq. (2.2). Taking the allowable stress as 12 N/mm^2 with a maximum power of 30 W (calculated at operating point), shaft diameter is found as 3.4 mm. In Arçelik dishwasher pumps, shaft is screwed to impeller. Leaving a thread tolerance, and to be on the safe side, a nominal size of 4.5 mm shaft is selected. Although 1.3 to 1.4 times the shaft diameter can be used as hub diameter, this is commonly preferred for metal impellers. If a plastic impeller is used, then the hub diameter may be taken as twice the shaft diameter due to its strength characteristics. Again leaving a thread tolerance, hub diameter is chosen as 10 mm.

For the outer diameter, Figure 2.3 is referred. With $n_q=41$, average value for head coefficient is taken, which is 0.90. From Eq. (2.3), outer diameter is calculated as 57 mm.

It is stated in Part 2.2.1 that 5 to 7 blade is suitable for pumps having a specific speed between 10 and 120. Since the pump in question has a specific speed in this range, number of blades is better to be 5, 6 or 7. By referring to Arçelik experience and practice, number of blades is selected as 6.

Choosing f_{d1} as 1.05 (corresponding to $n_q=40$), inner diameter of the impeller is found as 28.5 mm by Eq. (2.5). The shroud should not have to have the same diameter as the blade. In this design, ~10% increase is used for shroud inlet. Upon getting the diameters and number of blades, blade angles at inlet and outlet may be evaluated. Assuming a volumetric efficiency of 0.90, total flow rate, Q_{La} becomes $\sim 0.0011 \text{ m}^3/\text{s}$. Choosing a constant blade thickness of 1 mm, the blockage factor is calculated as 1.18 in an iterative way since it is an implicit equation with blade angle

(Eq's. (2.8-2.9)). This brings a blade inlet width of ~ 7.5 mm. With $c_{1m}=1.3$ m/s according to Eq. (2.7), flow angle is calculated as 24.5° . Assuming an incidence of 2° , inlet blade angle becomes 26.5° . For the outlet blade angle, outlet width is calculated first. Choosing a non-dimensional blade outlet width of 0.09 from Figure 2.4, b_2 becomes 5.1 mm. Again applying an iterative approach blockage factor is found as 1.069, and slip factor is found as 0.777 according to Eq's (2.13-2.16) . Using Eq's (2.17-2.21), flow angle at the outlet becomes 17.2° . An angle of deviation between 10 and 14° may be selected, [6]. By choosing 14° , the blade angle at the outlet then becomes 31.2° .

Table 2.3 presents the summary of impeller dimensions for preliminary design:

Table 2.3-Impeller dimensions:

Parameter	Value
d_w	4.5 mm
d_n	10 mm
d_1	28.5 mm
d_{1a}	32 mm
d_2	57 mm
z	6 blades
b_1	7.5 mm
b_2	5.1 mm
β_1	26.5°
β_2	31.2°
$e_{1,2}$	1 mm

Having defined the necessary geometric parameters, the impeller is ready to be drawn. The profiles for leading and trailing edges may be treated after getting the main blade profile. As mentioned in Part 2.2.1, there are three basic ways to draw the plan view of an impeller. In this study, all three methods are used to generate the blade profiles. By doing so, the designer had the chance to decide which one is the most appropriate. In Figures 2.26 to 2.28, plan view blade profiles by using three different drawing methods are illustrated:

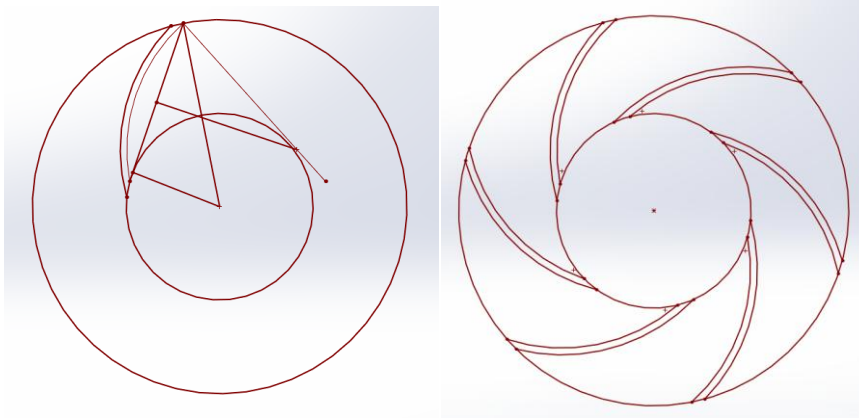


Figure 2.26- Blade profile by Single-arc method

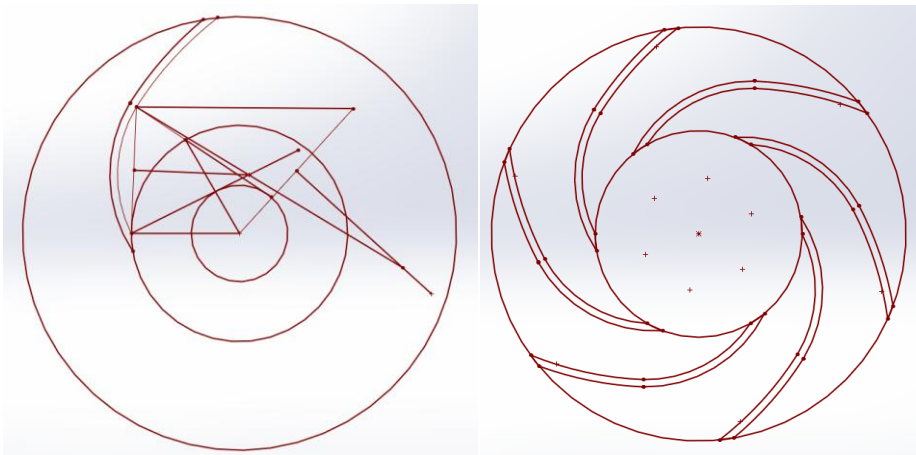


Figure 2.27- Blade profile by Double-arc method

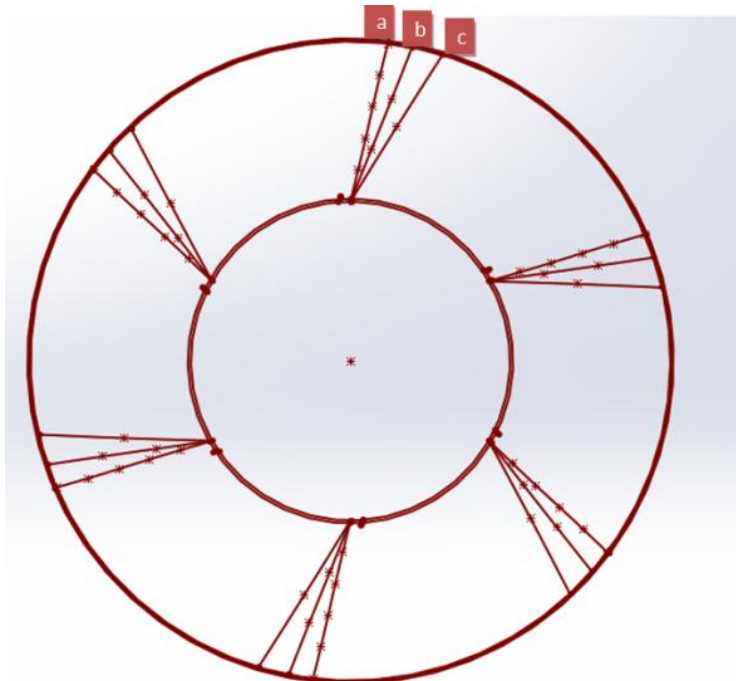


Figure 2.28- Blade profile Point-by-point method with: (a) 5 equal elements, (b) 3 equal elements, (c) 2 equal elements.

As seen in Figure 2.28, point-by-point method (assuming linear variation of blade angle) with different number of equal elements does not produce a satisfactory backward curved profile for these design dimensions. Hence, the designer is left with Single-arc method and Double-arc method. Figure 2.29 helps the designer compare both methods more easily:

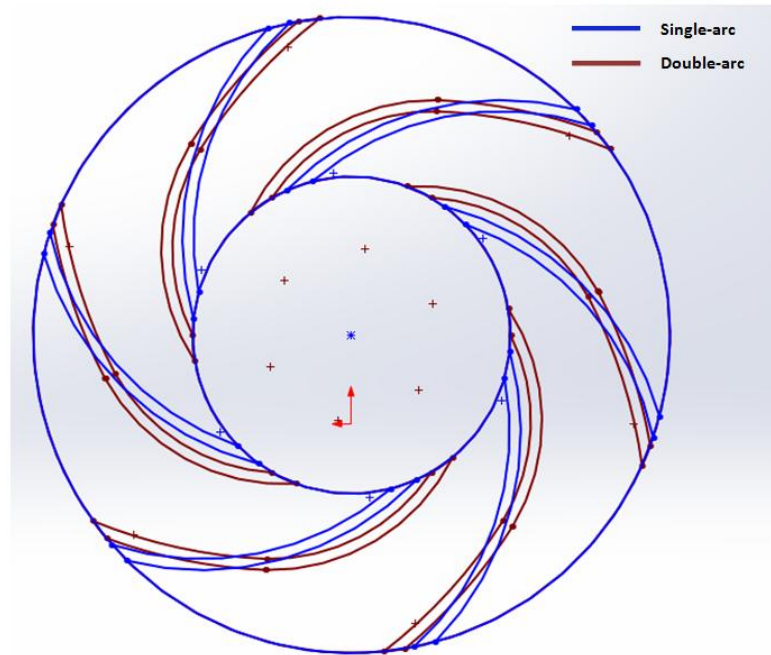


Figure 2.29- Comparison of Single-arc and Double-arc methods on the same plane

According to Figure 2.29, blade with Single-arc method is curved more uniformly than the other one. Blade with Double-arc has a uniform curvature until the end of the first arc. The section with the second arc has a nearly linear extension. As a result, choosing the one with Single-arc method seems to be better. However, in order to strengthen this argument, some other controls should be made as discussed in Part 2.2.1. Firstly, channel cross-section is checked as shown in Figure 2.12. According to that, a linear trend should appear for the connecting line of $a_x b_x$'s to guarantee the conservation of relative velocity. Figures 2.30 and 2.31 show the control results for both methods:

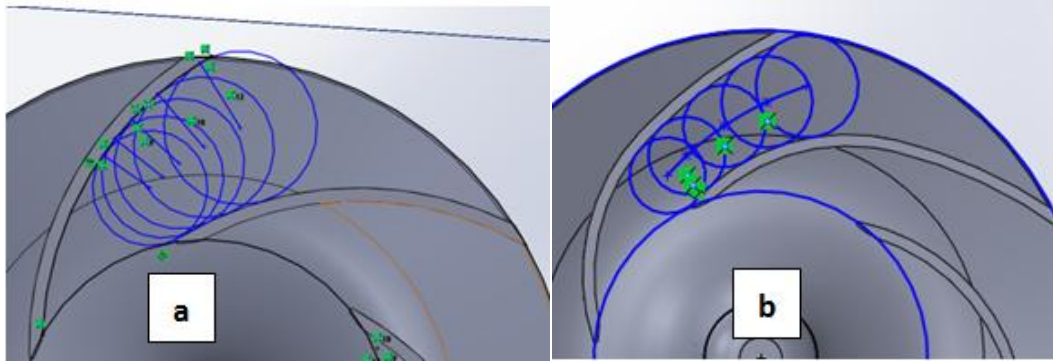


Figure 2.30- Channel cross-section control circles: (a) Single-arc (b) Double-arc

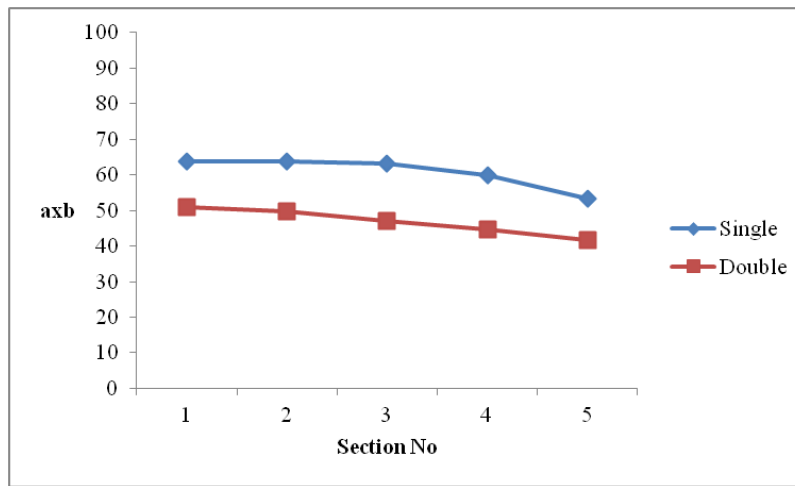


Figure 2.31- Channel breadth x blade width for the mid-stream line sections

As seen in Figure 2.31, both methods have similar trends (linear-like) for the indication of conservation of relative velocity. Thus, this check is successful for both methods. The other check is made about minimum surface area per unit blade as discussed in Part 2.2.1. By using Eq's (2.26-2.31) and Figure 2.13, parameters listed in Table 2.4 are calculated for the issue:

Table 2.4-Blade surface area per unit blade parameters

Parameter	Value	Parameter	Value
l	28.68 mm	β_{mean}	29.75°
t/l	0.779	ξ'_p/ξ_p	~1.05
$\tan(\beta_\infty)$	0.261	$(ztl)_{min}$	0.057
w_∞	19.52 m/s	l_{min}	9.5 mm
Γ_2	0.876		

By using the CAD geometries, arc lengths are measured as 26.2 mm and 34.6 for Single-arc method and Double-arc method profile, respectively. These values safely satisfy the minimum surface area per unit blade as compared to 9.5 mm.

Since controls are passed by both methods, designer is free to choose any of the two methods. Since Single-arc method produced a more uniform curvature, the designer decides to continue with this method.

Having chosen the plan view profile of the blade, the meridional view profile of the impeller is drawn as shown in Figure 2.32 by using the values presented in Table 2.3:

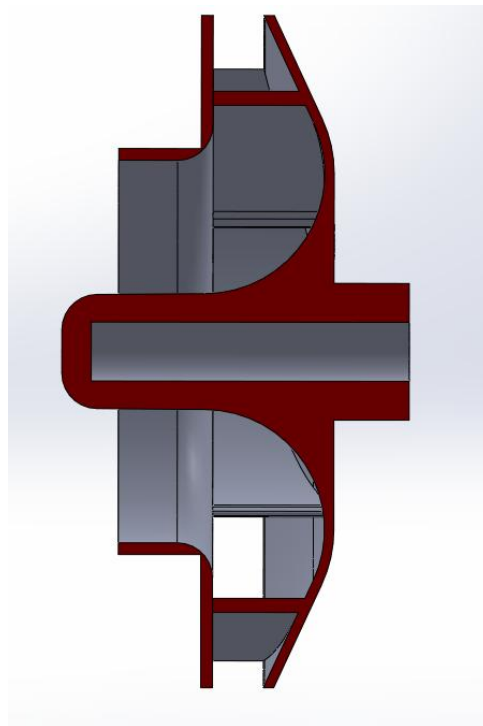


Figure 2.32- Meridional view of the impeller

For acceptable pressure distributions, leading edge is elliptically profiled as discussed in Part 2.2.1 and referring to Figure 2.7. However, trailing edge is kept as it is. If a head deficiency is observed, underfiling may applied after production. The final blade profile and impeller model are presented in Figure 2.33 and 2.34:

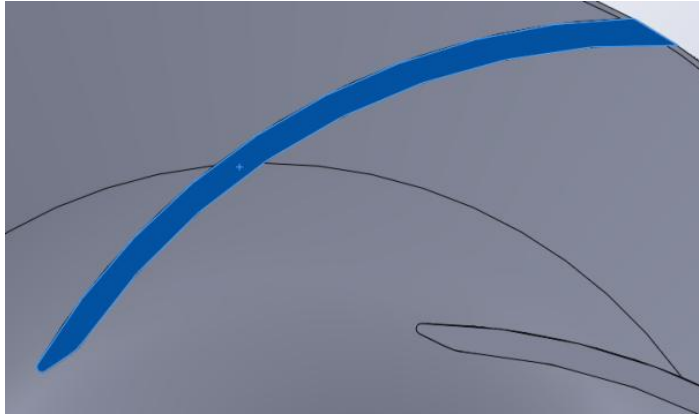


Figure 2.33- Final blade profile (plan view)

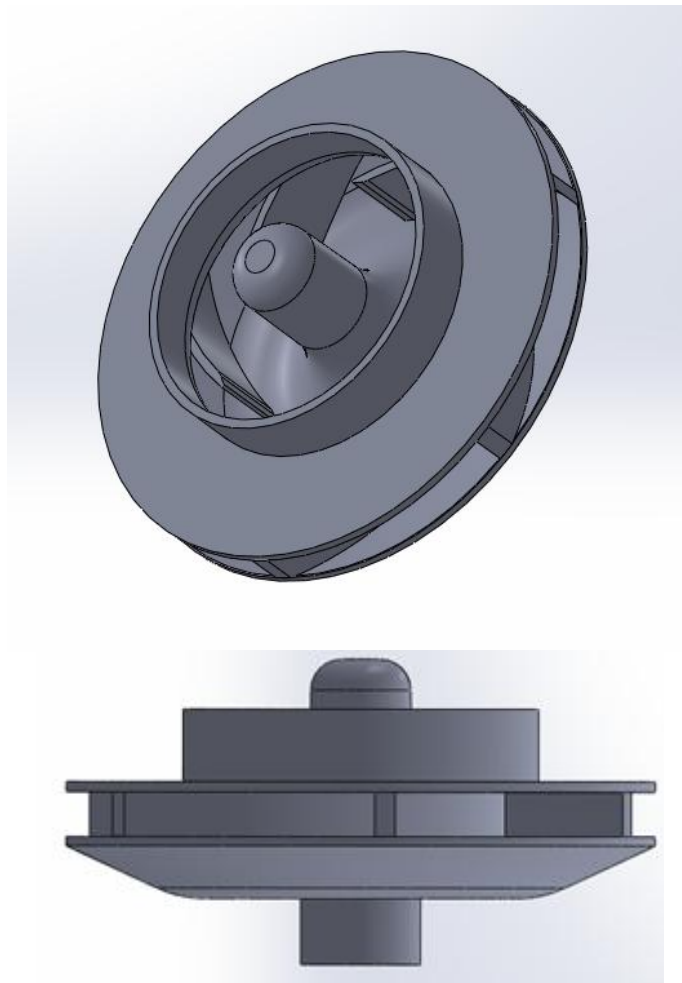


Figure 2.34- Final impeller model

2.3.2 Design of the Volute

The shape of the volute depends not only on impeller geometry, but also on other constraints such as pump installation as stated before. In Arçelik dishwasher, the circulation pump has the heating facility integrated on it. Since the company that produces the heater elements has a certain optimized design, volute design is

dependent to the shape of that heater elements, especially to the heating plate which is in direct contact with operating fluid. Another constraint is about the diameter and the height of the volute. The reason for this is that there are several components under a dishwasher tub and each of them has a certain location and size. Moreover, the pump is connected to the water sump forming a closed loop in a manner such that folding of hoses are strictly avoided in order not to disturb water flow. Furthermore, the pump is fixed to the dishwasher from the casing in order to prevent vibration. Combining all these constraints, the pump assembly –especially the volute since it is the topic of this study- has limited geometric flexibility.

In Arçelik dishwasher infrastructure, the pump casing, which forms the outer limits of the volute, has the form shown in Figure 2.35, inside which a volute design may be applied:

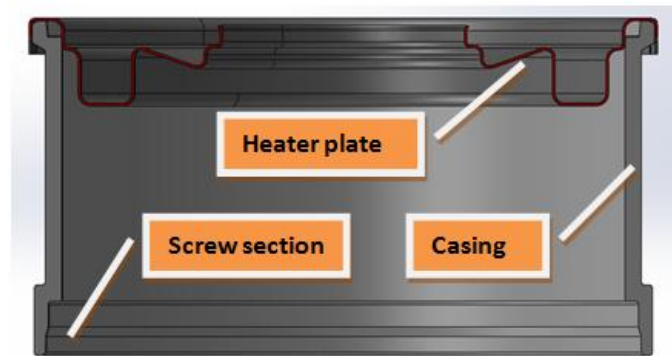


Figure 2.35- Volute outer limits

For the inner diameter of the volute, a clearance of 2.5 mm from the impeller outlet is given, resulting in $d_3=59.5$ mm. The last parameter for fixing the volute partial cross-section extension area is volute inlet width, b_3 . It may be taken as twice to four times of blade outlet width, [6]. This corresponds to 10.2 mm of volute inlet width. Having determined volute inner and outer constraints, the limits for partial cross-sections are set. Locating the impeller to the assembly, the limits are obtained as shown in Figure 2.36:

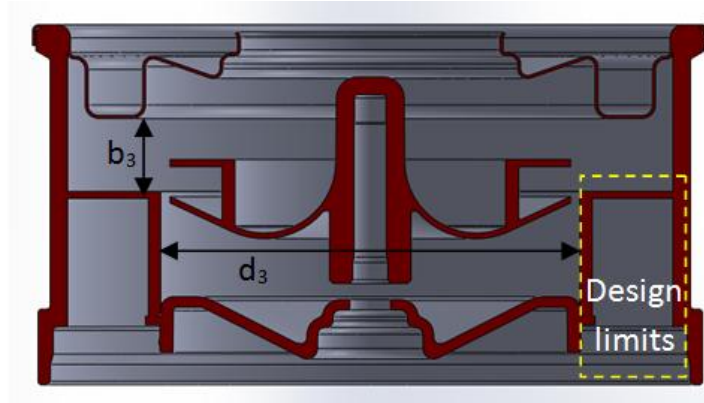


Figure 2.36- Design limits for partial volutes

As seen in Figure 2.36, partial volutes cannot extend radially outwards like shown in Figures 2.14 to 2.20. Thus, they are to extend downwards special to this design. It is commonly used to divide the volute into eight equal sections and draw eight partial volute cross-sections. Connecting these partial volutes produces the full volute, [29]. In order to draw each partial volute sections, throat areas should be calculated first. With the design parameters determined in this study, throat area for a circular cross-section volute is 285 mm^2 by using Eq's (2.38-2.39). This corresponds to a hydraulic diameter of 19 mm. For a rectangular-like cross-section, it is calculated as 16 mm by considering wall thicknesses, gap between inner and outer walls of the volute and inlet volute width. Adding the area between the outer wall of the volute and heater plate, calculated hydraulic diameters are approximately match. Assuming constant velocity inside the volute, which is the method suggested by Stepanoff, additional heights to volute inlet width are calculated as follows:

Table 2.5- Partial volute section heights (starting at a distance of b_3 (10.2 mm) from the heater plate)

Section No	Wrap angle, ε [°]	Additional height [mm]
1	0	1
2	45	2.6
3	90	4.7
4	135	6.9
5	180	9.1
6	225	11.3
7	270	13.4
8	315	16.4

Referring to the discussion made in Part 2.2.2 with Figure 2.18, rounded shapes exhibit better performance in terms of head, efficiency and radial force compared to those of rectangular cross-section. Taking this fact into consideration, bottom parts of partial volute sections are rounded to increase hydraulic diameter and to improve flow conditions. A volute spiral is obtained with the data shown in Table 2.5:

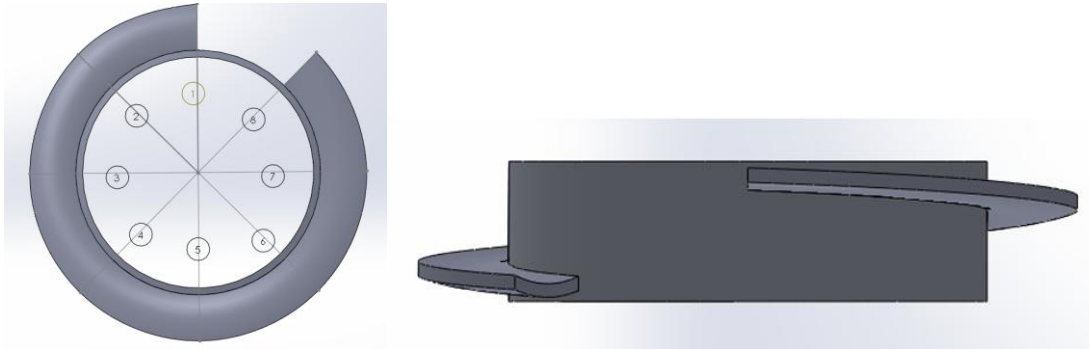


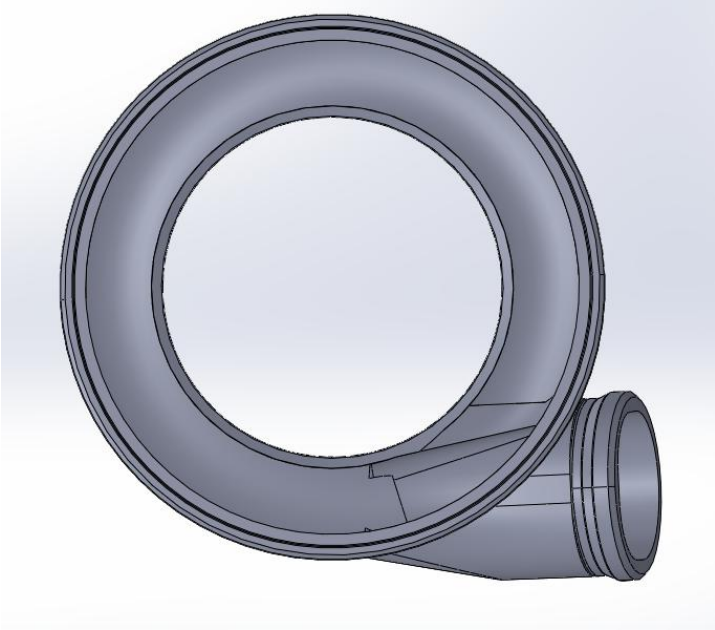
Figure 2.37- Volute bottom profile obtained by connecting 8 partial volute sections

Upon obtaining the volute profile, cutwater geometry is to be obtained. In general, volute cross-sections extend radially outwards as wrap angle increases as mentioned before. Hence, cutwater is located at the intersection of first partial volute section and diffuser which is the closest section to the center. In this specific design, on the other hand, since radial dimension of the volute sections are equal everywhere, distance from cutwater to the center is not the closest distance but is equal to volute outer diameter (~87 mm). According to Eq. (2.31), cutwater diameter should be greater than 64.5 mm, which is achieved in this case. Leading edge diameter, e_3 , may be taken as $0.02xd_2$ as suggested by Gülich (2010, p.415), [6]. This corresponds to a diameter of 1.1 mm. Camber angle of cutwater is calculated around 10° by Eq. (2.36). However, since cutwater is not very close to the point where the flow leaves impeller, it does not disturb the flow significantly. Thus, a wider angle may be used. Another compensator for cutwater blockage is cutwater correction as mentioned in Eq. (2.42). With 1.1 mm of cutwater tip diameter and 11.5 mm of throat area, amount of correction is evaluated as 0.021 mm which is negligible compared to 11.5 mm.

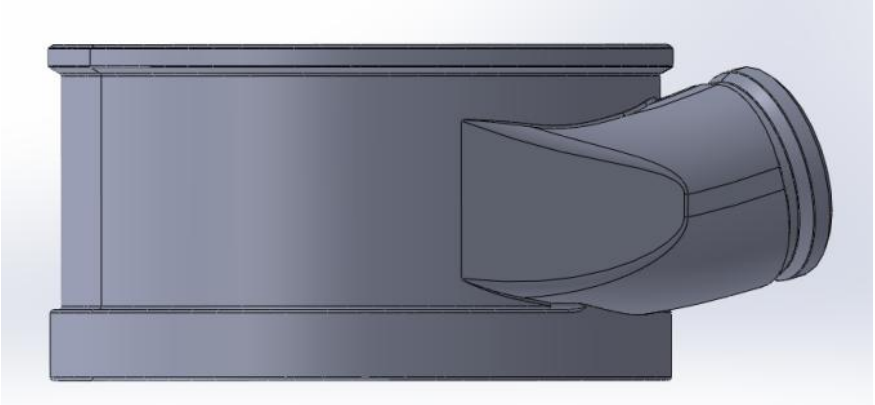
After deciding cutwater geometry, the final part of the volute, which is the diffuser, is to be designed. It is decided to use radial diffuser rather than a tangential one in order to keep diffuser length as short as possible to avoid separation. Benefitting from Arçelik's previous designs, a diffuser of ~60 mm length with an included angle of 15° to 10° (variable-angled) is used. With $R_I=5.75$ mm and $L=57$ mm, 10.4° of

allowable included angle is obtained by Eq. (2.44). Moreover, this is predicted to help flow attach to the diffuser wall as seen in Figure 2.25. Considering the pump position near the water sump of dishwasher, the diffuser should have an inclination for smooth hose connection. Thus, 15° inclination is chosen which exhibits moderate and acceptable volute efficiency values as referred to Figure 2.24.

Having determined all the required geometric parameters, the volute is constructed as seen in Figure 2.38:



(a)



(b)

Figure 2.38- Completed volute design (without heater plate): (a) top view, (b): side view

Combining all the designed and default parts, which are impeller, volute and heater, the pump assembly becomes shown in Figure 2.39:

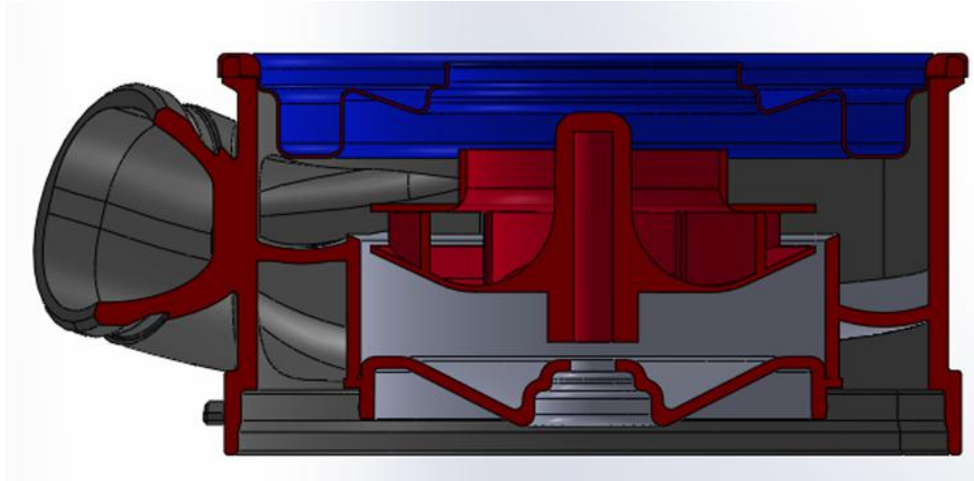


Figure 2.39- Pump hydraulic parts

2.3.3 Mechanical Parts and Electric Motor of the Pump

During the design of hydraulic parts, it is aimed to keep mechanical parts and electric motor common with the similar type of pumps used in Arçelik. The reason is that, the more the number of common parts, the easier to follow production planning especially with part suppliers. Moreover, these parts are auxiliary ones and their characteristics are already known. Since the designed pump dimensions suit these mechanical parts, new designs are not made.

There are several mechanical parts coupled with the pump. This pump is a “wet-rotor” pump in which the magnetic rotor is coated and sealed such that it is in contact with the operating fluid safely. The rotor encloses the shaft, which is 4.5 mm in diameter as calculated earlier. It is located in a well sealed cavity of the lower casing of the pump. Two radial coils, one at the lower part, the other at the upper part, are used for aligning and fixing the shaft to the casing. Under the lower casing, electric motor and motor card are present. The lower casing, in addition, enables fixing the pump assembly to the dishwasher base. There is an O-ring to prevent leakage located between volute and lower casing. The last mechanical part added to the assembly is the volute inlet pipe which allows hose connection to the volute.

The full assembly sectional view is as illustrated in Figure 2.40:

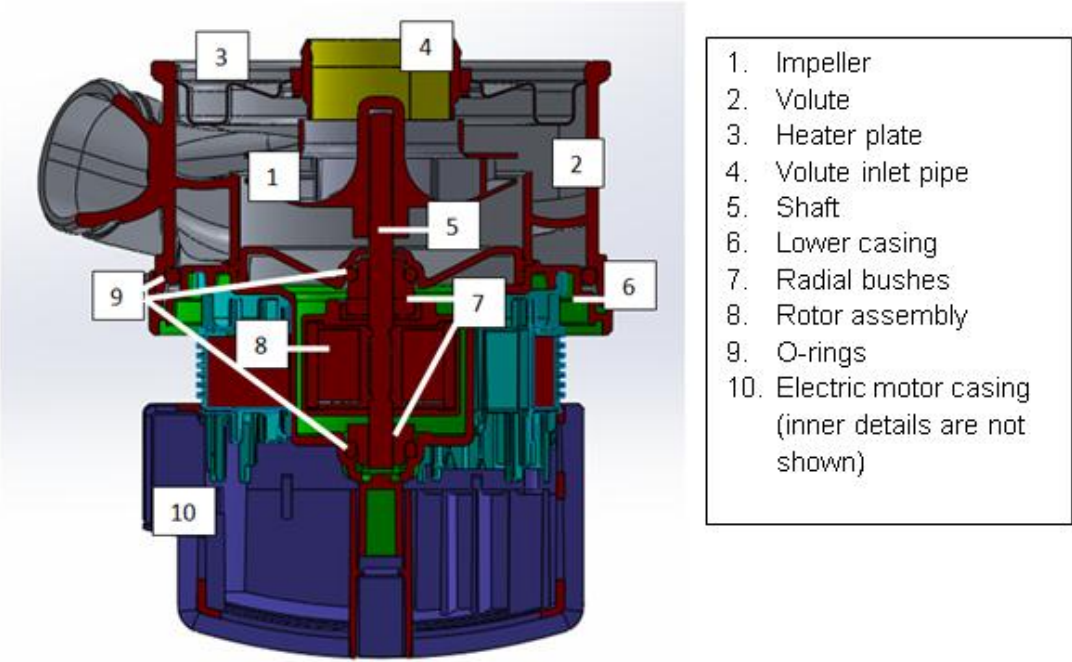


Figure 2.40- Full pump assembly

Electric motor of the pump is a BLDC type which enables variable speed, quieter operation and lower energy consumption compared to AC pumps. An electronic card designed by Arçelik is located inside the motor casing. This card has two electrical connection ports: one is for energizing; the other is for speed change. A wide range of various rotational speed values may be installed to the card by means of a certain software. However, the card has a certain capacity in terms of speed memory. To illustrate, one can install a speed combination of 1000, 2000, 3000 rpm; and another can install 1000, 1100, 1200 rpm to the three allowed speed memory. In this study, the design rotational speed is the nominal value to be used in general cleaning algorithms and equals to 3020 rpm. Other speed values may be determined depending on the application. Hence, it is not in the scope of this study.

CHAPTER 3

CFD ANALYSES OF THE DISHWASHER CIRCULATION PUMP

3.1 General Information on CFD Analyses and Software

Historical background, benefits, methods and logical background of CFD is discussed in Part 1.2.3 in detail. In this part, on the other hand, specific details of the application of numerical experimentations on the designed pump are presented.

CFD analyses allowed the designer to investigate the designed pump in several ways. First of all, problems in generated geometry are immediately captured by the software. Hence, the designer could revise the geometry knowing where the problems are. Secondly, hydraulic performance of the pump is predicted in a couple of days if a well-enough mesh quality is obtained. This helps the designer revise the design further if there is a lack of performance. Moreover, flow profile can be monitored in detail which contributes to noticing problematic regions that flow is disturbed. Separation and recirculation may be listed as concrete examples to this issue. This can only be achieved by means of very expensive tools such as PIV in laboratory environment.

There are two cases investigated by means of CFD analyses in this study. In the first case, designed impeller is analyzed with an existing volute design of Arçelik. In the second case, both the impeller and the volute are the ones designed in this study. By doing so, it is seen if there is need for launching the new volute design for mass production or the existing volute is sufficient for energy efficiency.

Since CFD software solve number of equations which are continuity (conservation of mass), conservation of momentum in x, y and z directions, energy and turbulence equations in an iterative way, capacity of the computer which solves these equations plays a very important role on the quality of the results. The used computer in this study has Intel® Core™ i7-3770 CPU operating at 3.4 GHz and a RAM of 8 GB with a 64 bit Windows 10 operating system. This capacity is quite sufficient for such CFD analyses.

In this study, used CFD software is Autodesk[®] Simulation CFD 2015. This software uses finite element method. By this way, algebraic equations are obtained from the governing partial differential equations which can be analytically solved in an easier way. “For numerical stability, the advection terms are treated with upwind methods along with the weighted integral method”, [34]. There are five upwind schemes to be chosen in the software. Each has certain methods, advantages and disadvantages. As a result, it is the application that determines which one to use. The software has intelligent selection criteria as well. If a rotating body is present in the analysis, which is the case for turbomachines, Petrov-Galerkin advection scheme is selected by default since it is recommended for pressure driven flows. In this advection scheme, moderate numerical stability is obtained. Moreover, it has less numerical diffusion, which is the case that “the simulated medium exhibits a higher diffusivity than the true medium, [35]], for random meshes, [34]. All rotating devices are solved by transient analysis method. In this case, implicit or backward difference method is used for discretization of transient terms.

For the solution of the governing equations, a special algorithm is used in Simulation CFD 2015 which is called Segregated Solver. The solver algorithm uses the following steps, [36]:

1. Read in geometry, boundary conditions, and analysis data
2. Create data structures
3. Solve x-momentum equation
4. Solve y-momentum equation
5. Solve z-momentum equation
6. Solve pressure equation and correct velocities
7. Solve energy equation
8. Solve turbulent kinetic energy equation
9. Solve turbulent energy dissipation equation
10. Check convergence (go to step 3)
11. Perform output calculations
12. Write out data
13. Exit

In order to deal with turbulence issues, the eddy viscosity and eddy conductivity variables are determined by using turbulent kinetic energy transport and dissipation equations in Simulation CFD. By default, k - ε turbulence model is utilized in the software. It is useful for many applications including most engineering issues with sufficient results. If, on the other hand, separation is of the question, RNG two

equation model exhibits better accuracy due to its firmer theoretical background, [37]. For a pump analysis where separation is not critical, $k-\varepsilon$ model is sufficient. Therefore, it is used in this study as well.

Simulation CFD most generally applies tetrahedral meshing in 3-D models, and triangular meshing for 2-D models. Other than those, quadrilateral, hexahedral, wedge and pyramid elements are available too, [38]. Auto-sizing is optional in the software. It can easily be applied to any geometries allowing the user interfere with local sections as well. On the other hand, the designer is free to use manual meshing, which is used in this study.

3.2 Pre-processing Steps for CFD Analyses

3.2.1 Solid Modeling

In order to analyze a pump, fluid domain should be generated first. This may be done in several ways. CFD software are usually capable of forming the fluid volume inside the volute. However, using a separate CAD software enables revising the fluid volume to be more suitable for CFD analyses. The reason is that, exact solid models which are drawn for manufacturing usually includes a lot of features like small fillets, chamfers, surfaces and so on. Nevertheless, a finite element software cannot resolve these small details and meshing errors arise in general. As a result, the designer should simplify the solid model as much as possible in order not to have problems in CFD analyses. Removing small fillets, chamfers, sharp edges do not affect the accuracy of analyses compared to real performance. The reason is that, these small details are usually included for manufacturing reasons rather than hydraulic performance. In this study, SolidWorks Premium 2013 and UG NX 9 are used for solid modeling since each has ease of use in different commands.

For the fluid volume, all the open parts of the volute are closed by planar surfaces. Then, an arbitrary larger solid body is created. Subtracting the volute wall from this larger solid body merged the inner volume of the volute as a solid part. Inappropriate features, surfaces, edges and so on are modified for CFD analyses. After that, pump inlet is extended 3 times the diameter and pump outlet is extended 5 times the diameter which is a rule of thumb for eliminating the boundary condition effects on the fluid flow.

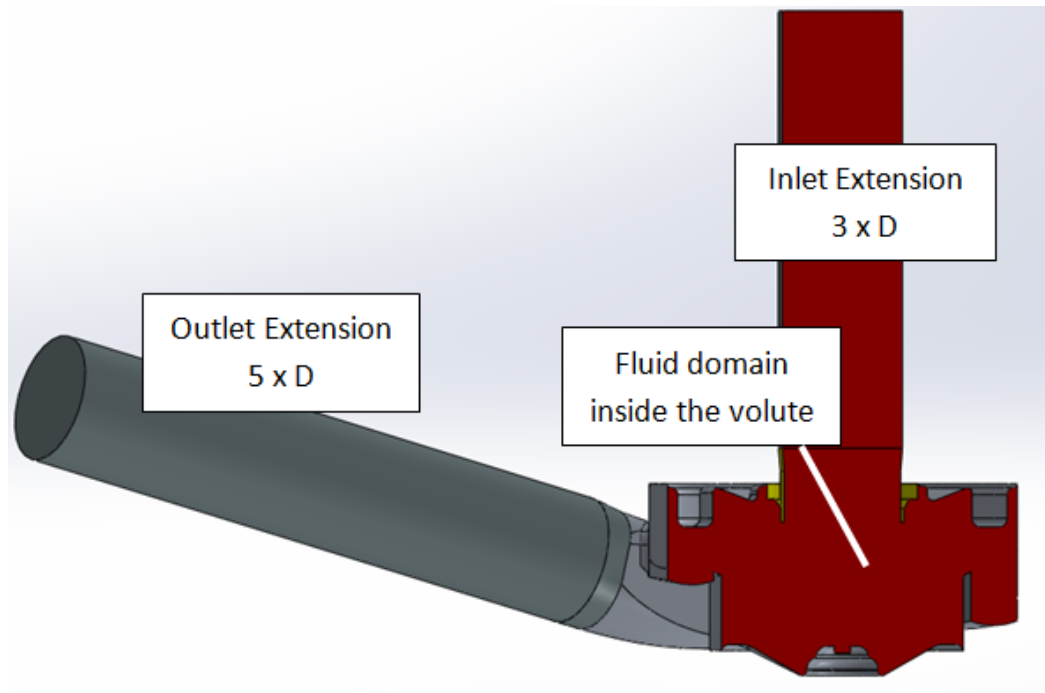


Figure 3.1- Fluid domain CAD model with inlet-outlet extensions

Impeller is modified for a suitable analysis as well. Mechanical parts are not included in the design since they are aligned in such a way that, even the shaft is not in direct contact with fluid. Hence, shaft hole is closed completely. Other small details are cleaned from the CAD geometry. At the end, impeller is attached to the fluid volume.

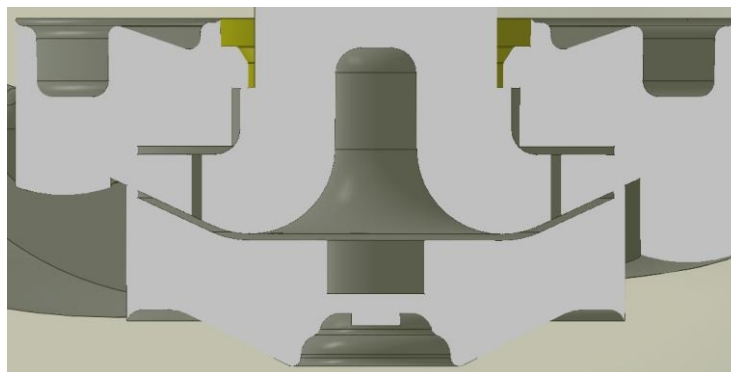


Figure 3.2- Impeller inside the fluid domain

In Simulation CFD, impeller is not directly rotated during analysis. Rather, a solid region between impeller and solid wall, called “Rotating Region” is used. This part should have the same axis of rotation with the impeller and should be symmetrical with respect to that axis. This part is drawn with the CAD software as well.

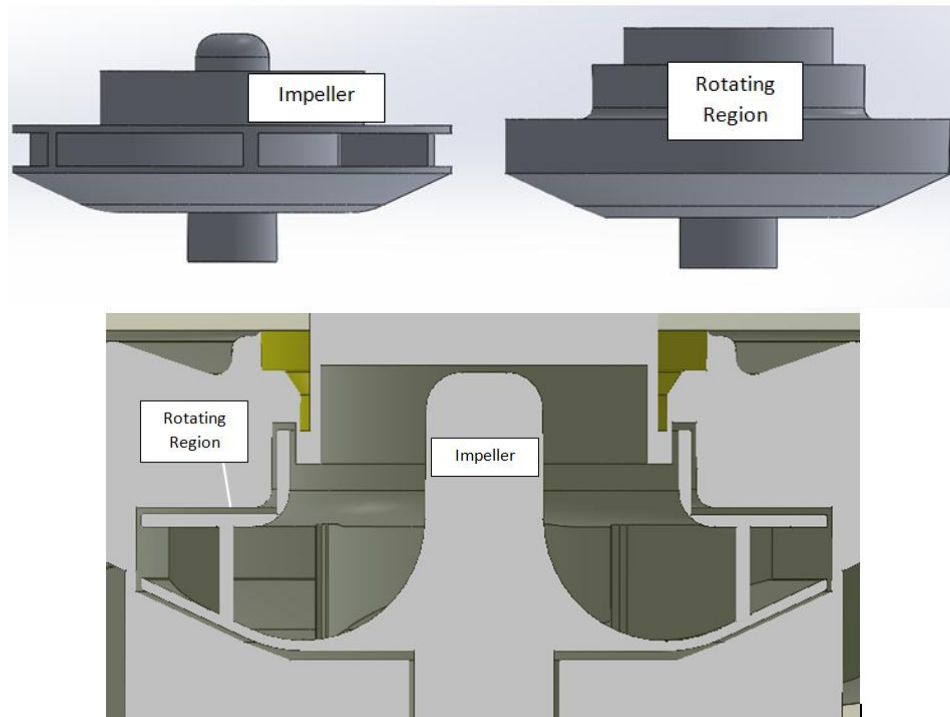


Figure 3.3- Rotating region between volute wall and impeller

3.2.2 Material Assignment

Simulation CFD has a material library from which the user can select large number of materials. Moreover, it enables adding more materials or material properties manually. In the pump design analyses, the fluid volume is selected as fixed water which means that the properties are constant. For the impeller, ABS (molded) is selected which is very close to the real impeller material. Rotation properties are assigned to the rotating region as stated before. Here, rotational speed is assigned for non-impulsive start up. This is not necessary but results in better flow development since ramping up of the impeller due to its inertia is simulated as in the real case. This is applied as follows: First, zero rotation at initial time is entered. Then, time passing between two successive blades with the known rotational speed is calculated (automatically or manually). 50 times this time step size is entered to the second row of rotational speed table with the nominal speed. Then, a comparably large time step is entered with the nominal speed again, [39]. For a 6-blade impeller with nominal rotational speed of 3020 rpm, the following data shown in Figure 3.4 is constructed.

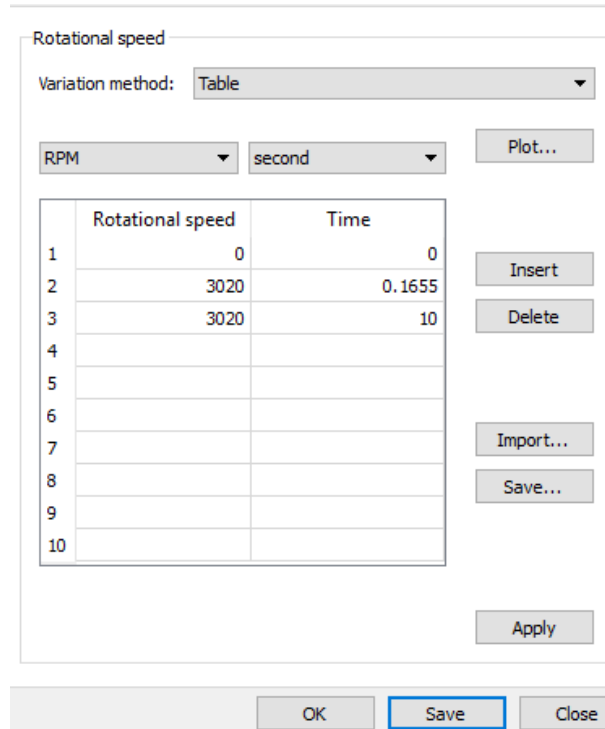


Figure 3.4- Rotating region speed-time table

3.2.3 Boundary Conditions

In analysis of centrifugal pumps, there are two ways of assigning flow boundary conditions (BC). Either pressure inlet-pressure outlet, or flow rate inlet-pressure outlet BC may be used. The former requires more computing time since computed data at each iteration changes the pressure distribution and analysis continues until the given BC's are matched. In the latter one, on the other hand, generated data at each iteration does not affect any parameter, and pressure distribution at the inlet is calculated for given BC's. At the end, total pressure rise through the pump is obtained more rapidly and compared to desired data. As an exception, the first analysis, which is for start-up, is performed with atmospheric pressure assigned to both inlet and outlet. This is the easiest way to start since all reference values for the pressure are equal to zero. At this step, ramping up of the impeller takes place as well. For the other operating points, flow rate inlet-pressure outlet BC's are used in this study as suggested.

3.2.4 Meshing

Upon importing the geometry and applying materials and BC's, "the geometry is broken up into small pieces called elements. The corner of each element is a node. The calculation is performed at the nodes. These elements and nodes make up the

mesh.”,[34]. The finer the mesh the better the accuracy; however, finer meshes require more memory and consume more time. As a result, there is a level of mesh size which gives acceptable results. Furthermore, after a certain mesh adjustment, the analysis may become mesh independent; that is no more considerable change in the result is obtained by further refinement.

Although automatic meshing is possible in Simulation CFD, manual meshing is used in this study by using previously exercised mesh sizes for the impeller having an approximately 60 mm outer diameter. The coarsest mesh is applied to the inlet and outlet extension pipes with a size of 4 mm. This is sufficient since these pipes are not critical for the fluid flow as other parts. Then, a mesh size of 3 mm is assigned to the volute. Impeller is suppressed, meaning that zero mesh size is assigned, since its shape is present at the rotating region as wall; however, leading edge of the blades and the hub are meshed by 0.5 mm surface meshing, which is the finest mesh size in these analyses. Rotating region, which is very critical since it represents the rotation of the impeller, is assigned with a mesh size of 2 mm determined by the size of the impeller. That is, $1/30^{\text{th}}$ of the outer diameter is chosen. These regions are the most critical ones since fluid flow is started to be guided here. In Simulation CFD, refinement regions may be created in addition to current parts present in the geometry. A cylindrical refinement region is drawn at the cutwater since it is another critical region where the flow is deflected. A size of 1.5 mm is used here. It is important to keep the ratio of neighboring elements' mesh sizes smaller or equal to 2. Otherwise, mesh structure is prone to be highly uneven. Default values are selected for the boundary layer meshing. There are 3 layers with a thickness factor of 0.45. By these values, 3 near-wall layers with a gap of 0.45 times the original element size are created, [40]. All the other parameters but the volume growth rate are kept as default since they are sufficient for this study. Volume growth rate is increased from 1.35 to 1.2 for finer mesh.

In order to ensure that the mesh sizes listed above are sufficient enough, a check for mesh independency is applied for the design point with case 1. Only mesh sizes are changed by a factor of 1.5 while other parameters such as enhancement factor, number of layer and so on are kept constant. Mesh sizes and corresponding number of elements are presented in Table 3.1:

Table 3.1- Number of elements with respect to different mesh size combinations

Mesh density	Mesh Size (mm)					Number of elements
	Volute	Extension pipes	Rotating region	Blade edges	Cutwater	
Coarse	4.5	6	3	0.8	1.25	405,400
Moderate	3	4	2	0.5	1.5	1,061,000
Fine	2	2.6	1.3	0.3	1	1,690,000

Analysis results for mesh sizes listed in Table 3.1 are presented in Figure 3.5:

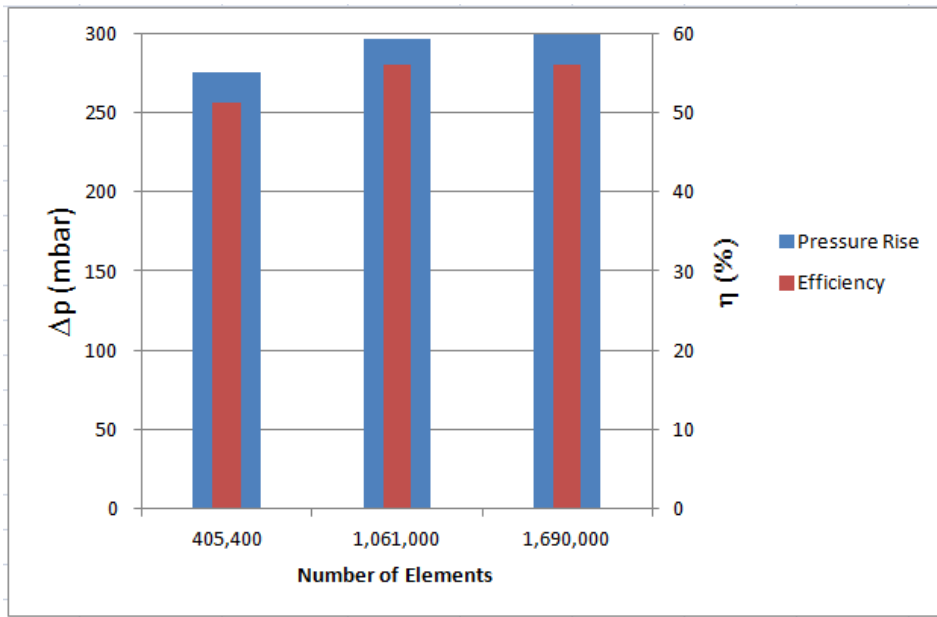


Figure 3.5- Analysis results for different mesh sizes at $Q=60$ l/min for case 1

Results in Figure 3.5 show that the coarse mesh results are far from the design point (300 mbar pressure rise and 55% efficiency) especially for the pressure rise with an error of 8%. However, the mesh size which is thought to be enough and the finer mesh results are in very good agreement for both pressure rise and efficiency. Moreover, their results match with the design point pressure rise and efficiency values as well. Hence, it can be said that, mesh independency is achieved with above mentioned mesh sizes.

3.3 Analyses and Results

For both cases, pre-processing parameters are chosen as the same since geometries are similar.

3.3.1 Analysis and Results for Case 1

In the first case, designed impeller is analyzed by existing volute design.

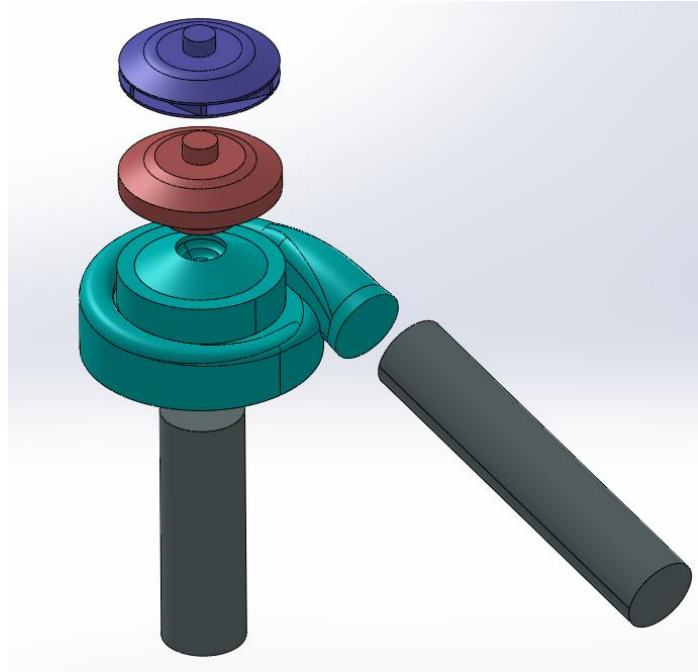


Figure 3.6- Exploded view of pump assembly for case 1

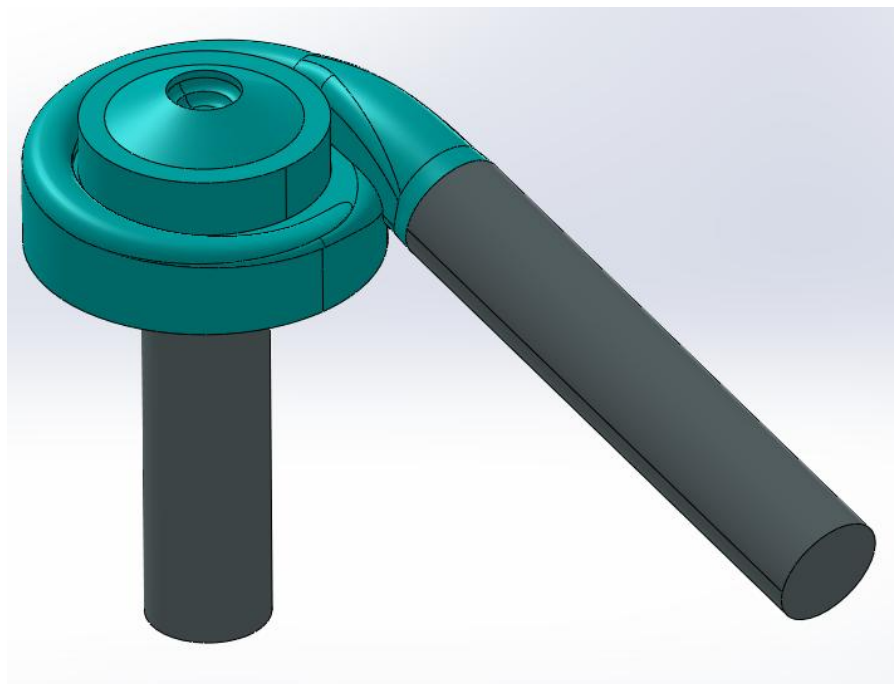


Figure 3.7- Pump assembly model for case 1

Using the mesh sizes as mentioned before, approximately 272,000 fluid nodes and 1,061,000 fluid elements are generated. Since the impeller is suppressed, there is no solid node and element. Hence, the numbers above represents the total number of nodes and elements. Relying on previous experiences and mesh independency check mentioned above, such a number of elements is sufficient for a dishwasher circulation pump . Mesh visuals are shown in Figures 3.8 to 3.12 :

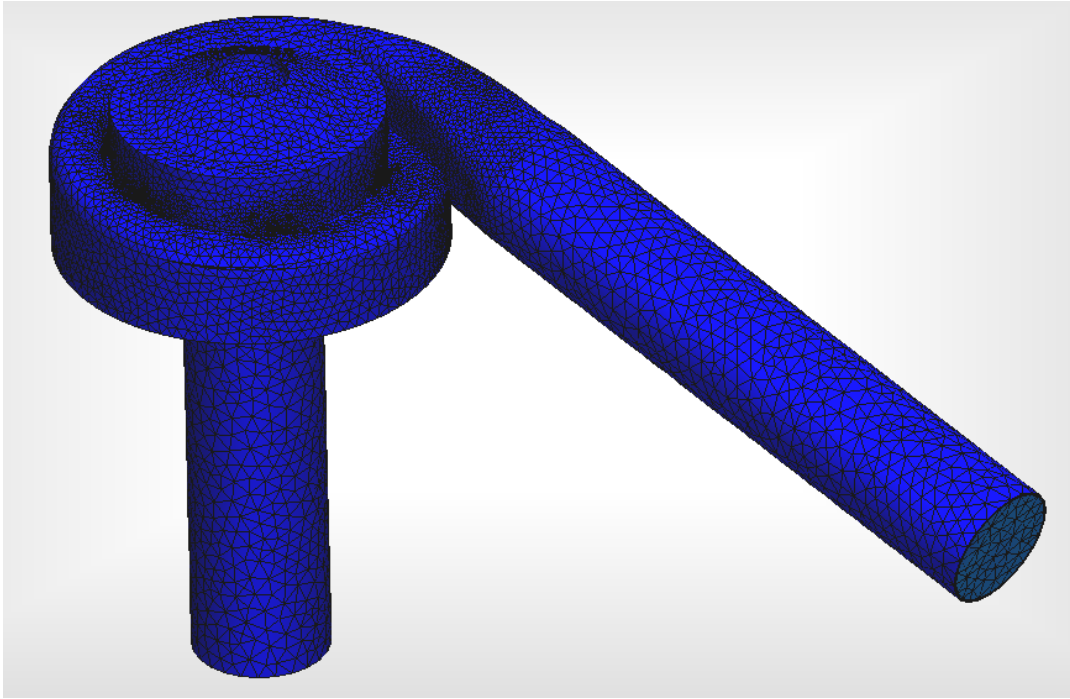


Figure 3.8- Generated mesh-general view (case 1)

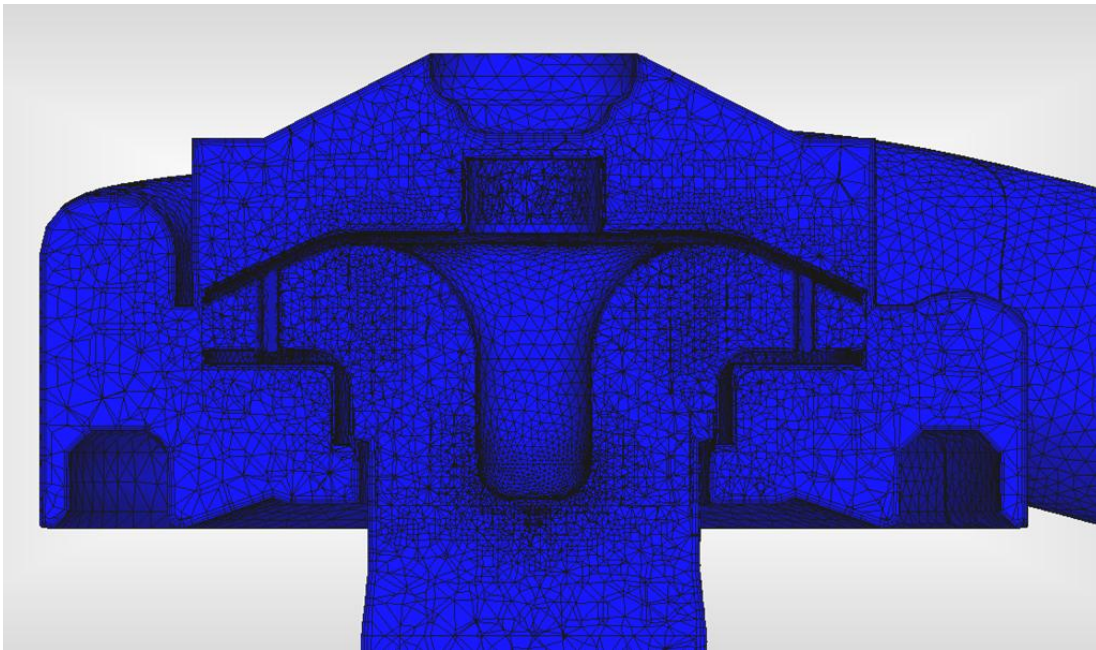


Figure 3.9- Generated mesh-sectional view (case 1)

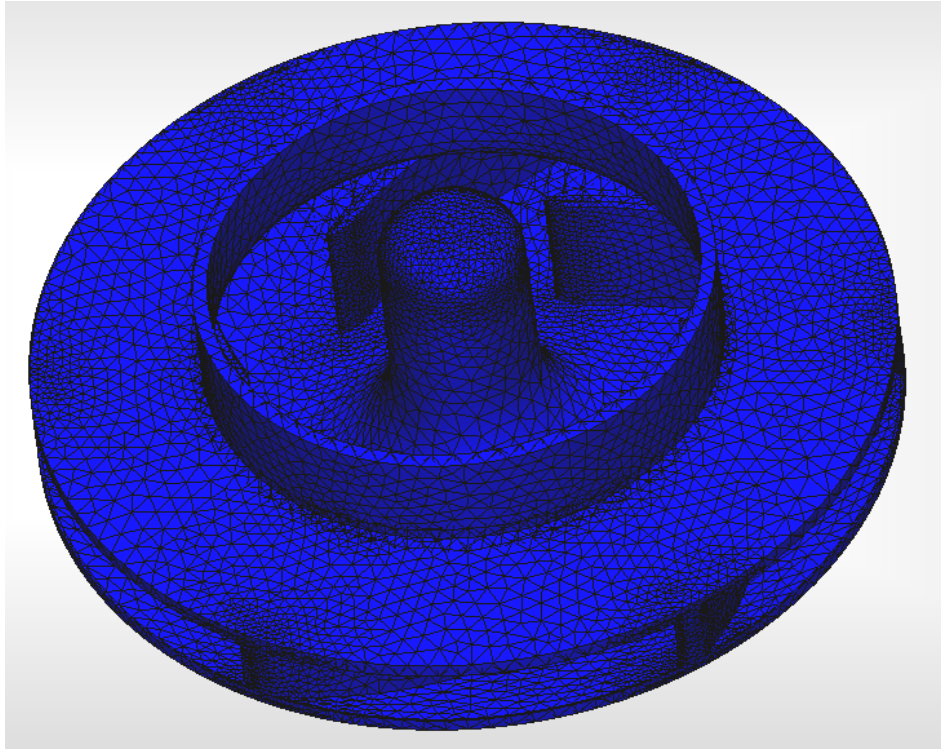


Figure 3.10- Generated mesh at impeller

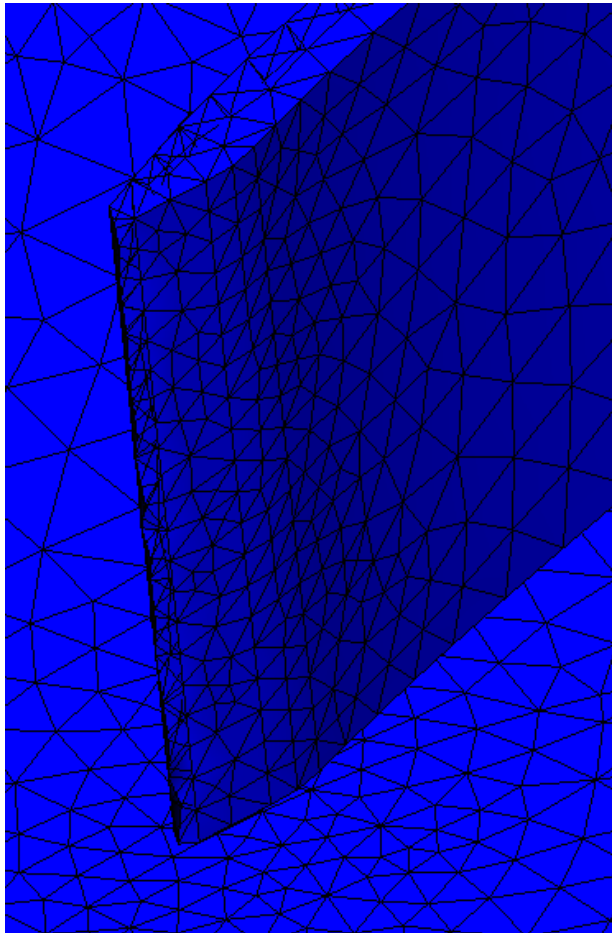


Figure 3.11- Mesh refinement at blade leading edge

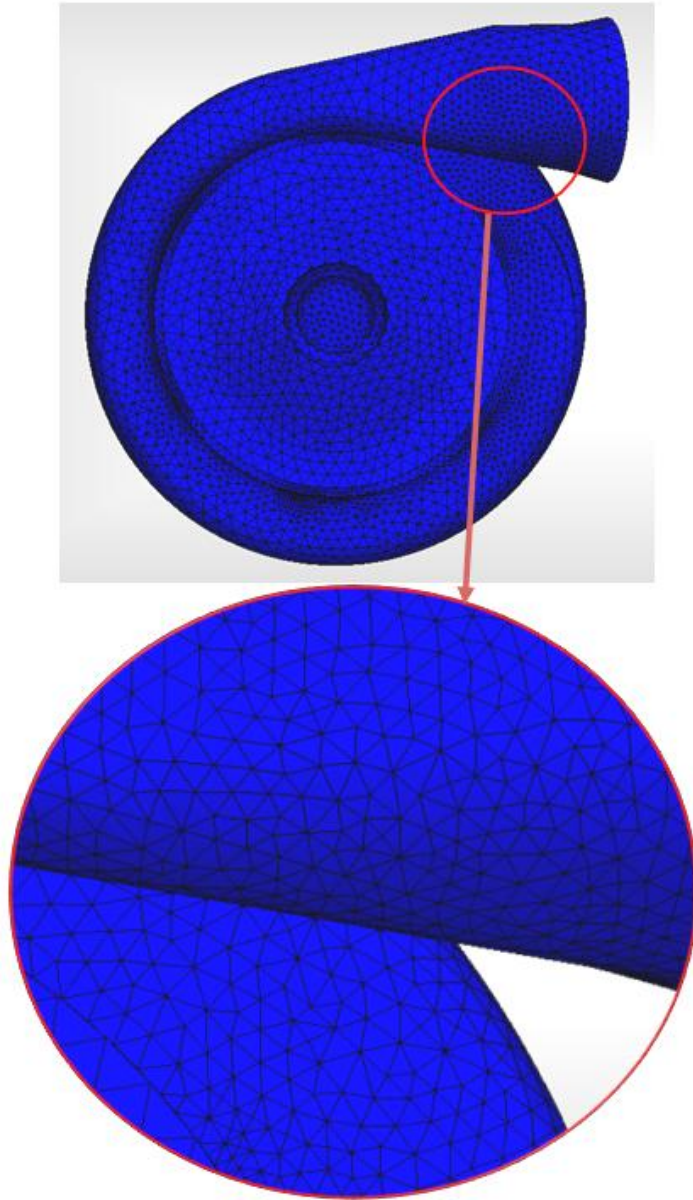
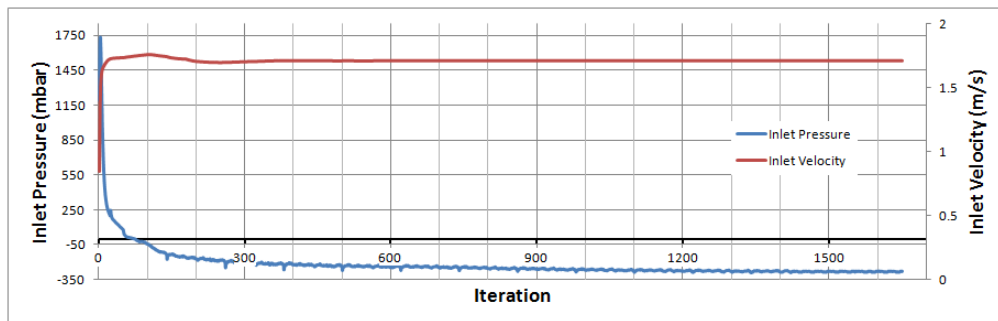


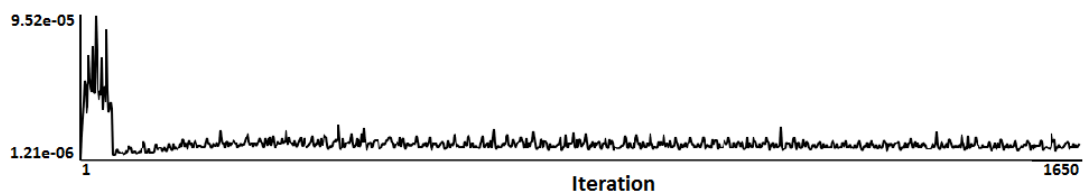
Figure 3.12- Mesh refinement at cutwater region (case 1)

For ramp up of the flow, the first analysis is run with atmospheric pressure BC at inlet and outlet. For the first 100 iterations, a time step size of 0.003311 seconds, which corresponds to blade to blade passage time with 3020 rpm for 6 blades, is used to ramp up the rotational speed. Then, a time step size of 0.0001656 seconds, which corresponds to three degrees per time step of a 6 blade impeller, is used. For the other operating points, outlet BC is kept at atmospheric pressure as before. Inlet BC's are assigned as fully developed volumetric flow rates of 120, 100, 90, 80, 70, 60, 50, 40 and 30 l/min. Apart from ramp up, all operating points are analyzed with 600 iterations corresponding to approximately 5 rotations of the impeller. There are no automatic convergence criteria for turbomachinery analyses in Simulation CFD.

Instead, pressure, velocities, generated torque may be monitored. If the amplitudes of oscillations and residuals fall to an acceptable range, then the analysis can be stopped manually. Successive operating point analyses are run from the time where the previous analysis finished. This reduces number of iterations for convergence since it is easier to change the flow rate by a small amount than ramping up from rest. To illustrate, approximately 1000 more iterations are required for convergence if 60 l/min operating point analysis is started at $t=0$. In order to better explain the convergence mechanism of Simulation CFD, an additional analysis is performed starting from $t=0$ to better show the dissipation of oscillations. Otherwise, since flow is developed at the very first operating point analysis, oscillations dissipate at the beginning of each analysis without convergence yet. That is, even convergence is not reached immediately, a reader who is not familiar with this software may not well distinguish dissipation of oscillations and convergence. In this study, manual convergence criteria are chosen as “change in inlet pressure and hydraulic torque between successive iterations should be less than 3% for the last 25 iterations, and pressure residuals over the entire domain should be less than $1.0e-05$. Since flow rate BC is assigned to inlet, velocity is forced and converged immediately. Convergence plots and hydraulic torque plot for the design point analysis are illustrated in Figures 3.13 and 3.14.



(a)



(b)

Figure 3.13- Convergence plots for design point analysis (case 1)
(a) Inlet pressure and inlet velocity, (b) residual values for pressure

Convergence criteria are achieved at the end of 1650 iterations with a maximum pressure change of 1.63% and with a maximum torque change of 2.53% between successive iterations at the last 25 iterations. Moreover, pressure residuals over the entire domain are approximately converged to 9.75e-06.

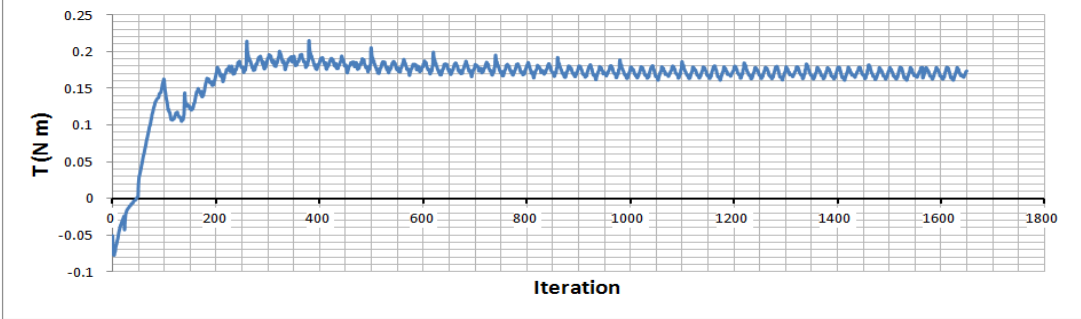


Figure 3.14- Hydraulic torque values for design point analysis (case 1)

Hydraulic performance results (average of last 25 data) of analysis at design point are in a good agreement with theoretically calculated values as shown in Table 3.2:

Table 3.2- Comparison of hydraulic performance parameters between theory and analysis (case 1):

	Q (l/min)	Δp (mbar)	T (N m)	η (%)
Theory	60	300	-0.172	55
Analysis	60	296	-0.167	56

In the Figures 3.15 to 3.22, results of analysis of the design point, which is 60 l/min of volumetric flow rate, are presented:

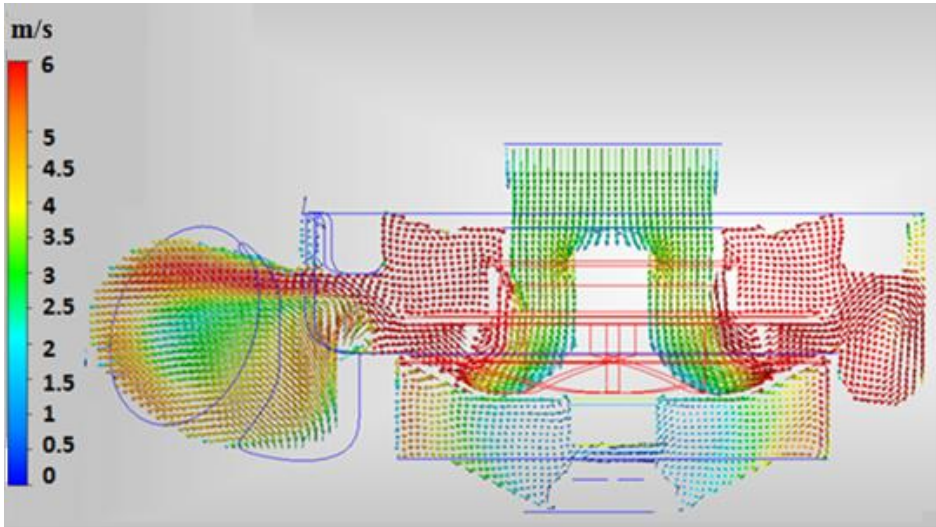


Figure 3.15- Absolute velocity vectors inside the pump on a vertical cut plane (case 1)

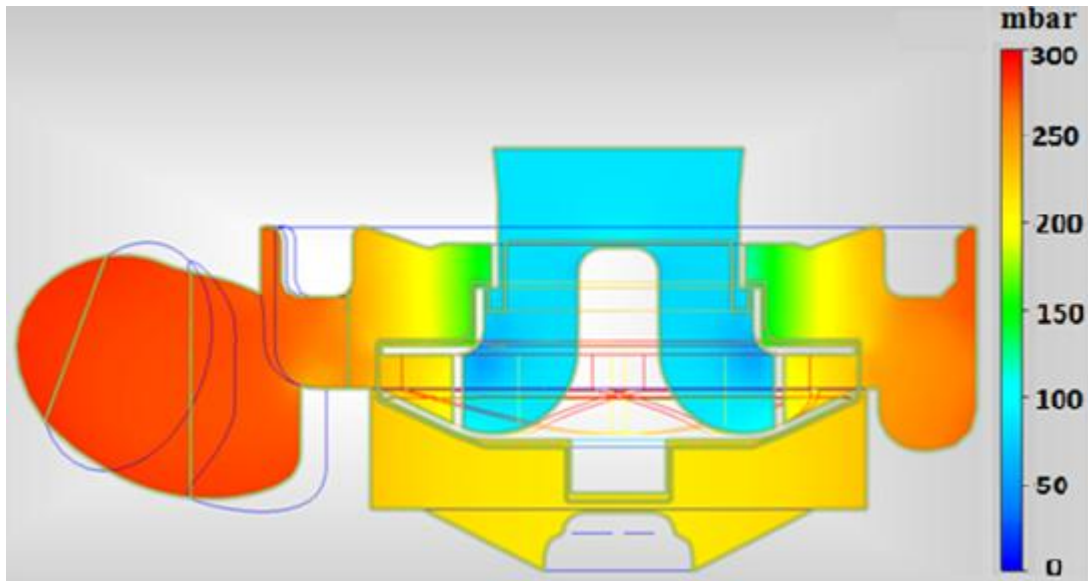


Figure 3.16- Static pressure distribution inside the pump on a vertical cut plane (case 1)

It is seen in Figures 3.15 and 3.16 that velocity and pressure are evenly distributed inside the pump. However, a non-uniform velocity profile is seen near the diffuser. This is due to the effects of cutwater and change in cross-sectional shape. This may be better seen in Figures 3.17 and 3.18:

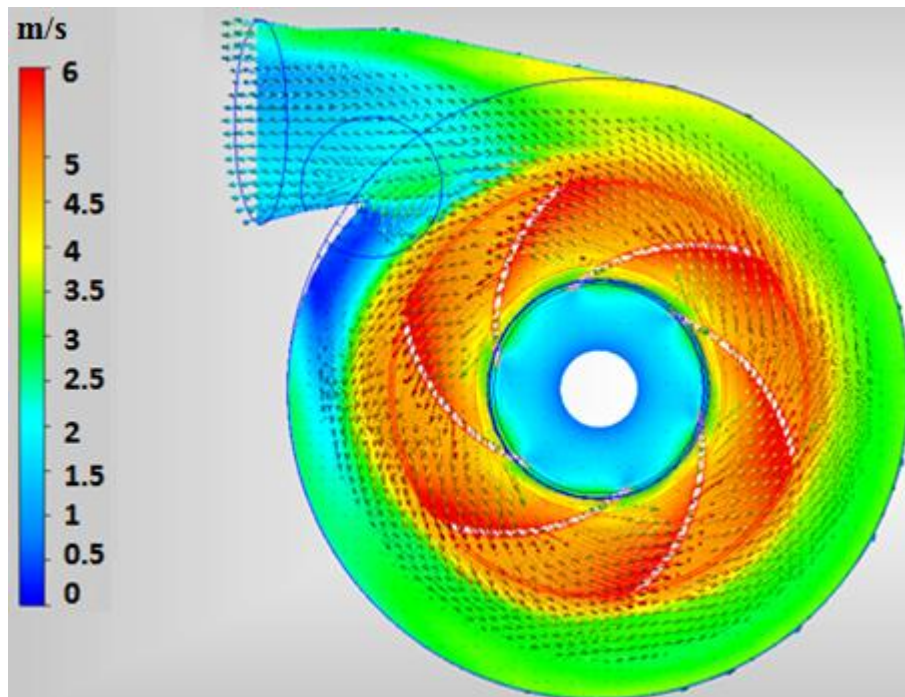


Figure 3.17- Absolute velocity vectors inside the pump on a horizontal cut plane (case 1)

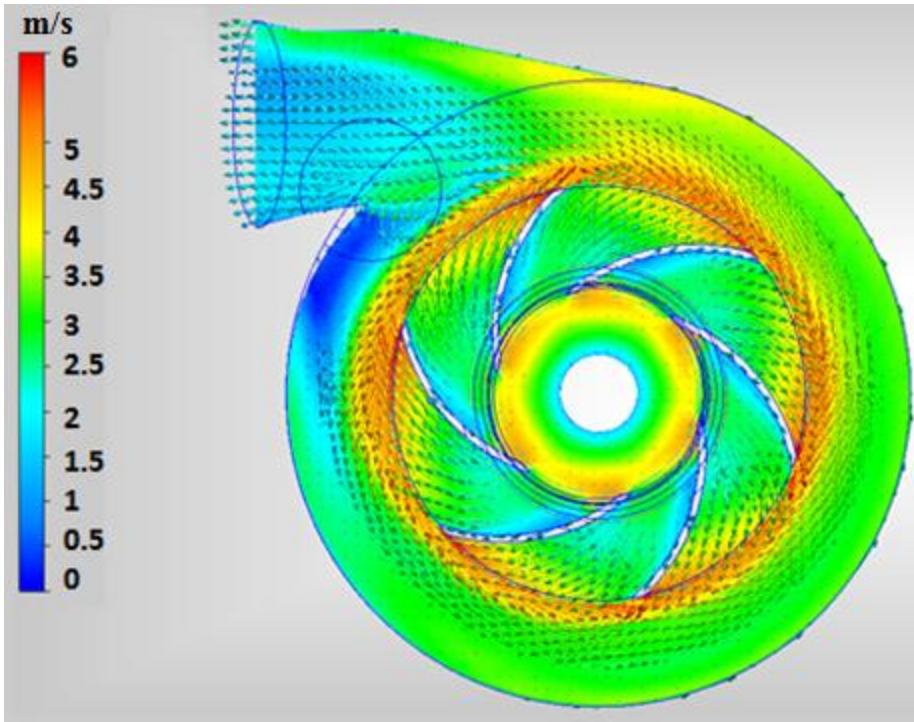


Figure 3.18- Relative velocity vectors inside the pump on a horizontal cut plane (case 1)

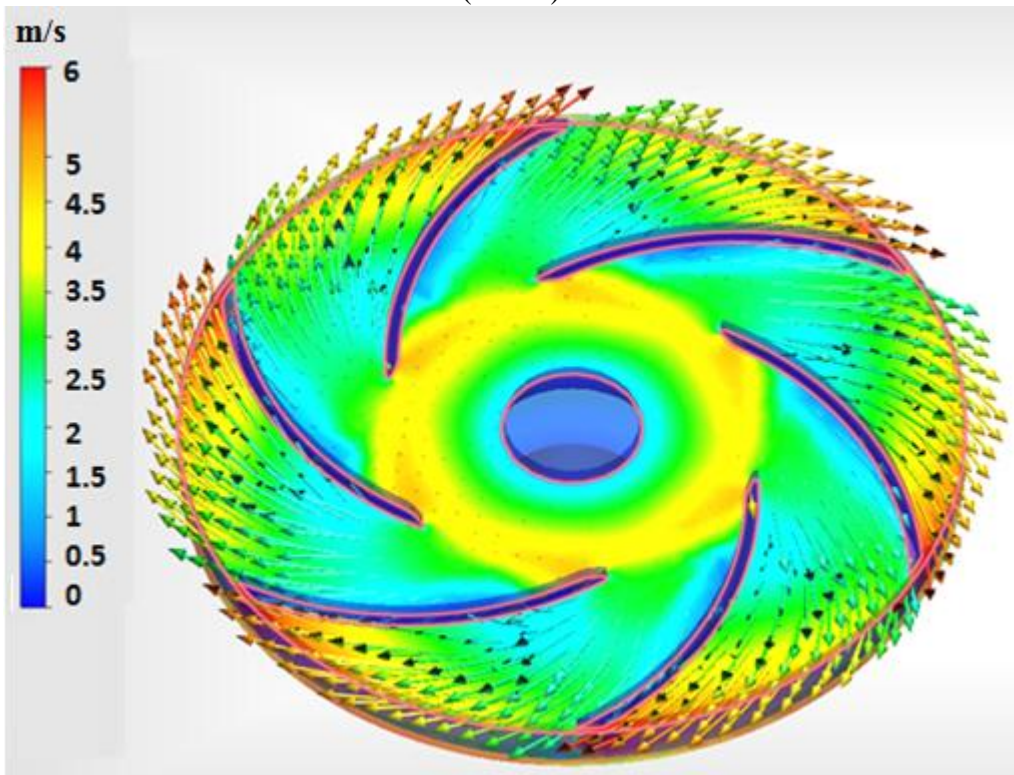


Figure 3.19- Relative velocity vectors through the blades (case 1)

Relative velocity vectors indicate that the fluid particles follow the blade surface in a desired manner. Thus, blade profile is good enough without any problematic regions. It is seen that the flow tries to keep its momentum near the outer wall even after

contracting with the diffuser opening, As a result, flow at the middle section does not have a high velocity. However, after leaving the diffuser, the flow is well developed within the extension pipe. This illustrates the help of extension pipe.

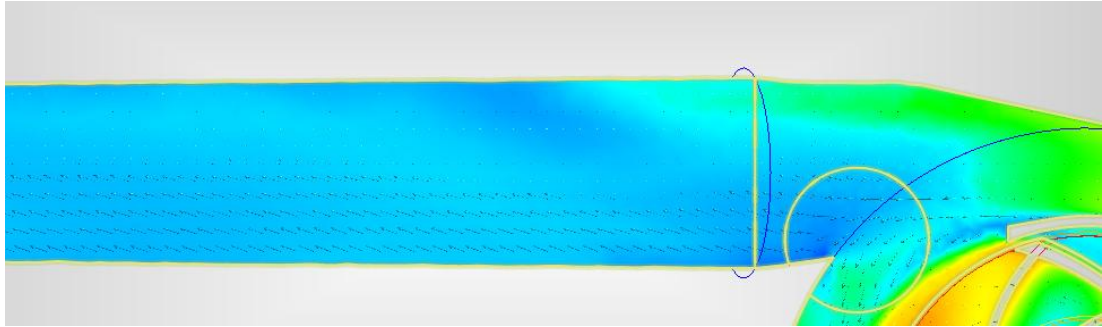


Figure 3.20- Flow development in extension pipe (case 1)

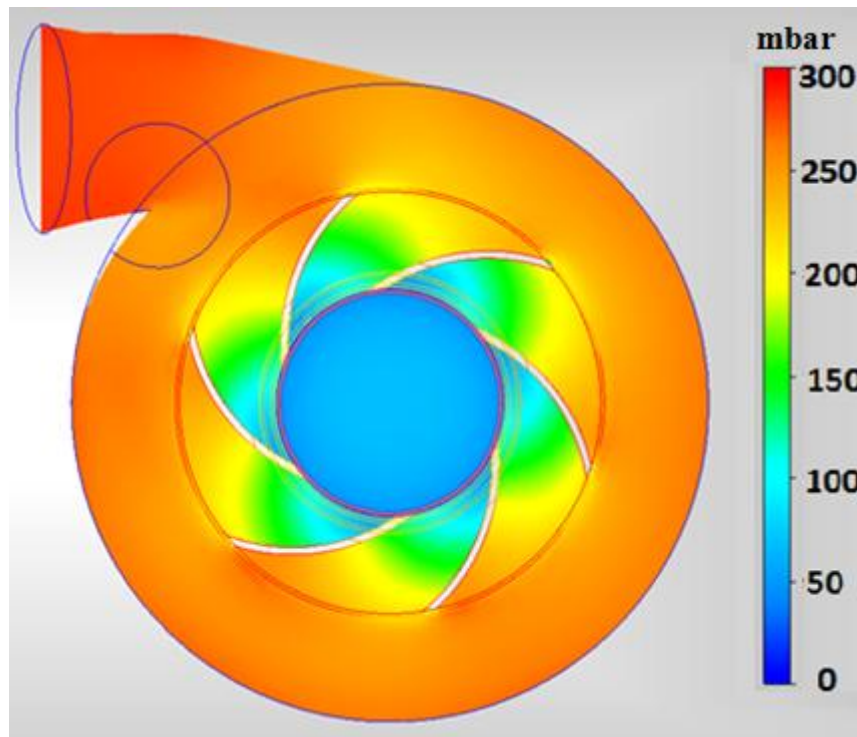


Figure 3.21- Static pressure distribution inside the pump on a horizontal cut plane (case 1)

It is seen that pressure is evenly distributed within the impeller. Pressure is gradually increasing through the blades. Hence, together with the above results, it can be said that the impeller design exhibits sufficient characteristics with the existing volute design of Arçelik.

Analysis results for 9 operating points are shown in Figure 3.22:

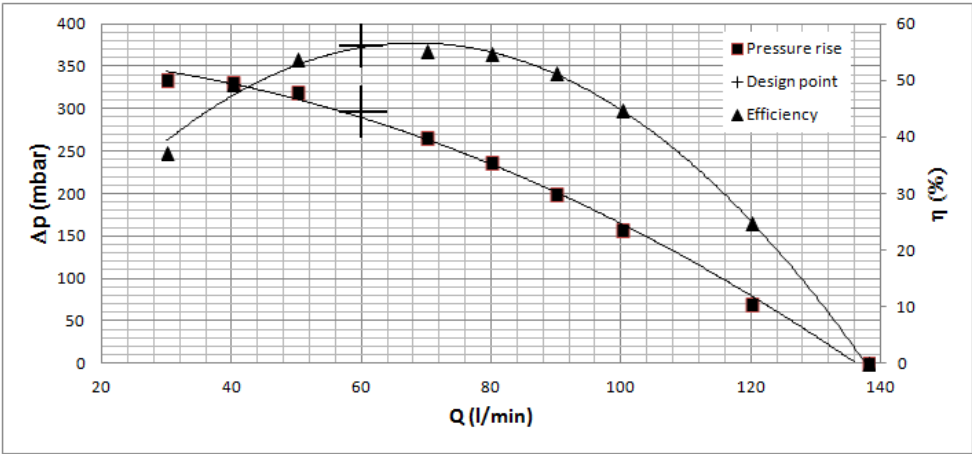


Figure 3.22- Pressure rise versus flow rate and efficiency versus flow rate curves obtained by CFD analysis (case 1)

3.3.2 Analysis and Results for Case 2

In the first case, designed impeller is analyzed by new volute design.

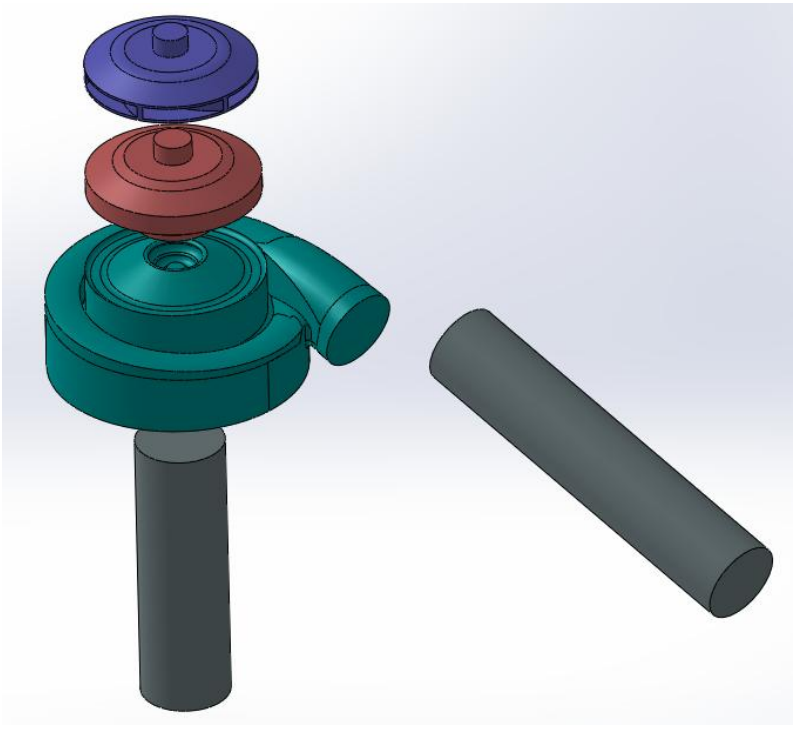


Figure 3.23- Exploded view of pump assembly for case 2

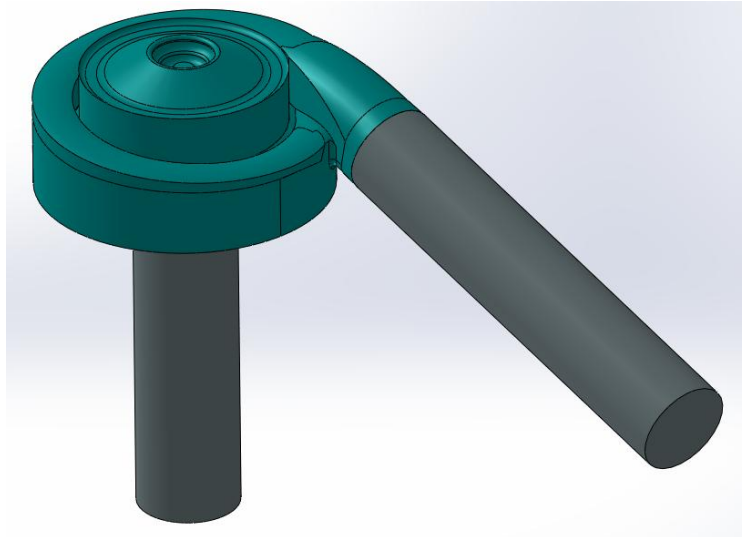


Figure 3.24- Pump assembly model for case 2

Using the same mesh sizes as those of case 1, approximately 199,750 fluid nodes (total nodes) and 773,400 fluid elements (total elements) are generated. This number of elements corresponds to 73% of that of case 1. The reason for this reduction despite the same mesh sizes is the simplicity of the geometry. Comparing Figure 3.24 to Figure 3.7, new volute design has lower amount of rounded surfaces. As a result, lower surface area is obtained resulting in less number of elements.

In Figures 3.25 and 3.26, mesh generation from different views are illustrated:

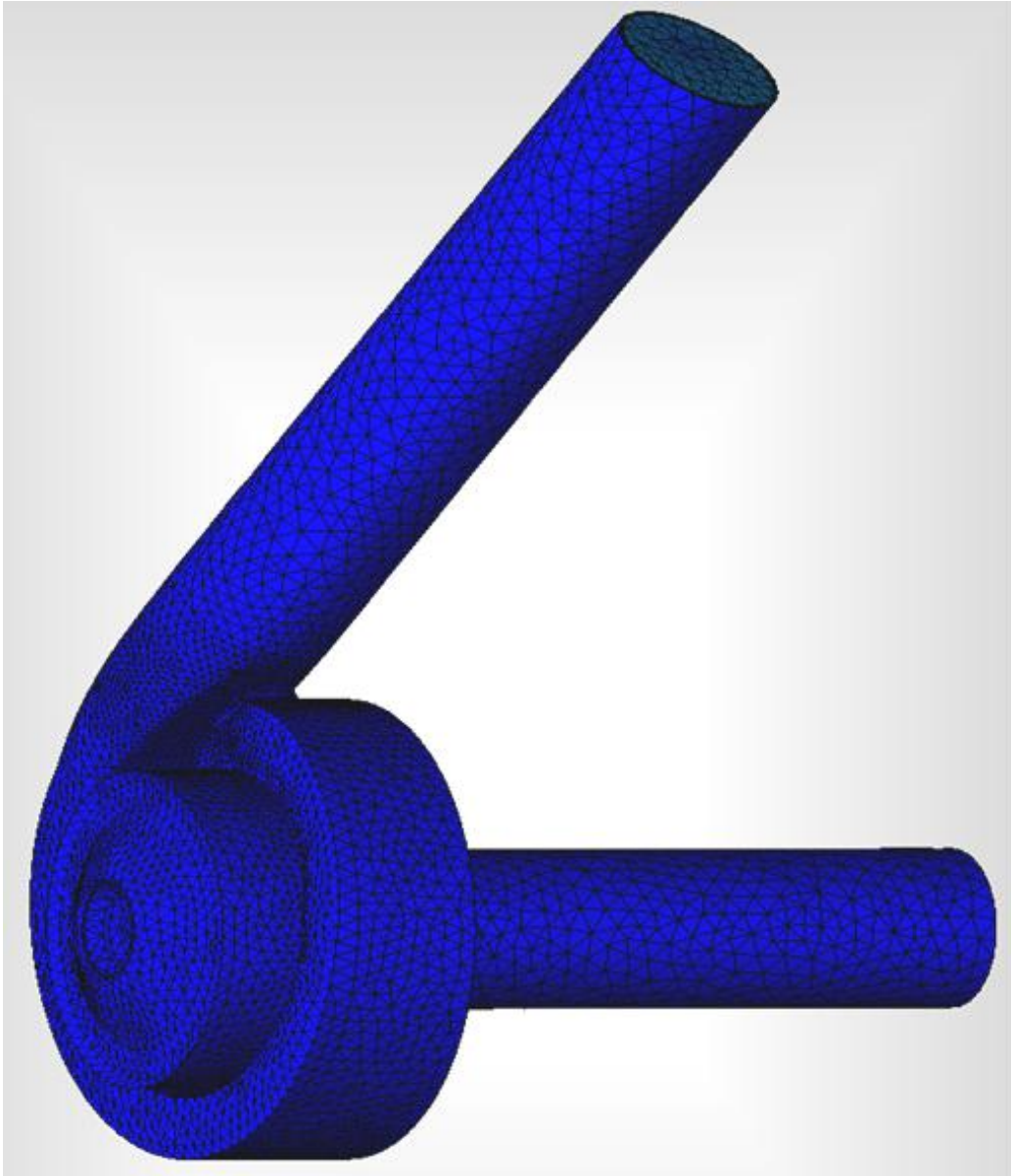


Figure 3.25- Generated mesh-general view (case 2)

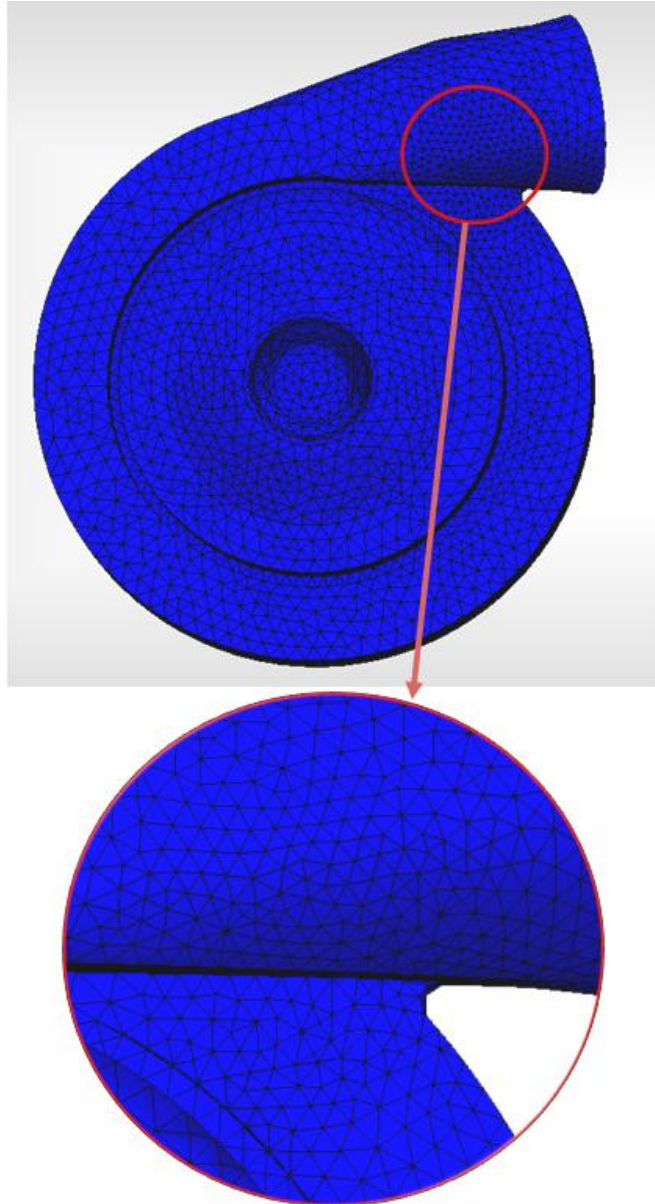
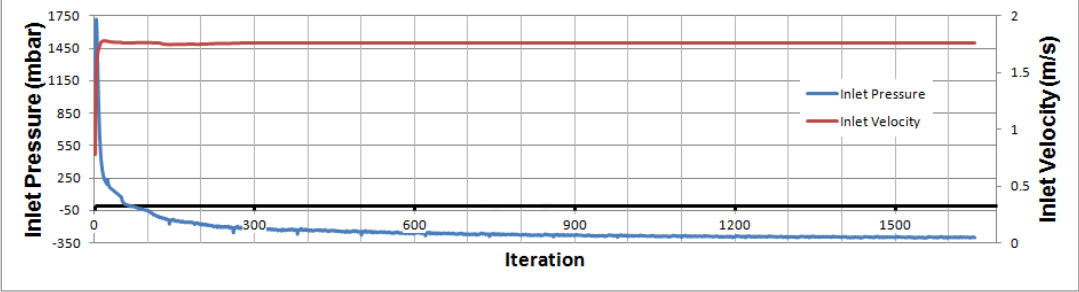


Figure 3.26- Mesh refinement at cutwater region (case 2)

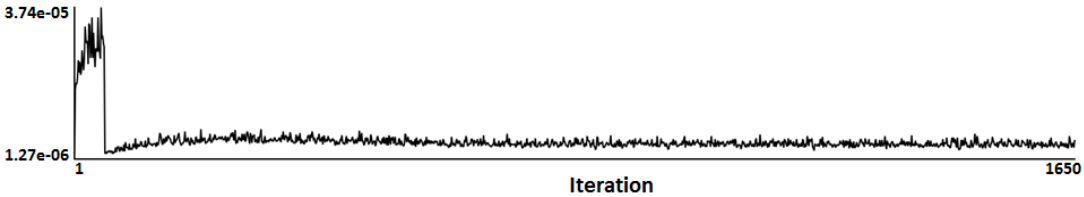
Impeller and blade mesh details are the same as those of case 1 since they have the same geometry and can be seen in Fig's 3.10 and 3.11.

Analyses of different operating points are run just in the same way done in case 1. The same time steps and ramp up conditions are applied. Due to the difference in maximum flow rate, operating points which are analyzed slightly differed for higher flow rates. Beginning with zero inlet and outlet gage pressure BC's, 130, 110, 90, 80, 70, 60, 50, 40 and 30 l/min of flow rates at inlet are analyzed in advance. As done in case 1, hydraulic torque is monitored for convergence. Analyses showed that 500 iterations per operating point is sufficient for aforementioned reasons in case 1. This corresponds to approximately 4.2 rotation of the impeller. However, an additional

analysis at design point starting from $t=0$ is performed as in case 1 for better illustrating convergence with the same criteria. Convergence plots and hydraulic torque plot are as shown in Figure 3.27 for design point:



(a)



(b)

Figure 3.27- Convergence plots for design point analysis (case 2)
 (a) Inlet pressure and inlet velocity , (b) residual values for pressure

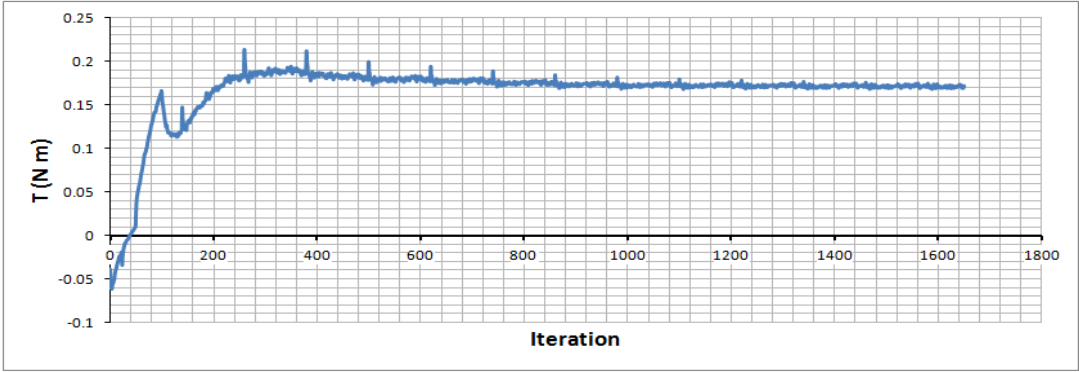


Figure 3.28- Hydraulic torque values for design point analysis (case 2)

Convergence criteria are achieved at the end of 1650 iterations with a maximum pressure change of 1.94% and with a maximum torque change of 1.98% between successive iterations at the last 25 iterations. Moreover, pressure residuals over the entire domain are approximately converged to $5e-06$.

Hydraulic performance results of analysis at design point are in a better agreement with theoretically calculated values compared to those of case 1. The results (average of last 25 data) are as shown in Table 3.3:

Table 3.3- Comparison of hydraulic performance parameters between theory and analysis (case 2):

	Q (l/min)	Δp (mbar)	T (N m)	η (%)
Theory	60	300	0.172	55
Analysis	60	302	0.170	56

In Figures 3.29 to 3.36, results of analysis of the design point, which is 60 l/min of volumetric flow rate, are presented:

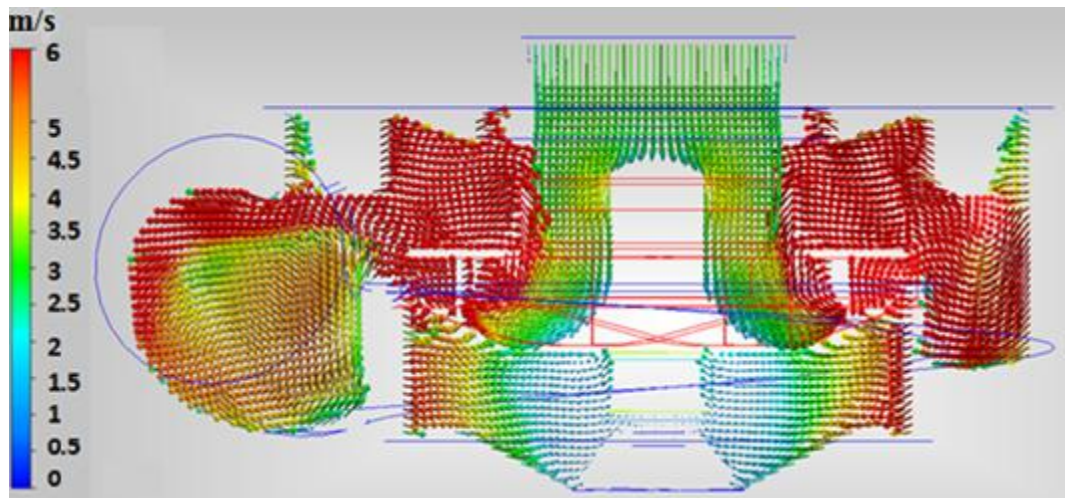


Figure 3.29- Absolute velocity vectors inside the pump on a vertical cut plane (case 2)

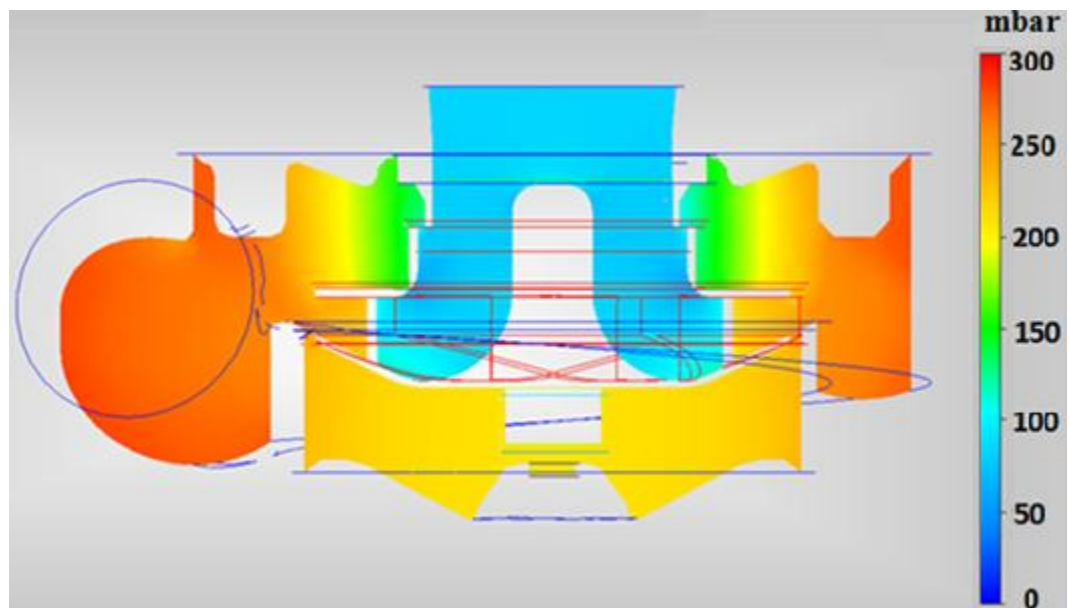


Figure 3.30- Static pressure distribution inside the pump on a vertical cut plane (case 2)

Results seen in Fig's 3.29 and 3.30 are similar to those of case 1. A slight difference is that the near wall velocities are higher in case 2.

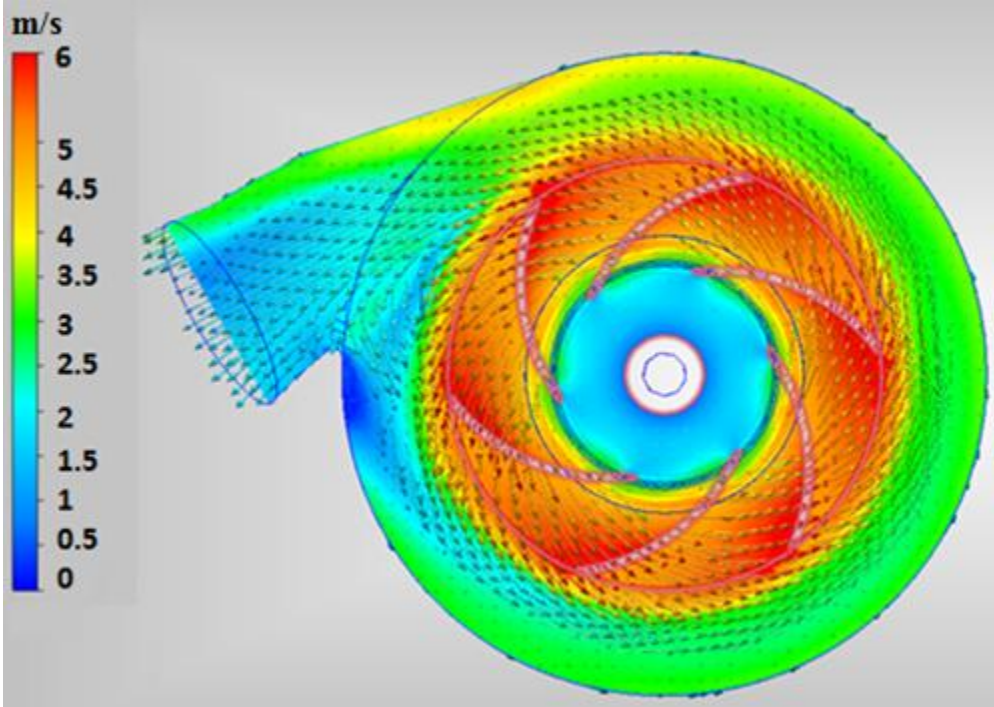


Figure 3.31- Absolute velocity vectors inside the pump on a horizontal cut plane (case 2)

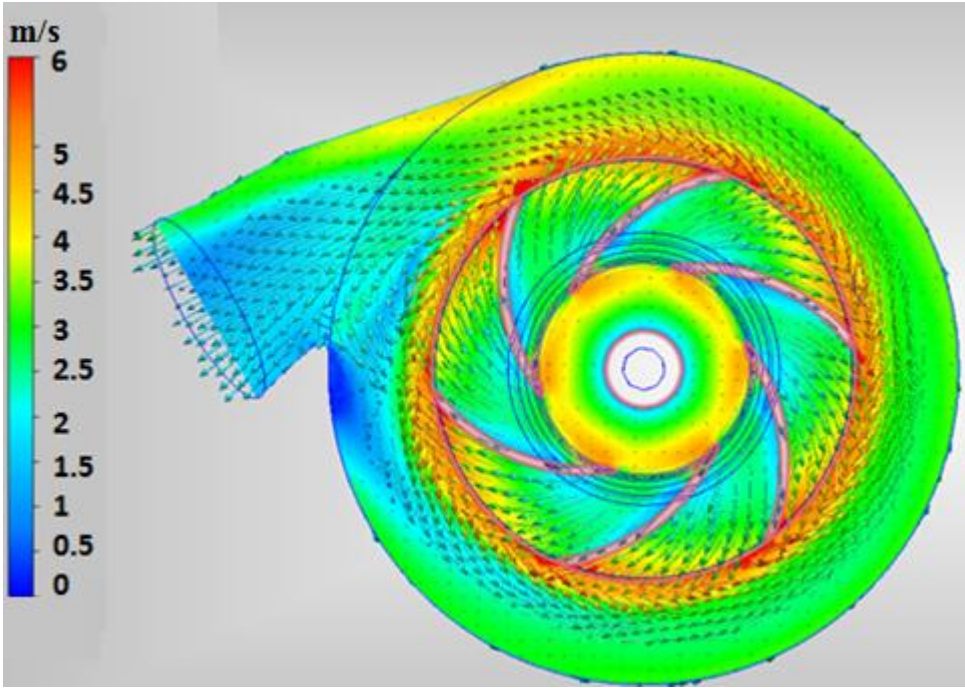


Figure 3.32- Relative velocity vectors inside the pump on a horizontal cut plane (case 2)

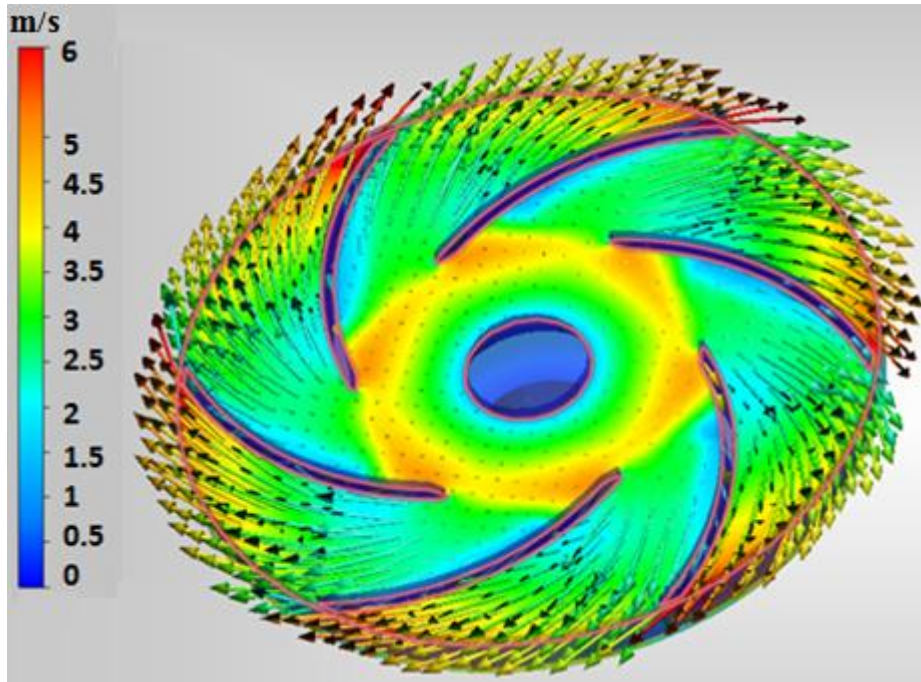


Figure 3.33- Relative velocity vectors through the blades (case 2)

Absolute and relative velocity vectors seen in Figures 3.31 and 3.32 are also similar to those of case 1. Similar effects of cutwater and diffuser entry are observed. Extension pipe at the outlet helps the flow develop as shown in Figure 3.34:

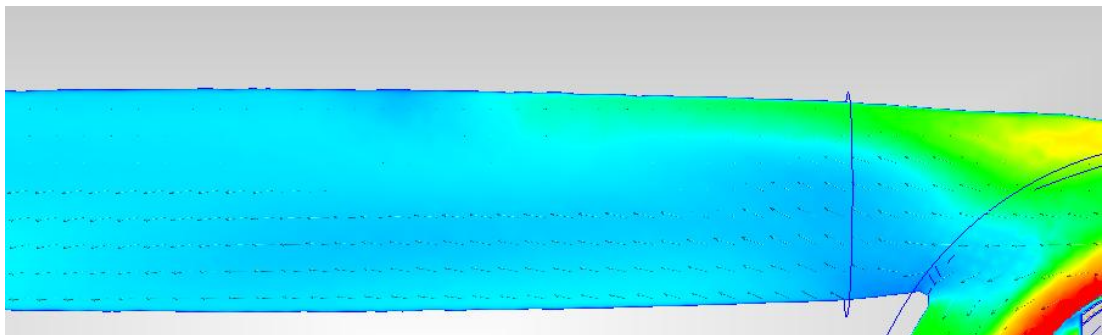


Figure 3.34- Flow development in extension pipe (case 2)

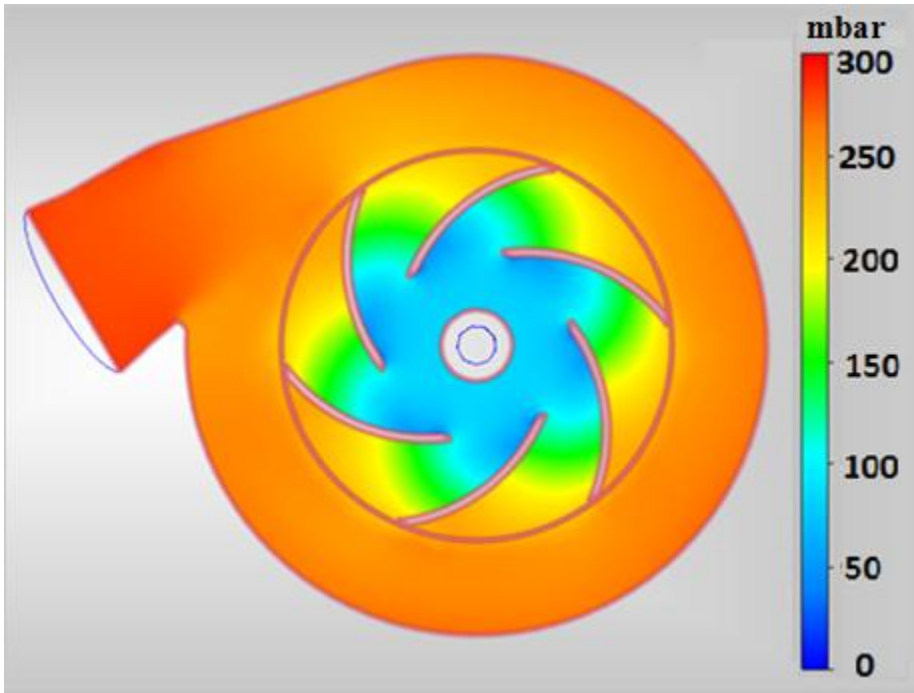


Figure 3.35- Static pressure distribution inside the pump on a horizontal cut plane (case 2)

An evenly distributed pressure profile is observed within the impeller. Compared to case 1, there is no significant change in pressure distribution. Considering this and all the above results, designed impeller and designed volute operate in harmony with good flow characteristics. Analysis results for 9 operating points are shown in Figure 3.36:

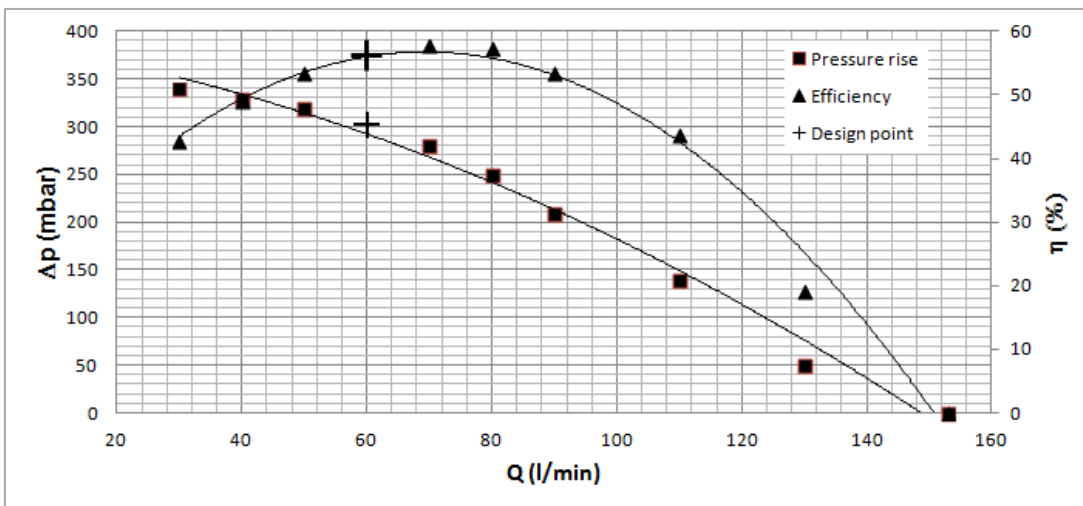
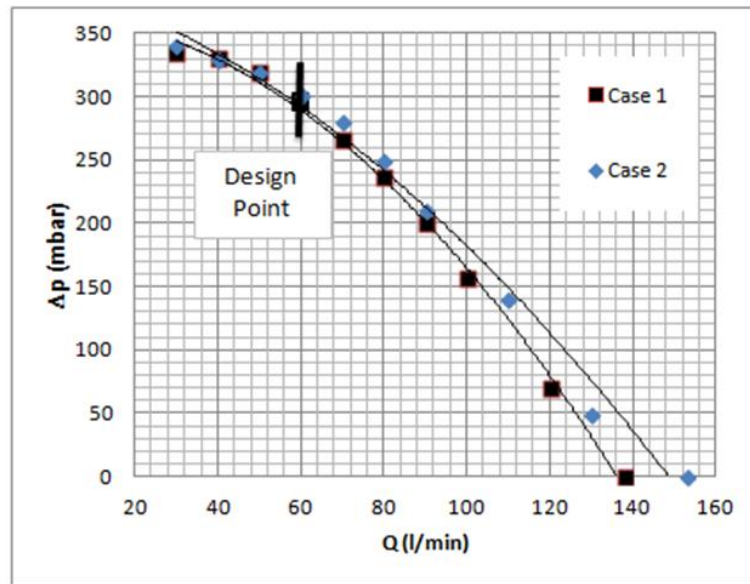
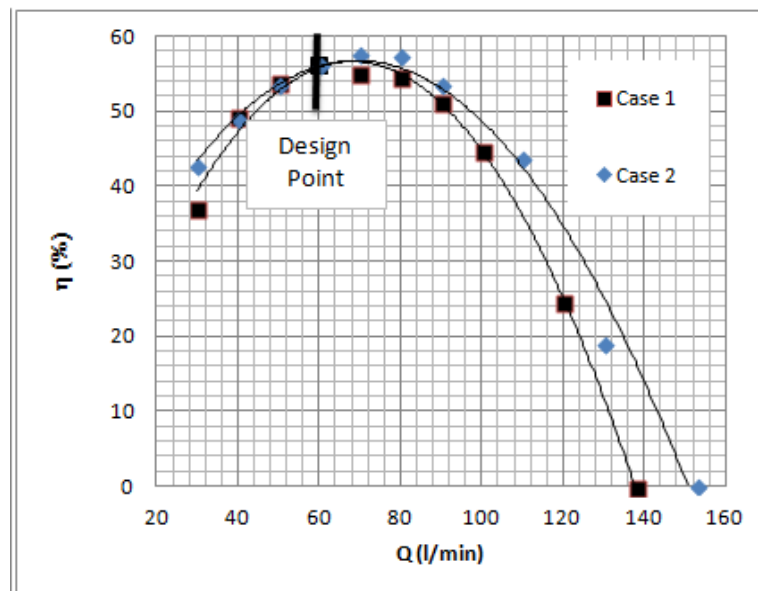


Figure 3.36- Pressure rise versus flow rate and efficiency versus flow rate curves obtained by CFD analysis (case 2)



(a)



(b)

Figure 3.37- Hydraulic performance comparison of case 1 and case 2 by CFD analyses –(a) pressure rise versus flow rate, (b) efficiency versus flow rate

Above results indicate that the new volute design exhibits higher pressure rise and efficiency at higher flow rates. However, performances are almost the same at the design point in both current volute and new volute designs. Considering the fact that the pump may not always operate at the design point, new volute design is more efficient according to CFD analysis results. This shows that the aim of this study, which is to design a more efficient pump for an energy efficient dishwasher, is achieved by numerical solution point of view.

CHAPTER 4

EXPERIMENTAL SETUP AND PROCEDURE

4.1 General about the Tests

Numerically analyzed impeller and volute are prototyped via Selective Laser Sintering (SLS). This is a technique in which a powdered material (glass fiber in this study) is sintered by a laser source in such a way that the laser fuses the powders into the desired solid shape, [41]. The shape is read from the CAD data of STereoLithography (STL) format. It is a file format which “describes only the surface geometry of a three-dimensional object without any representation of color, texture or other common CAD model attribute.”, [42]. The process of SLS is illustrated in Figures 4.1 and 4.2:

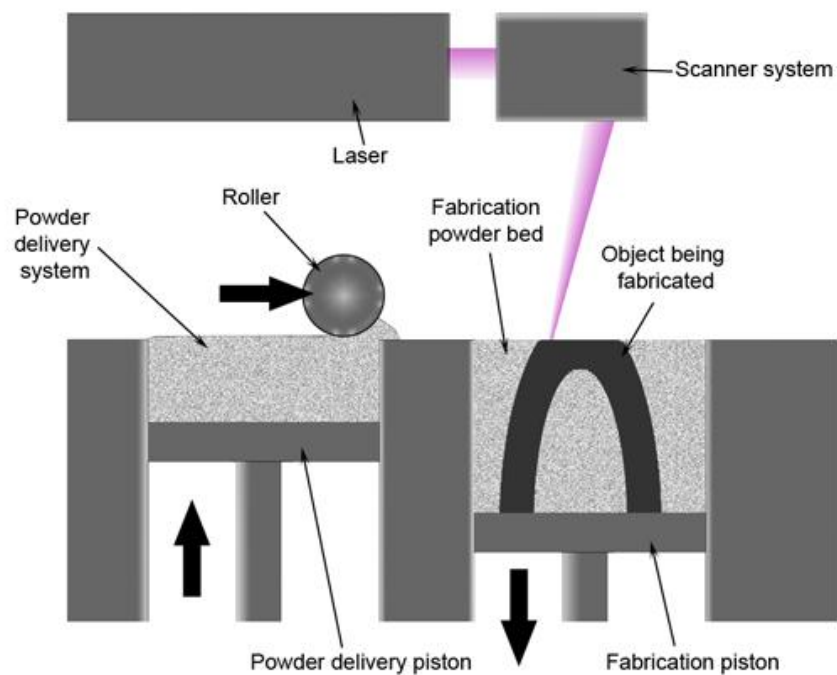


Fig. 4.1- SLS process-I, [41]

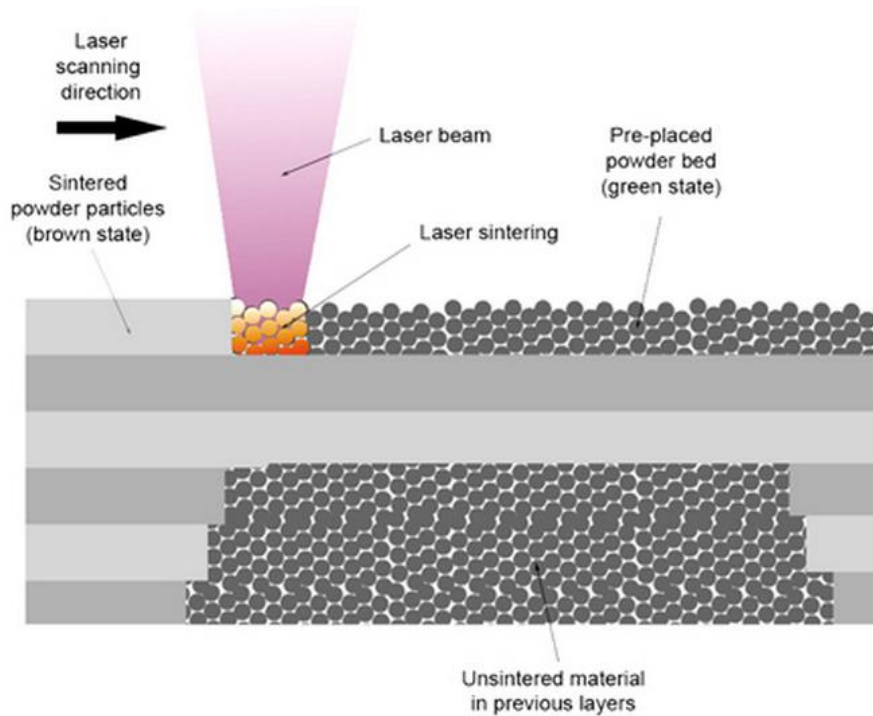


Figure 4.2- SLS process-II, [41]

Prototyped impeller is assembled to the existing volute and BLDC motor assembly of Arçelik for the test of case 1, whereas prototyped impeller and prototyped new volute are assembled to the existing BLDC motor of Arçelik for the test of case 2. After that, hydraulic performances for both cases are tested in Prof. Dr. Cahit Eralp Laboratory in Arçelik R&D Department.

4.2 Test Setup

In the test setup, pump assembly is installed to a pool of dimensions 125 cm x 160 cm x 45 cm (width, length, depth). Outlet of the pump is connected to a hose of diameter 45 mm. At a distance of 50 cm, a 1¼ inch butterfly valve is installed for flow rate adjustment. A pipe from the valve is connected to a magnetic flow meter of nominal size DN 25. Outlet of the flow meter is extended by 25 mm for increased accuracy. Pressure at the discharge is measured by a digital manometer. Electric motor is connected to a driver unit which contains the control board. The driver is plugged in a digital Wattmeter for electrical consumption measurement. Wattmeter is plugged in a 220 V-50 Hz mains. The pool is filled with fresh water at 20°C to a height of 20 cm in order to maintain a stagnant free surface. The test setup schematic is shown in Figure 4.3:

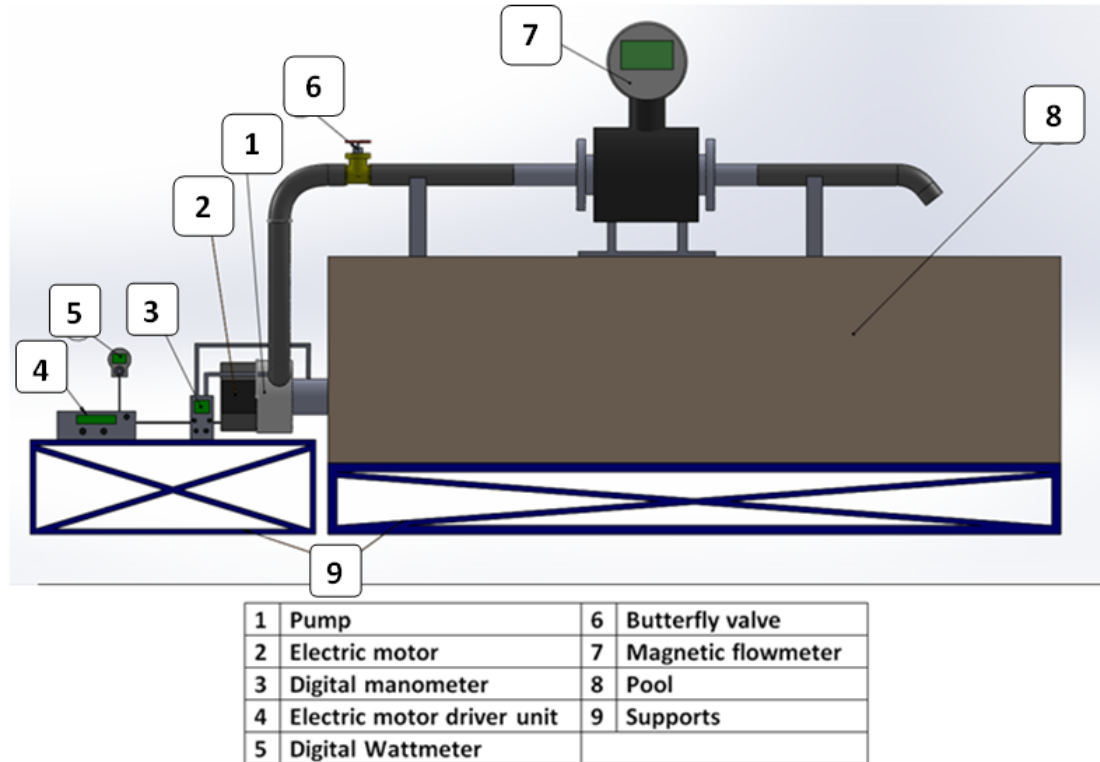


Figure 4.3- Test setup schematic

4.3 Experimental Procedure and Calculations

4.3.1 Experimental Procedure

In order to evaluate the pump performance characteristics, the following procedure is applied.

1. Prototype impeller is assembled to the shaft with interference fit using glue since prototype material might be damaged by threading.
2. Prototype volute is coated with special glue in order not to leak water due to its porous structure. Moreover, the upper part, which represents the heater plate, is strengthened by silicone since it is thin and recessed which might fail upon filled with water and pump is operated.
3. Impeller and volute are assembled to the lower case, which is already coupled with the electric motor.
4. Volute inlet and outlet pipes are drilled for pressure measurements. Fittings of 6 mm diameter are screwed to these threaded holes.
5. Pump assembly is installed to the pool with suitable hoses at inlet and outlet. Outlet hose is connected to the butterfly valve.

6. Flow meter is installed on a platform which stands inside the pool. Suitable hoses are connected between the valve and the flow meter. At the discharge of the flow meter, another hose is connected for aforementioned reasons related to flow. For hose connections, the flow meter has its own flanges at both ends.
7. Suitable small hoses (of pneumatic type) are connected between pressure taps on the pump and pressure sensors. These sensors are plugged into the digital manometer.
8. Driving unit of the motor is connected to the control card by electrical wiring.
9. Driving unit is plugged into the digital Wattmeter, and the Wattmeter is plugged into the 220 V-50 Hz mains plug socket.
10. Having completed the closed loop, pool is filled with fresh water to a certain height.
11. In order to evacuate trapped air inside the pressure hoses, pump is operated while hoses are disconnected from the sensor. Upon water flow is observed, hoses are cleaned from air and then re-connected to the sensors.
12. Digital manometer, magnetic flow meter and driving unit are turned on to start the experiment.
13. Starting at fully opened position, flow is adjusted by closing the butterfly valve for different operating points, taking the pressure value as reference. At each operating point, pressure, flow rate and power consumption values are recorded. In order the flow to reach steady-state, the participant waited for a certain time at each operating point.
14. The pump is stopped.
15. Excluding item 2 (about the prototype volute), procedure is repeated for the existing volute design (for case 1).

4.3.2 Data Processing and Calculations

Recorded data, which are raw yet, are entered into MS Excel[®] in a tabulated form. Units for all the measurements are in required form (mbar for pressure, l/min for flow rate and Watt for power consumption). After that, equations for efficiency calculations are entered. For the calculation of pump overall efficiency, motor efficiency should be known since the ratio of fluid power to electrical power consumption gives pump-electrical motor assembly overall efficiency. Motor

efficiency values with respect to certain torque values are taken from Arçelik Inc. Electric Motor Plant in Çerkezköy. Thus, all the required values are entered into the table. Finally, pump characteristic curves for both cases are plotted using processed data.

4.4 Experimental Results

In Figures 4.4 and 4.5, test results for case 1 and case 2 are presented:

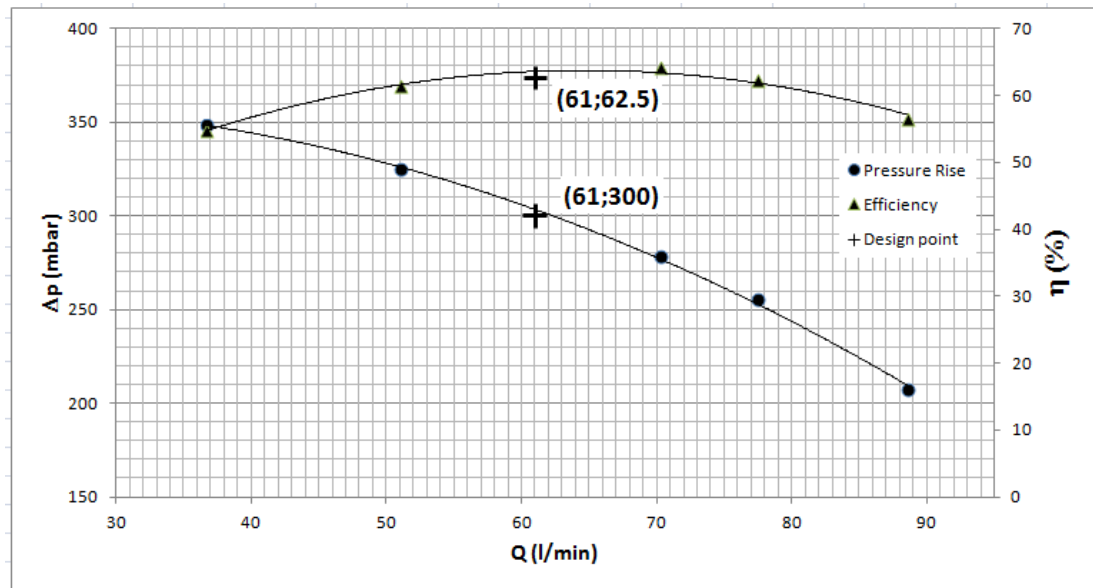


Figure 4.4- Test results for case 1

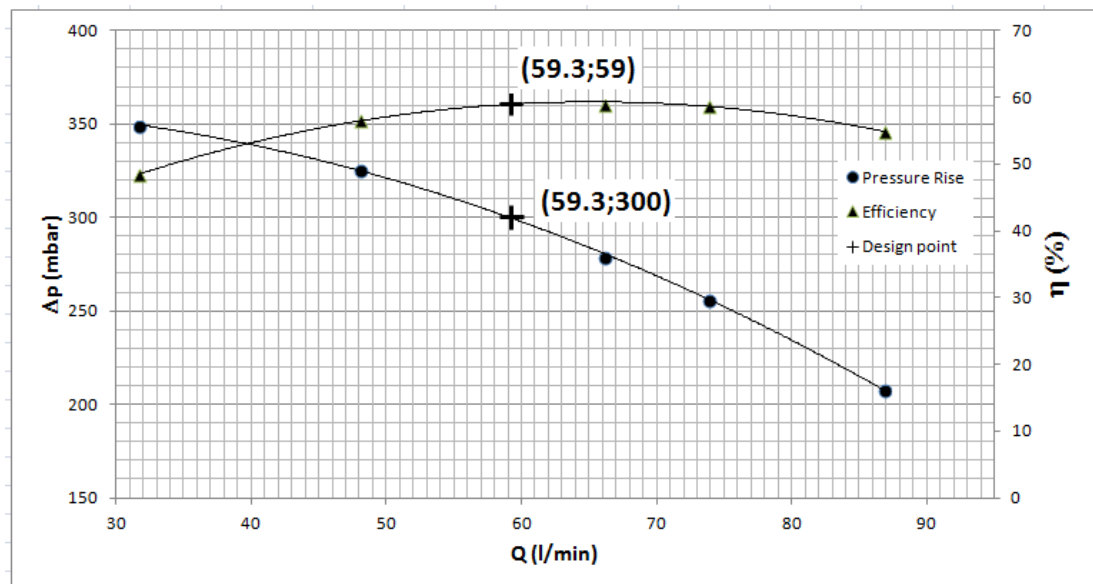


Figure 4.5- Test results for case 2

As seen in Figures 4.4 and 4.5, flow rates at 300 mbar are in good agreement with the theoretical design (+1.67% for case 1 and -0.5% for case 2). Moreover, design

point coincides with BEP, which is one of the ultimate goals of a design. However, tested pump efficiency values are higher than the assumed value of 55% in both cases (+13.6% for case 1 and +7% for case 2). There are three efficiency components in overall efficiency: hydraulic, volumetric and mechanical. Small deviations in these three components may result in larger changes in the overall efficiency. During the design stage, 55% overall efficiency is assumed by a 5% of reduction from the corresponding plot reading to be on the safe side, [29]. This means that 60%, which is very close to the test results, might have been selected as well. As a result, inconsistency between design assumption and test result is not surprising. Indeed, it is a desired case to have higher efficiency in real case. On the other hand, new volute design has lower efficiency values at both design point and at other points. This conflicts with the results of CFD analyses presented in Chapter 3. Nevertheless, this is expected to occur since the existing volute design used in case 1 is of mass production and made from Polypropylene (PP) whereas the new design prototype used in case 2 is produced by SLS with high level of surface roughness. Moreover, to prevent leakage, glue is applied inside and outside the volute which may have been unevenly distributed over the surface. Hence, it is expected that the new design would have higher efficiency values at higher flow rates if it is manufactured as in the same way as that of the existing volute.

4.5 Validation of CFD Analysis Results

Upon conducting laboratory experiments, CFD analysis results are compared with test results. This is made to validate the CFD results. If acceptable agreement is achieved, then design procedure is completed successfully. If, on the other hand, there are considerable differences, CFD analyses should be repeated by certain improvements.

In Figures 4.6 and 4.7, comparison between CFD and test results for both cases are illustrated:

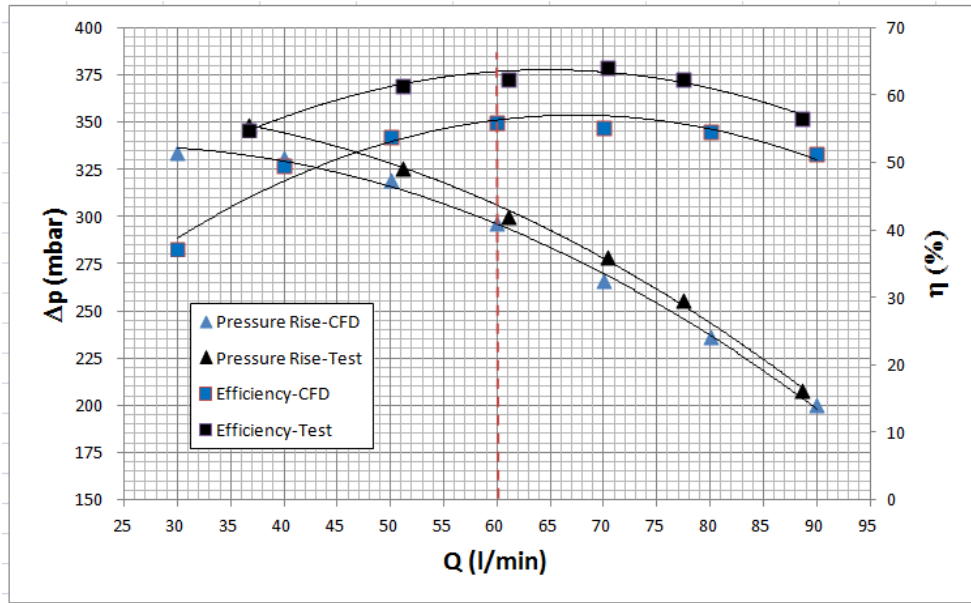


Figure 4.6- Comparison of CFD and test results for case 1

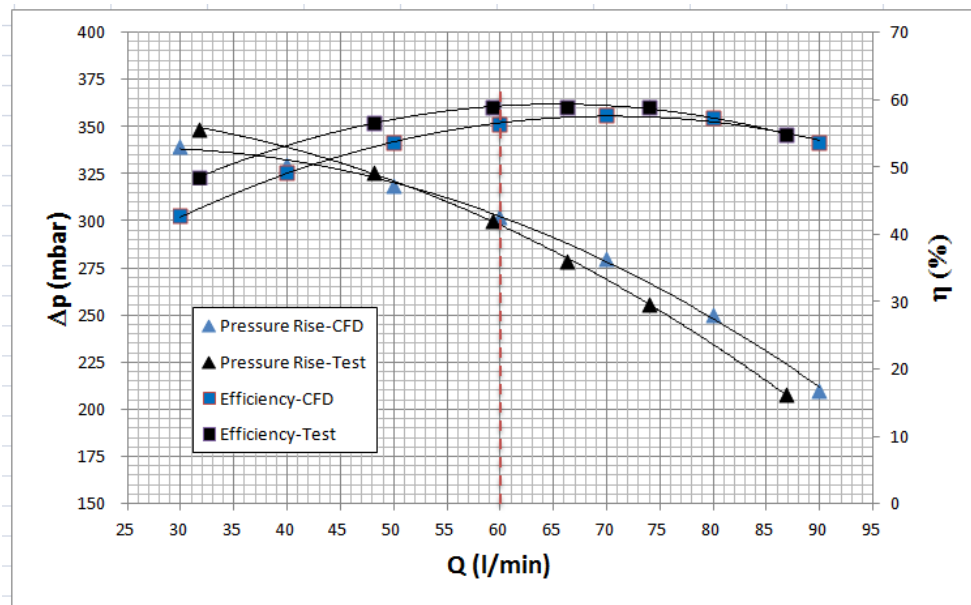


Figure 4.7- Comparison of CFD and test results for case 2

Pressure rise results are in appreciably good agreement especially for case 2. In addition, BEP is achieved at design point for CFD and test results of both cases. On the other hand, CFD analyses predicted less efficiency values for case 1. The reason for this discrepancy is expected to be due to higher volumetric, mechanical and hydraulic efficiency values being higher than the assumed ones. As stated above, it is desirable to have higher efficiency in reality.

In order to decrease the level of inconsistency between CFD and actual test results, leakage passage between impeller and volute may be closed for CFD analyses for future works.

4.6 Improvement in Energy Efficiency Compared to Current Pump

The ultimate goal of this study is to increase the energy efficiency of certain dishwasher models of Arçelik. Hence, new pump design should be compared to the existing one used in those certain models. In Figure 4.8, efficiency values of current pump and new designed pump are illustrated. Due to company policies, numerical values are hidden:

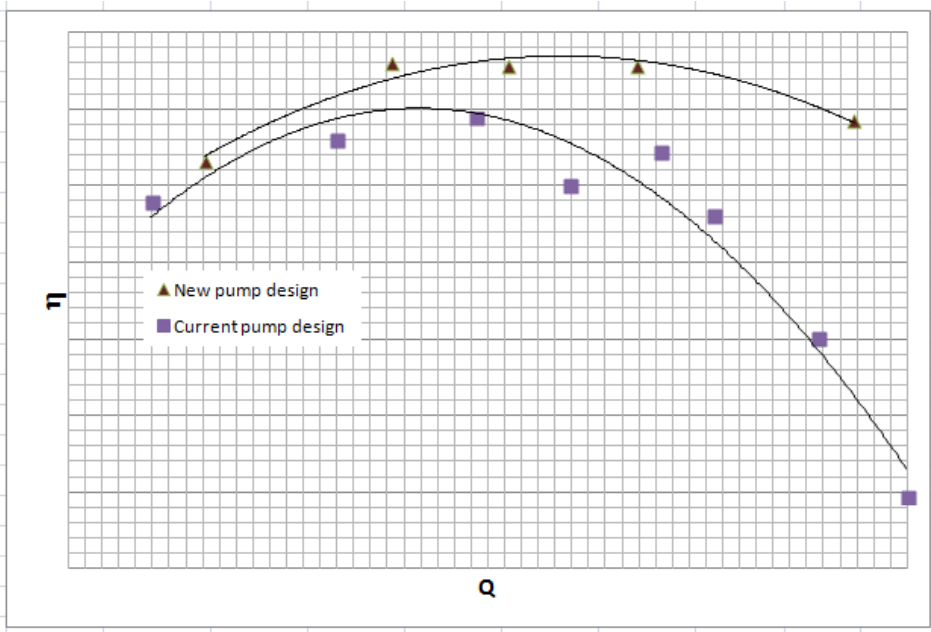


Figure 4.8- Efficiency comparison of current and new pump designs

As seen in Figure 4.8, new pump design has appreciably higher efficiency at all operating points. In addition to getting the desired performance at the design point, higher efficiency goal with respect to the existing pump is achieved. This should be noted that, current pump design is not the same as the pump investigated in case 1. In case 1, impeller is newly designed, while volute is that of one of the current pump models which is used in higher segment dishwashers. On the other hand, “the existing pump” whose efficiency is presented in Figure 4.8 has completely different impeller and volute. As a result, newly designed pump, including impeller and volute, is more efficient than the existing one used in the same segment dishwashers.

CHAPTER 5

SUMMARY AND CONCLUSION

5.1 Summary

In this thesis, a centrifugal circulation pump for an energy efficient Arçelik dishwasher is designed. Furthermore, designed pump is analyzed by means of CFD and tested in laboratory using a prototype produced by SLS technology.

There are certain methods in literature to design a centrifugal pump. However, it is the application area that defines the design constraints, hence the final design. Dishwasher circulation pumps have certain design characteristics as well. Hence, not only empirical methods present in literature, but also Arçelik's previous experience and data base played a significant role during the design stage.

The design point of the pump in question is defined according to the needs of Arçelik. To be more clear, the pump is desired to deliver 60 liters of water per minute against a system which causes the pump to operate at pressure of 300 mbar at the BEP. The pump has a nominal rotational speed of 3020 rpm with the current control system. Moreover, the pump is to have a heating facility integrated on it. The heater plate being fixed in shape, and electric motor being the current model, pump volute outer geometry is fixed as well. A design effort is spent on the impeller and on the inner shape of the volute in this study.

Design procedures for impeller and volute are discussed in Chapter 2 in detail. Final dimensions and CAD models are presented as well. Auxiliary mechanical parts for the pump assembly are chosen from one of the current pumps in order to communize as many parts as possible, which contributes to financial improvement as well as planning.

Having designed the hydraulic parts, numerical experimentation is conducted in order to predict the performance of the designed pump. Being discussed in depth in Chapter 3, two different cases, one with current volute and designed impeller and the other with designed volute and designed impeller, are investigated. Results showed that the new impeller achieves to match with theoretical design point for both

volute. Moreover, new volute design acts similar to the existing one while at higher flows it is expected to be more efficient.

Upon finalizing CFD analyses, designed parts are prototyped by means of SLS technology. Being made of glass fiber, the parts are highly rough compared to PP which is the actual material used in mass production. Moreover, prototype volute is coated with special glue for leakage retardation. Furthermore, since production tolerances are coarse in SLS, parts are manually treated in order to be assembled comfortably. Hence, new designed volute's actual test performance is less efficient than that of the existing volute which has superior surface characteristics and assembly quality. Thus, if a higher quality material is used for manufacturing of the new design of volute, the performance is expected to increase.

Finally, new designed pump exhibits higher efficiency compared to the existing pump at any operating point. As a result, energy efficient dishwasher aim is achieved.

5.2 Conclusion

The designed centrifugal pump for an energy efficient dishwasher complies with design specifications according to both CFD analyses and actual test results. Indeed, overall efficiency value obtained during tests is higher than the theoretically assumed one considering the design point. As a result, it can be deduced that the designed pump fulfills the requirements of Arçelik dishwasher.

Having explained earlier in depth, CFD results for pressure rise are in appreciable agreement with test results; whereas, efficiency values differ in some points which can be improved by some modifications in solid models prepared for CFD. Considering the mesh sizes, acceptable convergence is obtained in all operating points for both cases. Having checked for mesh dependency, used mesh sizes for different parts of the pump may be considered as default values whenever analyzing a pump of similar geometry and size. Hence, the CFD part of this study brings appreciable benefits in Arçelik's database.

Since two cases are discussed in this thesis, there exists an opportunity for comparing current volute design and new volute design. Although the existing design exhibits higher efficiency values in tests, CFD analyses give a green light to the new design that it may have similar efficiency values near the design point and even better

efficiency values above the design point. As discussed in Chapter 4 and earlier in this chapter, manufacturing the new volute as in the same way as the existing one will help the designer make more realistic comparison. If, on the other hand, the efficiency is not increased sufficiently, some modifications may be made on the pump, such as applying underfiling on the trailing edge as discussed in Chapter 2. In this case, an increase in performance is expected, [6].

During the design, although empirical methods introduced by Gülich, Lazarkiewicz, Pfleiderer, Stepanoff and so on are highly used, Arçelik's previous experiences and experimental database are also taken as strong references since the ones in literature represent the general case, while Arçelik's previous studies stand for specific area of application. To illustrate, outer profile of the impeller and the volute are taken from current designs in used in Arçelik dishwashers. The contribution of this thesis is obtained by new blade design and new volute inner profile since the pump is to be used in different types of dishwashers than those use the current ones.

In this study, mold designs for the designed parts are not discussed. The reason is that, Arçelik Inc. outsources for the mold designs. Arçelik Inc. supplies the mold companies with CAD model and technical drawing and then they decide the manufacturing method and design molds accordingly. In general, PP volute and impeller are produced by injection molding. Hence, the designed parts in this thesis are also to be manufactured in the same manner. Moreover, none of the mechanical parts, which are used in current pumps of the similar type, are changed. As a result, additional effort for those parts is not spent in the scope of this thesis.

5.3 Additional Contributions and Future Work

The studies made in this thesis constitute one of the three work packages of a TÜBİTAK TEYDEB 1501 project about an energy efficient dishwasher. By the help of this thesis, corresponding work package is automatically finished by success. With the new designed pump, certain types of dishwasher models of Arçelik are to be more efficient than their previous condition. As a result, Arçelik Inc. became entitled to be promoted by TÜBİTAK.

Another contribution of this study is that a declaration is prepared to be presented at POMSAD 9th Pump-Valve-Compressor Conference, which is to be held on May 4th-6th, 2016. The topic of the declaration is similar to that of this study; but, a different

impeller design is made for a different type of circulation pump of Arçelik dishwasher. MS Excel[®] pump design sheet prepared in this thesis is used for the design discussed in the declaration. Moreover, effect of underfiling, which is discussed in Chapter 2, is covered in that study.

Having contributed to a TEYDEB project and to a POMSAD declaration, this thesis is a reference material for future pump design projects of Arçelik Inc. Furthermore, any designer may benefit from the studies covered in this thesis in the future.

In order to improve the design of this study, modifications in design parameters may be tried. Their effects on the performance may be observed by using CFD analyses which helped a lot throughout this study as discussed earlier. Since analysis and test results of the designed pump are present in this thesis, one may establish a correlation between newer designs.

Lastly, energy efficiency and life cost become more and more important as the time passes. Hence, further improvements for pump efficiency (and overall dishwasher efficiency in advance) are an inevitable aim of Arçelik Inc., whose slogan is “Respects the Globe, Respected Globally”. Considering this fact, more efficient and long-lasting pump designs are to be made in the light of this thesis.

REFERENCES

1. Wikipedia, <http://en.wikipedia.org/wiki/Dishwasher>, [last visited on October 2013]
2. Arçelik Dishwasher Plant, System Design Team, R&D Department. (2013). *Grundig project:Dishwasher hydraulic system report* (Report No. 1.3.7.17). Ankara: Arçelik Inc.
3. LG Electronics Inc., (2013). *Dishwasher and control method therfor*. US20130139854A1.
4. Ingram, G. (2009). *Basic concepts in turbomachinery*. Frederiksberg: Ventus Publishing ApS.
5. Karassik, I. (1986). *Pump handbook* (2nd ed.). New York: McGraw-Hill.
6. Gülich, J. F. (2010). *Centrifugal pumps* (2nd ed.). Berlin: Springer-Verlag.
7. Wikipedia, http://en.wikipedia.org/wiki/Centrifugal_pump#cite_note-Ladislao_Reti_290-2, [last visited on October 2013]
8. Üçer, A. Ş. (1982). *Turbomachinery*, Class Notes (ME-METU), Ankara
9. Sert, C. (n.d.), *ME 306 fluid mechanics II part 3: Turbomachinery* [Powerpoint slides]. Retrieved from <http://users.metu.edu.tr/csert/me306/ME%20306%20Part%203%20Turbomachinery.pdf>, [last visited on November 2013]
10. *The Centrifugal Pump Handbook* (n.d.) Grundfos Industrie, Denmark
11. Özerengin, F. (1972). *Santrifüj ve eksenel akımlı pompalar: Özellikler, hesap metodları, konstrüksiyon*. İstanbul: Kutulmuş Matbaası.

12. Oto-Hui, http://mechanical-engg.com/forum/uploads/1247310097/gallery_53_11_16271.jpg, [last visited on October 2013]
13. Roymech, http://www.roymech.co.uk/images/volute_diffuser.gif, [last visited on October 2013]
14. Fitzgerald, A., & Kingsley, C. (1971). *Electric machinery: The processes, devices, and systems of electromechanical energy conversion* (3rd ed.). New York: McGraw-Hill.
15. Fletcher, C. (1991). *Computational techniques for fluid dynamics 1: Fundamental and general techniques* (2nd ed.) (R. Glowinski, M. Holt, P. Hut, H. Keller, & J. Killeen, Eds.). Berlin: Springer-Verlag.
16. Wendt, J. (2009). *Computational fluid dynamics: An introduction* (3rd ed.). Berlin: Springer.
17. Jameson, A. (2012). *Computational fluid dynamics past, present and future* [Powerpoint slides]. Retrieved from http://aero-comlab.stanford.edu/Papers/NASA_Presentation_20121030.pdf, [last visited on November 2013]
18. Blazek, J. (2005). *Computational fluid dynamics principles and applications* (2nd ed.). Amsterdam: Elsevier.
19. MDPI, Open Access Journals Platform, <http://www.mdpi.com/2073-431X/4/1/24/htm> [last visited on December 2015]
20. Consumer Information, <http://www.consumer.ftc.gov/articles/0072-shopping-home-appliances-use-energyguide-label>, [last visited on November 2013]

21. Gov.uk,
https://www.gov.uk/government/uploads/system/uploads/attachment_data/file/69295/pb13466-eu-energy-label.pdf, [last visited on November 2013]
22. Energy Rating, <http://www.energyrating.gov.au/>, [last visited on November 2013]
23. European Commision, http://europa.eu/rapid/press-release_IP-10-584_e.htm, [last visited on November 2013]
24. Dries, J. (n.d.), *Fundamentally increasing dishwasher efficiency*, Dries Engineering
25. ETSU, AEAT PLC, *Study on improving the energy efficiency of pumps*, European Commission, 2001, Retrieved from http://www.waterymex.org/Waterymex%20Toolkit/resources/53_Improving%20Energy%20Efficiency%20of%20Pumps.pdf, [last visited on November 2013]
26. Sahoo, T. (2012). *Strategies to increase energy efficiency of centrifugal pumps*, Centrifugal Pumps, Dr. Dimitris Papantonis (Ed.), ISBN: 978-953-51-0051-5, InTech, Retrieved from <http://www.intechopen.com/books/centrifugal-pumps/strategies-to-increase-energy-efficiency-of-centrifugalpumps>, [last visited on November 2013]
27. Lazarkiewicz, S. and Troskolanski, A. T. (1965). *Impeller pumps*, Oxford: Pergamon Press Ltd.
28. Pflaiderer, J. (1978). *Akım makinaları* (4th ed.) (H. Petermann, Ed.; K. Edis, Trans.). İstanbul: İstanbul Teknik Üniversitesi Matbaası
29. Baysal, K. (1975). *Tam santrifüj pompalar: Hesap, çizim ve konstrüksiyon özellikleri*. İstanbul: İstanbul Teknik Üniversitesi Matbaası.

30. Liu, H. et al (2010). Effects of blade number on characteristics of centrifugal pumps. *Chinese Journal of Mechanical Engineering*, 23(06), p. 742
<http://dx.doi.org/10.3901/CJME.2010.06.742>
31. Kovats, A., & Desmur, G. (1971). *Pompalar, vantilatörler, kompresörler* (2nd ed., Vol. 856, pp. 142-146). İstanbul: İstanbul Teknik Üniversitesi Matbaası.
32. Alemi, H. et al (2013). Effects of volute curvature on performance of a low specific-speed centrifugal pump at design and off-design conditions, *Journal of Turbomachinery*, 137(4), (n.p.). doi: 10.1115/1.4028766
33. Schlichting, H. (1979). *Boundary-layer theory* (7th ed.). New York: McGraw-Hill.
34. Help-Autodesk, <http://help.autodesk.com/view/SCDSE/2016/ENU/?guid=GUID-DEE0664D-771B-4446-9ED4-1498267D13FB>, [last visited on November 2015]
35. Wikipedia, https://en.wikipedia.org/wiki/Numerical_diffusion, [last visited on December 2015]
36. Help-Autodesk, <http://help.autodesk.com/view/SCDSE/2016/ENU/?guid=GUID-C23BBBB0-8938-460D-8061-50964D3A6CEE>, [last visited on November 2015]
37. Help-Autodesk, <http://help.autodesk.com/view/SCDSE/2016/ENU/?guid=GUID-61C4EB55-362C-48A0-8B22-20F9148D190D>, [last visited on November 2015]
38. Help-Autodesk,
<http://help.autodesk.com/view/SCDSE/2015/ENU/?guid=GUID-BE8C3B02-3613-4237-AD18-033FE3002C34>, [last visited on November 2015]
39. Help-Autodesk, <http://help.autodesk.com/view/SCDSE/2015/ENU/?guid=GUID-013A783C-807F-4340-BB8B-16A3AF52EECA>, [last visited on November 2015]

40. Help-Autodesk, <http://help.autodesk.com/view/SCDSE/2015/ENU/?guid=GUID-F9C4DDB4-8111-4F25-8EDE-D7C38B3BAD99>, [last visited on November 2015]
41. Wikipedia, https://en.wikipedia.org/wiki/Selective_laser_sintering, [last visited on November 2015]
42. Wikipedia, [https://en.wikipedia.org/wiki/STL_\(file_format\)](https://en.wikipedia.org/wiki/STL_(file_format)), [last visited on November 2015]

APPENDIX A

PICTURES OF PROTOTYPES AND EXPERIMENTAL SETUP

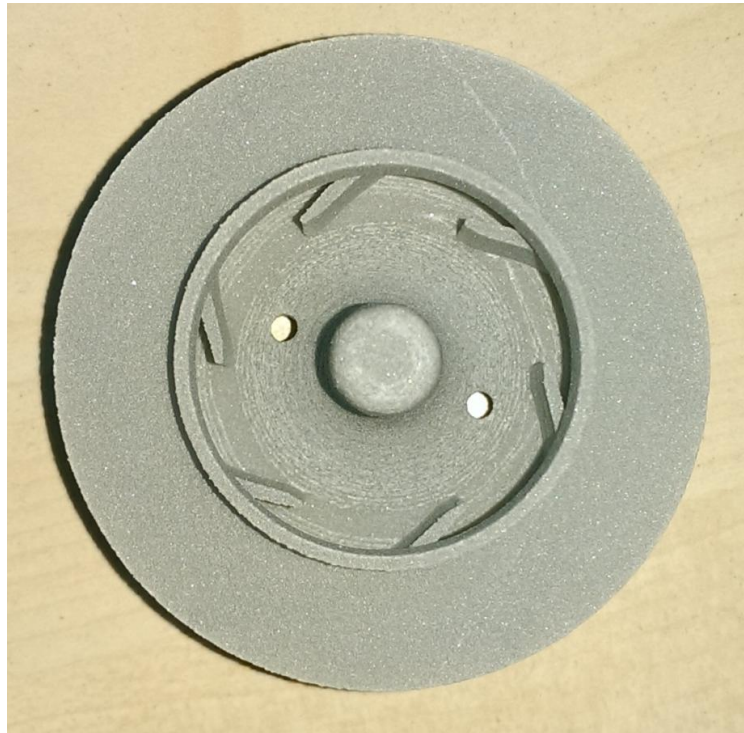


Figure A.1- Prototype of designed impeller (top view)

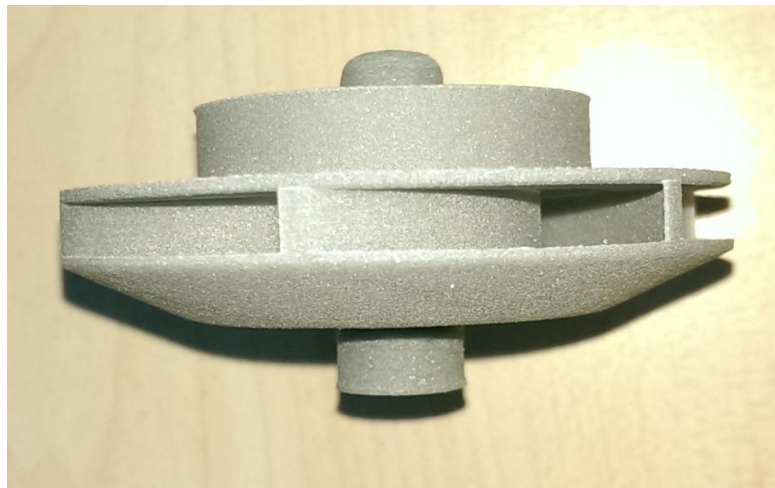


Figure A.2- Prototype of designed impeller (side view)



Figure A.3- Prototype of designed impeller (isometric view)



Figure A.4- Prototype of designed impeller assembled to shaft and wet rotor

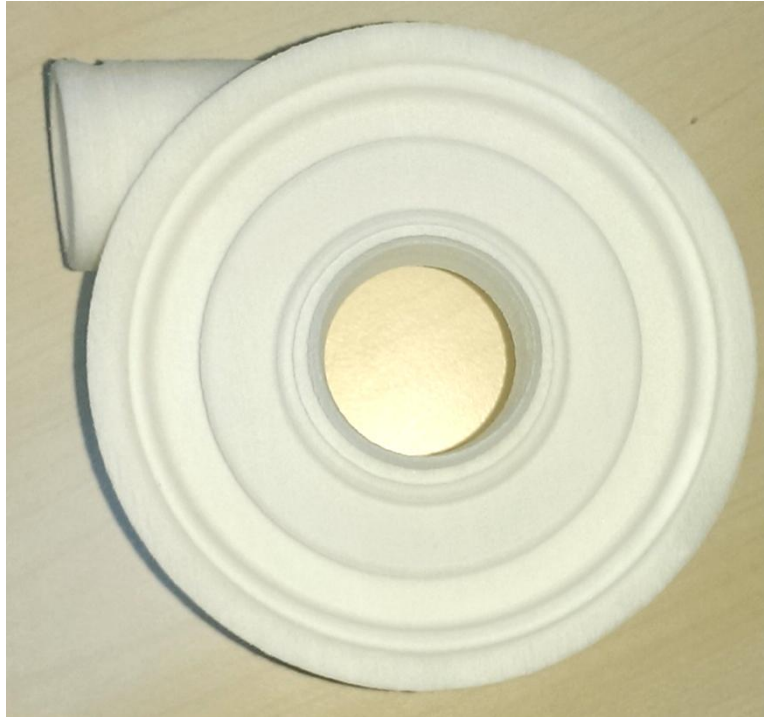


Figure A.5- Prototype of designed volute (top view)



Figure A.6- Prototype of designed volute (side view)



Figure A.7- Prototype of designed volute (front view)



Figure A.8- Prototype of designed volute (bottom view)



Figure A.9- Prototype of designed volute assembled to electric motor and inlet hose (with water-resistant glue on it)

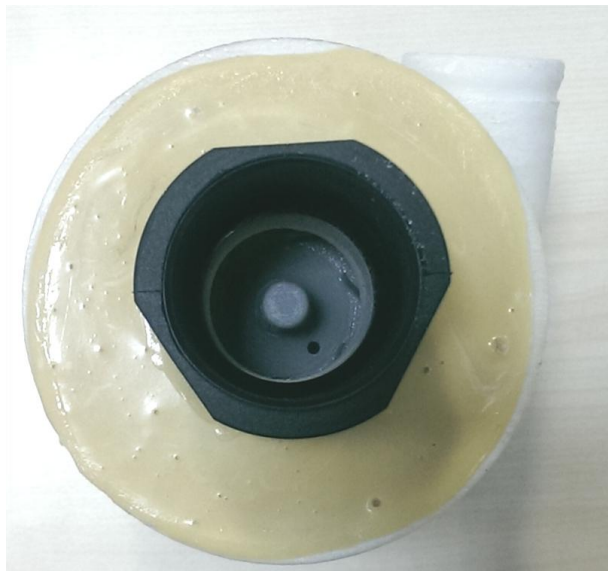


Figure A.10- Silicon reinforcement at the top of the volute prototype



Figure A.11-Experimental setup in Prof. Dr. Cahit Eralp Laboratory in Arçelik Dishwasher Plant

APPENDIX B

SAMPLE VISUALS OF MS EXCEL[®] PUMP DESIGN SHEET

INPUTS		SPECIFIC SPEED		PHYSICAL PROPERTIES		EFFICIENCIES	
N	3020 rpm	Ω	316 1/s	N_s	0.78	ρ	997 kg/m ³
Q	0.001 m ³ /s			nq	41	g	9.81 m/s ²
H	3.07 m					τ	1.2E+07 N/m ²
						pi	3.14159
						η	0.55
						η_v	0.92
						η_h	0.9

Shaft and Hub Diameter

Pmax 30.0 W dw 0.0034 m dn **0.0097 m**

$$d_{sh} = \left(\frac{1.03 P_{max}}{\pi \tau} \right)^{1/3} = 3.65 \left(\frac{P_{max}}{\tau} \right)^{1/3}$$

Impeller Outlet Diameter

$V_{tip} = 1.21 \omega r_{tip} \approx 1.21 \Omega r_{tip}$ Plot 0.88 $d_2 = \frac{60}{\pi N} \frac{2\pi H_{net}}{V_{tip}} = \frac{60 H_{net}}{N V_{tip}}$ **0.0569 m** (plot)

Blade Number

Z **7** $10 < z_1 < 120$ with 5 to 7 blades.

Impeller Inlet Diameter

$A_1 = \frac{Q}{V_1} = \frac{Q}{\omega r_1} = \frac{Q}{\Omega r_1}$ $d_1^* = d_1/d_2$

tan $\alpha_1 = \infty$ $\delta r = 1$ fd_1 1.15–1.05 (nq: 15–40) 1.05

d1 **0.0285 m** d1a **0.032** d1b **0.030** d1m **0.032**

Inlet blade angle

$u_1 = \pi d_1 \omega / 60$ 4.99 m/s $\beta_1 = \arctan \frac{Q_{1a}}{V_1 A_1}$ $A_1 = \frac{\pi}{4} (d_1^2 - d_h^2)$ A1 0.0006 m²

flow w/o blockage 21.2 deg flow w/blockage $\beta_1^* = \arctan \frac{c_{1a}}{u_1 - c_{1a}}$

blockage blade thickness e1 **0.001 m** $c \cdot d_1 = 0.016$ to 0.022 0.018

RUN Calc'd 1.21 0.8904 5.6085

β_1^* 25.1 deg i 2 deg 2.214

0.0349 rad

blade angle

β_{1B} **27.1 deg** 0.4725

Outlet width

$nq/nref = \frac{Q_{net} \sqrt{H_{net}}}{Q_{net,ref} \sqrt{H_{net,ref}}}$ nq/nref 0.41

b2 **0.0064 m** or b2* **0.09** b2 **0.0051**

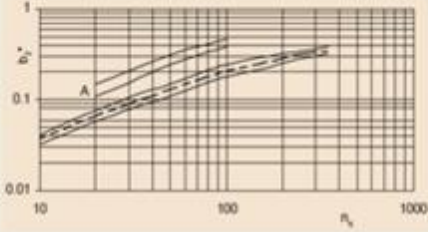
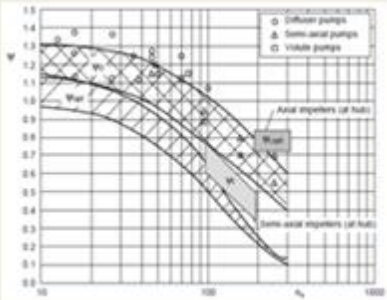
Outlet blade angle

$u_2 = \pi d_2 \omega / 60$ u2 9.00 m/s $A_2 = \pi d_2 b_2$ 0.0009 m²

RUN $c_{2a} = \frac{Q_{2a}}{V_2 A_2}$ c2m 1.187 m/s $\beta_{2,a} = \arctan \frac{c_{2a}}{u_2}$ 0.132

blockage blade thickness e2 **0.001 m** $c \cdot d_2 = 0.016$ to 0.022 0.018

β_{2a} **1.078788** Calc'd 1.079



slip factor $\epsilon_{lim} = \exp\left(\frac{8.16 \sin \beta_{2B}}{z_{Ls}}\right)$ $k_w = 1 - \left(\frac{d_{im} + \epsilon_{lim}}{1 - \epsilon_{lim}}\right)^3$ $\frac{1.000}{k_w} = 1$

0.535314 Calc'd 0.535

$\gamma = f_1 \left(1 - \frac{\sqrt{\sin \beta_{2B}}}{z_{Ls}^{0.7}}\right) k_w$ Radial: $f_1 = 0.98$ 0.002

0.796233 Calc'd 0.796

Prediction $c_{2u} = u_2 \left(\gamma \cdot \frac{c_{2m} \tau_2}{u_2 \tan \beta_{2B}}\right)$ 0.0004 $c_2 = \sqrt{c_{2m}^2 + c_{2u}^2}$ 5.289 m/s $W_{2u} = u_2 - c_{2u}$ 3.85 m/s $W_2 = \sqrt{c_{2m}^2 + W_{2u}^2}$ 4.02 m/s

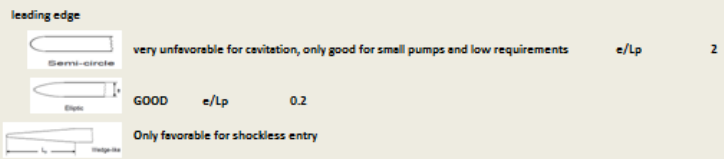
Calculation from measured head H $c_{2u} = \frac{g H}{\eta_b u_2} + \frac{u_{2m} c_{2u}}{u_2}$ 3.718 m/s vs 5.154

5.154208 m/s Calc'd 5.149 m/s

flow w/blockage $\beta_2 = \arctan c_{2m} \tau_2 / W_{2u}$ 0.0949

$\beta_2 = 18.4$ $5' 10$ to $14'$ 14 $\beta_{2B} = 32.4$ deg 0.566 red

Blade edge profiles



!!!BUT, non-profiled blades are also preferred for possibility of underfilling in case of deficit in head and also for cost reasons

Blade loading

$c_{ul} = \left(\frac{h_{q,Ref}}{h_q}\right)^{0.77}$ 0.978 with 10% tolerance $c_{ref} = \frac{2\pi V_{opt}}{\eta_b z_{Ls} L_{ch} (w_1 + w_2)}$ 0.881

$h_{q,Ref} = 40$ Band width $\pm 15\%$

$w1^* = 0.595$ $Lsch = 0.055$ m

Throat area

$A_{1q} = a_1 \cdot b_1$ a_1 (from CAD) 0.007 m $A_{1q} = 0.00004$ m²

$W_{1q} = Q_{Ls} / (z_{Ls} \cdot A_{1q})$ 3.722785 m/s

$w_{1m} = 5.36$ m/s

CHECK $w_{1q}/w_{1m} = 0.75-0.85$ 0.70

Blade distance a2

$\beta_{s2} = \arcsin a_2 / t_2$ $\sin \beta_{s2} / \sin \beta_{2B}$ 0.65 $\sin(\beta s2)$ 0.35

$t = \pi \cdot d / z_{Ls}$ 0.026 $a_2 = 0.0089$ mm

FINAL DIMENSIONS

a1a	21.6 mm
a1b	30.0 mm
a2	56.9 mm
aw	3.4 mm
dn	9.70 mm
d1	28.5 mm
β_{1B}	27 deg
β_{2B}	32 deg
b1	7.2 mm
b2	5.1 mm
e1	1 mm
e2	1 mm

APPENDIX C

CODES OF MACROS FOR ITERATIONAL CALCULATIONS

Macro 1: β_{1B} calculations

Sub beta_1b()

Dim t As Double

Dim tc As Double

Dim b As Double

Dim c As Double

Dim pi As Double

pi = Range("m6").Value

t = 1

tc = 5

Do While Abs(t - tc) / Abs(tc) * 100 > 0.1

c = tc

tc = Range("g42").Value

t = c

Cells(42, 4) = t

Loop

End Sub

Macro 2: β_{2B} calculations

Sub beta_2b()

Dim t As Double

Dim tc As Double

Dim e As Double

Dim ec As Double

Dim g As Double

Dim gc As Double

Dim c As Double

Dim cc As Double

Dim xt As Double

Dim xe As Double

Dim xg As Double

Dim xc As Double

t = 1.25

Cells(71, 4) = t

tc = 1.5

e = 0.5

Cells(78, 4) = e

ec = 0.75

g = 0.5

Cells(84, 4) = g

gc = 0.75

c = 2

Cells(89, 4) = c

cc = 5

Do While Abs(c - cc) / Abs(cc) * 100 > 0.1 Or Abs(g - gc) / Abs(gc) * 100 > 0.3 Or
Abs(e - ec) / Abs(ec) * 100 > 0.3 Or Abs(t - tc) / Abs(tc) * 100 > 0.3

x1 = tc

x2 = ec

x3 = gc

x4 = cc

tc = Range("g71").Value

ec = Range("g78").Value

gc = Range("g84").Value

cc = Range("g89").Value

t = x1

Cells(71, 4) = t

e = x2

Cells(78, 4) = e

g = x3

Cells(84, 4) = g

c = x4

Cells(89, 4) = c

Loop


```
End Sub
Macro 3: Cutwater blockage calculations
Sub volute_blockage()
    Dim t As Double
    Dim tc As Double
    Dim c As Double
    t = 1
    tc = 5

    Do While Abs(t - tc) / Abs(tc) * 100 > 0.1
        c = tc
        tc = Range("g206").Value
        t = c
        Cells(206, 4) = t
    Loop
End Sub
```